DOCTORAL THESIS

Thermodynamic Study on Thermochromic Phase Transitions in Transition Metal Complexes

by

Akihito NISHIMORI

Microcalorimetry Research Center
Faculty of Science
Osaka University

1993

ACKNOWLEDGMENTS

This thesis owes very much to many persons. First of all, I would like to express my most sincere gratitude to Professor Michio Sorai for many valuable instructions and patient encouragements to me. I thank very much Professor David N. Hendrickson of University of California at San Diego for kindly providing the sample of $[Cu(dieten)_2](ClO_4)_2$.

Elemental analyses were performed by Mr. Masakazu Okumiya and Ms. Kazuyo Hayashi, infrared spectra were recorded by Mr. Shin-ichi Ishikawa. I express my sincere thanks to them.

I am also grateful to Dr. Hiroshi Shimomura for his advice and helpful discussions. I am deeply indebted to Dr. Motohiro Nakano, who kindly helped me to prepare this thesis. Without his support, this thesis would not have been completed.

I wish to express my sincere appreciation for warm supports and fruitful discussions from fellows of Microcalorimetry Research Center and Matsuo's Laboratory.

Finally, I express my heartfelt thanks to my parents.

ABSTRACT

Thermal properties of six thermochromic complexes have been studied by means of heat capacity measurements. These six complexes are classified into two groups. One is $[M(dieten)_2]X_2$ (M = Cu(Ⅱ) and Ni(Ⅱ); dieten = $(C_2H_5)_2NCH_2CH_2NH_2$; X = BF_4^- and ClO_4^-); bis(*N,N*–diethylethylenediamine) copper(Ⅱ) tetrafluoroborate, bis(*N,N*–diethylethylenediamine)copper(Ⅱ) perchlorate, bis(*N,N*–diethylethylenediamine)nickel(Ⅱ) tetrafluoroborate and bis(*N,N*–diethylethylenediamine)nickel(Ⅱ) perchlorate. The other is $(IPA)_nCuCl_{n+2}$ (IPA = $(CH_3)_2CHNH_3^+$; n = 1: isopropylammonium trichloro–cuprate(Ⅱ), n = 2: bis(isopropylammonium) tetrachlorocuprate(Ⅱ)). $[M(dieten)_2]X_2$ is described in Chapter 1 and $(IPA)_nCuCl_{n+2}$ in Chapters 3 and 4. All these compounds exhibit a reversible color change with a phase transition in the solid state. This abrupt color change is very attractive and interesting from a view point of the mechanism of thermochromic phenomena. When the temperature is varied, the color of the sample changes as follows,

$[Cu(dieten)_2](BF_4)_2$; red ⇌ blue–violet,
$[Cu(dieten)_2](ClO_4)_2$; red ⇌ blue–violet,
$[Ni(dieten)_2](BF_4)_2$; orange ⇌ red,
$[Ni(dieten)_2](ClO_4)_2$; orange ⇌ red,
$(IPA)CuCl_3$; brown ⇌ orange,
$(IPA)_2CuCl_4$; green ⇌ yellow.

In Chapter 2, heat capacities of four $[M(dieten)_2]X_2$ compounds measured between 13 and 420 K are described. Each compound shows a large phase transition and a heat capacity anomaly spreading over a wide temperature region from ~200 K to the phase transition point. Transition temperatures, entropies and enthalpies are as follows,

$[Cu(dieten)_2](BF_4)_2$; 302.64 K, 55.3 J K^{-1} mol^{-1}, 16.62 kJ mol^{-1},
$[Cu(dieten)_2](ClO_4)_2$; 317.64 K, 55.2 J K^{-1} mol^{-1}, 17.43 kJ mol^{-1},
$[Ni(dieten)_2](BF_4)_2$; 374.86 K, 57.4 J K^{-1} mol^{-1}, 20.85 kJ mol^{-1},
$[Ni(dieten)_2](ClO_4)_2$; 382.01 K, 54.7 J K^{-1} mol^{-1}, 20.18 kJ mol^{-1}.

There exist large differences in the transition temperatures, from 302.64 K for $[Cu(dieten)_2](BF_4)_2$ to 382.01 K for $[Ni(dieten)_2](ClO_4)_2$. However, the transition entropies are almost the same, about 55.7 J K^{-1} mol^{-1} ($\approx R \ln 800$). The Boltzmann principle relates the entropy to the degrees of molecular freedom. So almost the same degrees of freedom, in other words the same degrees of disorder, are excited in the process of thermochromic phase transition from the low– to the high–temperature phase. Correlation among structures, electronic spectra and thermal properties is studied. The thermodynamic quantities are discussed by use of puckering motion of the chelate ring, Chesnut exciton model and angular overlap model (AOM). Observed excess heat capacities, transition entropies and transition enthalpies are well reproduced by the application of the Chesnut model. The magnitudes of transition entropies and enthalpies are interpreted by means of the ring puckering and AOM. The change of structure, the change of color and the thermodynamic quantities due to the thermochromic phase transition are reasonably well explained.

Calorimetric studies on $(IPA)CuCl_3$ are given in Chapter 3. The high–temperature phase is undercooled down to liquid helium temperature. The thermochromic phase transition was observed at 335.63 K, with $\Delta_{trs}H$ = 5.54 kJ mol^{-1} and $\Delta_{trs}S$ = 16.5 J K^{-1} mol^{-1}. On the other hand, two anomalies were found in the heat capacity of the quenched metastable phase. One is a glass transition at 154 K and the other is a higher–order transition at 207.75 K. The residual entropy due to the glassy state is 5.53 J K^{-1} mol^{-1}. The enthalpy difference between the stable phase and the metastable phase

at 0 K can be estimated to be 3.55 kJ mol^{-1}.

Calorimetric studies on $(IPA)_2CuCl_4$ are described in Chapter 4. Four endothermic peaks were found by means of DTA measurements. Two peaks at 330 and 352 K are observed in the stable phase and two at 250 and 286 K in the metastable phase. The peak at 330 K corresponds to the thermochromic phase transition. The peaks in the metastable phase could not be measured by the adiabatic calorimetry. The enthalpy relaxation from the metastable to the stable phase prevented the heat capacity measurement. The enthalpy of the metastable phase was found to be higher than that of the stable one by 4.47 kJ mol^{-1} at 0 K.

CONTENTS

Chapter 1. General Introduction

§1-1. Phase Transitions Occurring in the Solid State

The most obvious phase transitions one encounters are fusion and vaporization occurring between two different condensed states of matter. However, a wide variety of physical systems exhibit phase transitions in the solid state, known as "cooperative phenomena in crystals". Study of phase transitions plays a diagnostic role in the elucidation of the intermolecular interactions that stabilize the crystal lattice of a given system. From a thermodynamic point of view, a phase transition takes place between two given phases when their Gibbs free energies become equal. Ehrenfest [1] has defined general transitions of nth order by requiring that at the transition point the Gibbs free energy and its derivatives up to the $(n-1)$st order be continuous, while the nth derivatives are to be discontinuous and the $(n+1)$st derivatives are to be infinite. The case $n = 1$ thus comprises the ordinary changes in phase, which are therefore called "first order" transition [2]. In spite of this clear definition, phase transitions characterized by n other than $n = 1$ are often loosely denoted as "second order" or "higher order" transitions.

According to molecular basis responsible for the transition mechanism, phase transitions hitherto well-known are classified as the order-disorder type and the displacive type. In the order-disorder type [3], the onset of orientational disordering of molecular axes or spin axes brings about characteristic phase transitions. Ammonium halides are well-known examples of this type of transitions, in which ammonium cations having tetrahedral forms are involved in the order-disorder mechanism. In magnetic phase transitions leading to ferro- or antiferromagnetic state the orientational

alignment of electron spins plays an important role. Brass exhibits another type of order–disorder phase transition, in which constituent atoms show positional order–disorder effect. Displacive type phase transitions are often encountered in dielectric materials, where small displacement of atoms and/or ions changes the crystal symmetry to lead to a phase transition. In general, entropy gain at a phase transition is much larger in the order–disorder type than in the displacive type.

Since the intramolecular electronic energy is much greater than the intermolecular potential energy, the molecular structure remains unchanged before and after a phase transition for these systems; a change in the electronic energy of a molecule is sufficiently small to be neglected. Recently, however, new types of phase transitions have drawn many scientists' attention. Here electrons are directly involved and a change in the electronic state is strongly coupled with a change in the lattice. These transitions involve the spin–crossover phenomena occurring between high– and low–spin states, the intramolecular electron–transfer in mixed–valence complexes, the metal–nonmetal transition known as the Peierls transition, the thermochromic phenomena, the neutral–ionic transition due to charge–transfer mechanism and so on [4].

§1–2. Aim of the Present Study

Among various types of phase transitions occurring in the solid state those in which electrons are directly involved are of particular interest in that the onset of dynamics associated with ligands, counter ions and even solvate molecules in crystals can be dramatically coupled with the electrons in a molecule. This category of phase transition includes spin–state transformation in spin–crossover complexes [5], intramolecular electron transfer in mixed–

valence compounds [4], thermochromic phenomena [6–8], neutral–to–ionic transition due to charge transfer mechanism [9] and others.

The thermochromic phenomena are very attractive because they exhibit a dramatic color change when a phase transition takes place. The manifestation of thermochromism is full of variety, it can be reversible or irreversible, continuous or discontinuous, and can occur either in the solid state or in a solution. The present study is concerned with heat capacity measurements of thermochromic materials, whose color change occurs reversibly and discontinuously in the solid state. There are two series of thermochromic complexes in this thesis. One is $[M(dieten)_2]X_2$ (M = Cu(Ⅱ) and Ni(Ⅱ); dieten = *N,N*–diethylethylenediamine; X = BF_4^- and ClO_4^-), in which the coordination number remains unchanged through a phase transition, while the other is $(IPA)_nCuCl_{n+2}$ (IPA = $(CH_3)_2CHNH_3^+$; n = 1: isopropyl–ammonium trichlorocuprate(Ⅱ), n = 2: bis(isopropylammonium) tetrachloro–cuprate(Ⅱ)), in which the coordination number does change through a phase transition. A considerable amount of physicochemical study, mainly spectroscopic measurements, have been for these complexes. The spectroscopic methods are very useful for the study of the microscopic aspects. But they do not provide us with information about phases recognized as a macroscopic aspect. In order to make clear the relationship between the microscopic aspects hitherto reported and the macroscopic energetic and entropic aspects, precise heat capacity measurements by adiabatic calorimetry will be reported in the present study. Adiabatic calorimetry enables us to directly evaluate the enthalpy and entropy. The entropy of transition, $\Delta_{trs}S$, is an important thermodynamic quantity, because the Boltzmann principle relates the entropy of transition to the degrees of molecular freedom, W. That is, the relation can be written as

$$\Delta_{trs}S = R \ln (W_f / W_i), \qquad (1-1)$$

where subscripts i and f indicate initial and final states, respectively. So the calorimetric entropy can be interpreted as a measure of disorder.

§1–3. Calorimetry

Heat capacities of the thermochromic complexes described in this thesis were measured by means of adiabatic calorimeters [10–12]. Adiabatic calorimetry has a very high accuracy and precision. Molar heat capacity at constant pressure is the ratio of the heat given to a unit amount of a substance to the consequent rise in its temperature. The averaged heat capacity of the system, C, which consists of the calorimeter sample cell and sample, is equal to

$$C = \Delta E / \Delta T, \qquad (1\text{–}2)$$

where ΔE indicates the supplied energy and ΔT is the temperature rise.

In this experiment, two adiabatic calorimeters were used to measure the heat capacity. One worked in the temperature range between 13 and 530 K [12] and the other between 13 and 395 K [10]. The automatic measuring system had already been constructed in the former, while in the latter it had not been done. Therefore, that calorimeter was improved in advance to the present experiment [11]. The automatic measuring system is a very convenient technique for heat capacity measurement, for it takes long time to get heat capacities. The heat capacity measurement is composed of two major operations. One is the measurement of the input energy, ΔE. The other is the measurement of the temperature rise, ΔT. ΔE is the Joule energy supplied from a constant D.C. current generator (Yokokawa Electric Work, model 2555). The electric current through and the potential drop across the

heater wire are measured by a digital multimeter (Keithley, model 195A) and the energy-input interval is measured by a universal counter (Advantest, model TR5822). The temperature was measured with a platinum resistance thermometer calibrated on the basis of IPTS-68. The resistance of the Pt-thermometer is measured by an A.C. bridge (Automatic System Laboratory, model F17A). Since the A.C. bridge is sensitive to the line noise, the power supply for the bridge is separated from those for other electric devices by a noise cut transformer (Elgar, HIT-1.0-0.005). These apparatuses and home-built relay circuit are controlled by a personal computer (NEC, PC-9801VM2). They are connected by GP-IB or RS-232C. The block diagram of the automatic measuring system is drawn in Fig. 1-1.

The molar heat capacity at constant pressure, C_p, is determined as follows,

$$C_p = (C - C_{\text{cell}})F, \qquad (1\text{-}3)$$

where C_{cell} stands for the heat capacity of the sample cell which has been determined in an auxiliary measurement and F is the mole factor, which is determined as the ratio of the relative molecular mass to the mass of the sample contained in the sample cell. To establish a good adiabatic condition, the sample cell is surrounded by two [10] or four [12] radiation shields and the space around the cell is evacuated with an oil diffusion pump and a rotary pump. The heat leakage through the electric lead wires and radiation are minimized by adequate temperature control of the radiation shields. When the adiabatic condition was well maintained, the temperature drift of the sample cell was less than 0.02 mK min^{-1}.

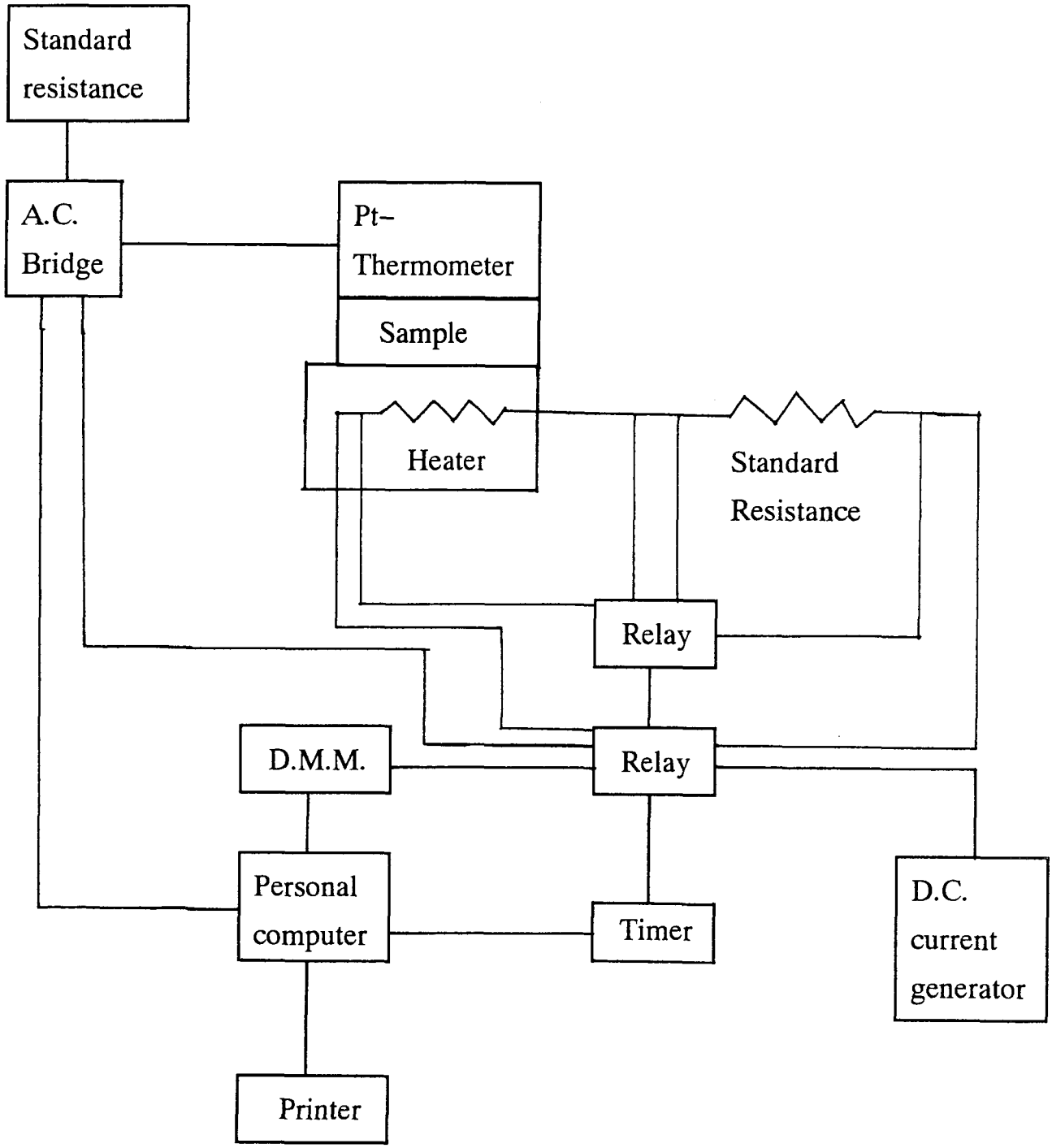

Fig. 1-1. Block diagram of measuring system.

References to Chapter 1.

[1] P. Ehrenfest, *Commun. Kamerlingh Onnes Lab. Univ. Leiden*, Suppl. 75b (1933).

[2] A. Münster, "*Statistical Thermodynamics*", Vol. I, Springer-Verlag (1969), Chap. 4.6.

[3] N. G. Parsonage and L. A. K. Staveley, "*Disorder in Crystals*", Oxford Univ. Press (1978).

[4] M. Sorai and D. N. Hendrickson, *Pure & Appl. Chem.*, **63**, 1503 (1991).

[5] P. Gütlich, *Struct. Bonding*, **44**, 83 (1981).

[6] K. Sone and Y. Fukuda, "*Inorganic Thermochromism*", (Inorganic Chemistry Concepts, Vol. 10) Springer-verlag, Berlin (1987).

[7] D. B. Bloomquist and R. D. Willett, *Coord. Chem. Rev.*, **47**, 125 (1982).

[8] J. H. Day, *Chem. Rev.*, **63**, 65 (1963).

[9] J. B. Torrance, J. E. Vazquez, J. J. Mayerle and V. Y. Lee, *Phys. Rev. Lett.*, **46**, 253 (1981).

[10] M. Yoshikawa, M. Sorai, H. Suga and S. Seki, *J. Phys. Chem. Solids*, **44**, 311 (1983).

[11] A. Nishimori, Y. Nagano and M. Sorai, *unpublished result.*

[12] M. Sorai, K. Kaji and Y. Kaneko, *J. Chem. Thermodyn.*, **24**, 167 (1992).

Chapter 2. Thermochromic Phase Transitions in $[M(dieten)_2]X_2$

§2-1. Introduction

A number of substances are known to be thermochromic [1]. There are many types of thermochromism, it can be reversible or irreversible, continuous or discontinuous, and can occur either in the solid state or in a solution. The series of compounds $[M(dieten)_2]X_2$, where M is Cu^{2+} or Ni^{2+}, dieten *N,N*-diethylethylenediamine, and X BF_4^- or ClO_4^-, is particularly well-studied [2]. They show a remarkable color change as they undergo solid state phase transitions. Thermochromism in $[Cu(dieten)_2](ClO_4)_2$ was first reported in 1938 by Pfeiffer *et al.* [3]. The color of the copper complex compounds changes from red to blue-violet upon heating. The color of a similar nickel complex compounds changes from orange to red. Both color changes are reversible. Infrared [4], far-infrared [4], electronic and spectra [4,5], magnetic measurement [5], ESR [5], DSC [6], X-ray diffraction [7,8] and NMR [8,9] have been reported. At first it was supposed that the thermochromism was caused by an increase of axial approach of the anions to the copper or nickel ion [5,6]. But, when the crystal structures of the low- and high-temperature phases were reported [7,8], that idea was turned out to be wrong. There exists no axial coordination of the counter anions in either phases because the bulky alkyl groups on the nitrogen atoms prevent the counter anions from approaching the central metal atom. Then the mechanism of the thermochromism proposed next was as follows. In the high-temperature phase the chelate rings pucker up and down while it stays stationary in the low-temperature phase. Such ring-motions affect the ligand field strength, leading to the color changes. This mechanism is consistent with the experimental data so far available. However, the relationship

between the microscopic aspects hitherto reported and the macroscopic energetic and entropic aspects is still unclear.

§2-2. Review of Previous Investigation

2-2-1. Structure

The structure of $[Cu(dieten)_2](ClO_4)_2$ has been determined in both low- and high-temperature phases [7,8]. The red low-temperature is triclinic, P1, Z = 1, a = 8.131(8) Å, b = 8.762(13) Å, c = 9.786(12) Å, α = 65.33(10)°, β = 65.98(11)°, and γ = 63.34(8)° at 25° C, and the blue-violet high-temperature phase is monoclinic, I2, Z = 4, a = 13.34(1) Å, b = 8.414(5) Å, c = 9.978(5) Å, and β = 97.43(5)° at 60° C. The crystal structure of the low- and high-temperature phases are shown in Figs 2-1 and 2-2 respectively. In the low-temperature phase, the perchlorate anions are separated from the central Cu atom. The distance between Cu and the closest O is 3.65(1) Å. In the high-temperature phase, this interatomic distance is 4.16(2) Å. In the case of $[Cu(eten)_2](ClO_4)_2$ [8], perchlorate anions coordinate on the copper atom and the Cu-O distance is 2.594 Å. Therefore, both the low- and high-temperature phases, the perchlorate anions do not coordinate on the copper atom. The coordination number does not change on going from one phase to the other. Thermal ellipsoids of the chelate ring atoms are very large in the high-temperature phase, and the interatomic distances in the rings in the high-temperature phase are much shorter than those of the low-temperature phase. These features in the high-temperature phase are probably due to either dynamic or static disorder of the chelate rings. The structures of the other three complexes seem to have an

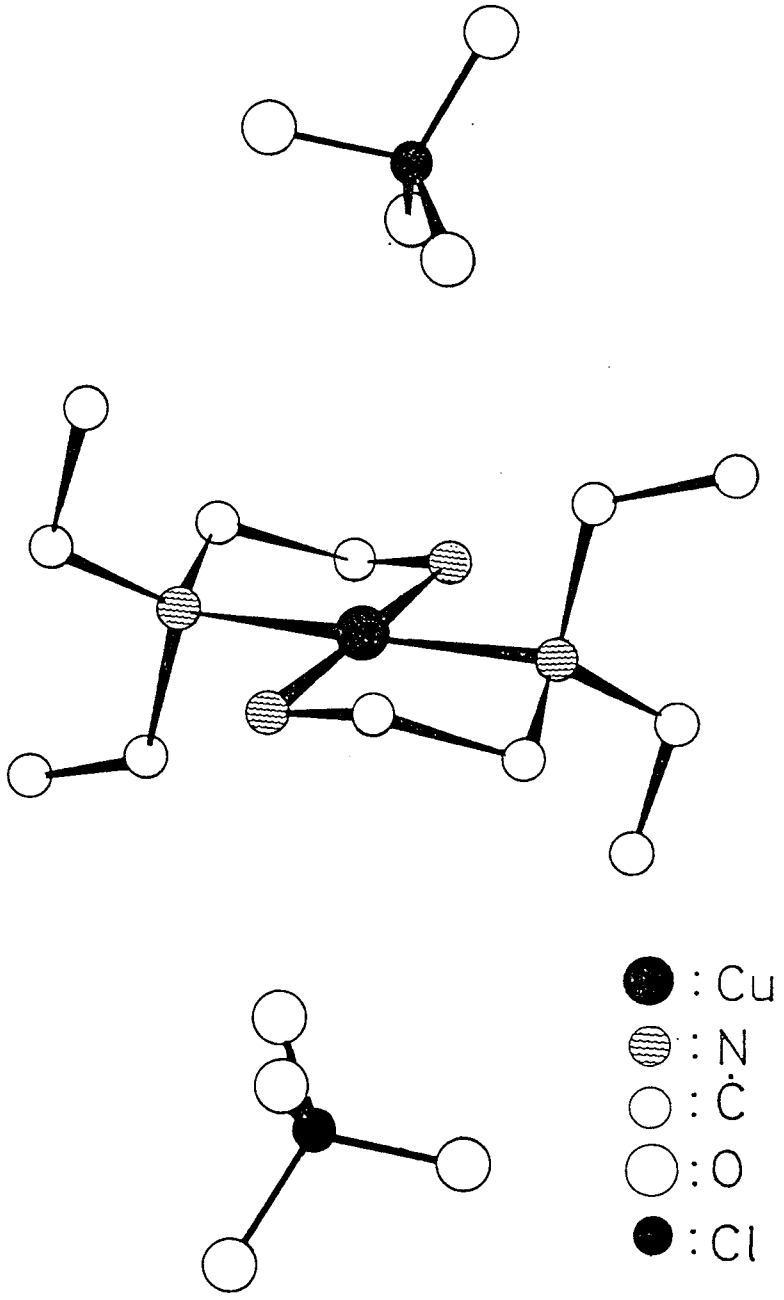

Fig. 2–1. Structure of $[Cu(dieten)_2](ClO_4)_2$ in the low–temperature phase (after ref. 8).

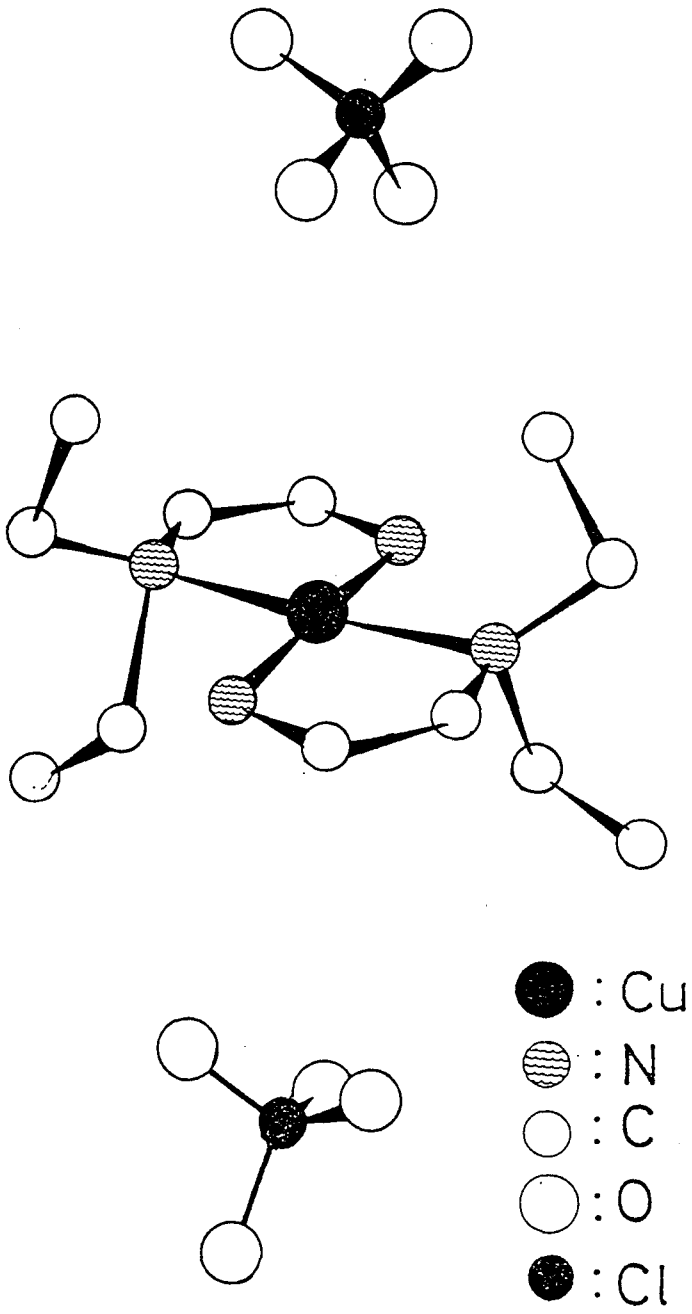

Fig. 2-2. Structure of $[Cu(dieten)_2](ClO_4)_2$ in the high-temperature phase (after ref. 8).

identical structure with that of $[Cu(dieten)_2](ClO_4)_2$ by the X-ray diffraction patterns.

2-2-2. Electronic Spectra

The visible absorption spectra of the Cu and Ni complexes show red shift when the sample is heated [4-6]. The red shift may be viewed as the tendency of the complex to go from a planar toward an octahedral environment (increased axial interaction of the anions from above and below the MN_4 plane) [4].

2-2-3. Differential Scanning Calorimetry (DSC)

Differential scanning calorimetry (DSC) has been carried out to determine the enthalpy change associated with the endothermic transition between low- and high-temperature phases by Fabbrizzi *et al.* [6]. They found endothermic peaks at the same temperatures where a sharp spectral transformation occurred. The transition could be repeated indefinitely by successive heating and cooling cycles, as long as the temperature was kept low to avoid decomposition. The enthalpy gain, ΔH, was 10.0 and 8.9 kJ mol^{-1} for the BF_4^- and ClO_4^- salts of the copper complexes, respectively, while ΔH was 5.7 and 6.7 kJ mol^{-1} for those the of nickel complexes.

2-2-4. Nuclear Magnetic Resonance (NMR)

Solid state proton NMR measurements have been done [8,9]. The line widths varied only slightly with temperature in the low and high temperature

phases. However, a significant line narrowing has been observed at the color change. ^{1}H NMR second moments of this series of complexes show a discontinuous change at the thermochromic transition temperatures. These results indicate different degrees averaging of the local magnetic field in the two phases. Solid state ^{19}F NMR resonance of the $[Cu(dieten)_2](BF_4)_2$ complex has also been measured [9]. In contrast to the proton NMR, there is no change in the ^{19}F NMR spectra at the phase transition temperature. The second moment of ^{19}F NMR signal is 2.0 G^2 and shows no change at the transition. Theoretical calculations show that a BF_4^- anion undergoing threefold rotation about a B–F axis would have a second moment of 1.9 G^2. The authors [9] suggested an alternative possibility that the motion is not the simple one described above but a combination of various motions. It was concluded that no change in the dynamic state of the BF_4^- anion occurs at the phase transition.

§2–3. Aim of the Present Investigation

Heat capacity is one of macroscopic physical quantities obtained as a bulk property of a given system. In this sense, heat capacity measurement is the most suitable experimental method for identification of phase and detection of phase transition in a thermal equilibrium state. In the case of thermochromic phase transition, electronic spectroscopy provides a direct information about a color change reflected by the energy difference between an electronic ground state and its excited state at a given temperature. On the other hand, one can get an information about the energy difference between a ground state of low–temperature phase and a ground state of high–temperature phase from calorimetric data such as T_{trs}, $\Delta_{trs}S$, $\Delta_{trs}H$ and others. This study aims at understanding the mechanism of the thermochromic

phenomenon in $[M(dieten)_2]X_2$ by combining the knowledge of the macroscopic aspects obtained from thermodynamic study with that of the microscopic aspects gained by various spectroscopies and X-ray diffraction analysis.

§2-4. Experimental

2-4-1. Preparation of Samples

$[Cu(dieten)_2](BF_4)_2$

This complex was prepared according to the method described by Lever *et al.* [5]. Tetrafluoroboric acid was added to excess copper carbonate. When the reaction was complete, ethanol was added, and the solution was filtered to remove unreacted copper carbonate. This solution was added to a stirred ethanolic solution of the ligand, *N,N*-diethylethylenediamine, at 315 K. Blue-violet precipitate was formed. The solution with the precipitate was cooled in a refrigerator. The red product was filtered and washed with ether three times, then dried in a vacuum desiccator. The total yield of product was 63.3 %. The elemental analysis for the complex was good.

$[Cu(dieten)_2](ClO_4)_2$

This complex was prepared by David N. Hendrickson *et al.* at University of Illinois. The elemental analysis for the complex gave a good result.

$[Ni(dieten)_2](BF_4)_2$

This complex was prepared by the method of Lever *et al.* [1] and Goodgame *et al.* [10]. Tetrafluoroboric acid was added to excess nickel carbonate. When the reaction was complete, ethanol was added, and the

solution was filtered to remove unreacted nickel carbonate. This solution was added to a stirred ethanolic solution of the ligand at 315 K. The orange precipitate was formed. The solution with the precipitate was cooled in a refrigerator. The product was filtered and washed with ethanol five times, then dried in a vacuum desiccator. The total yield of product was 61.9 %. The values of elemental analysis were in good agreement with the calculated values.

$[Ni(dieten)_2](ClO_4)_2$

This complex was prepared by the method of Lever *et al.* [5] and Goodgame *et al.* [10]. Perchloric acid was added to excess nickel carbonate. The rest of the procedures was the same as for $[Ni(dieten)_2](BF_4)_2$. The total yield of product was 62.7 %. The elemental analysis for the complex was good.

The results of elemental analyses are tabulated in Table 2–1 ~ 2–4.

2–4–2. Differential Thermal Analysis (DTA)

Qualitative nature of thermal properties of the samples were examined by the use of a home–built DTA apparatus in the temperature range from 82 K to their melting temperatures.

2–4–3. Infrared and Far–Infrared Absorption Spectra

Infrared spectra in the range from 400 to 4000 cm^{-1} were recorded with an infrared spectrophotometer (Japan Spectroscopic Co., Ltd., Model DS–402G) and far–infrared spectra in the range from 30 to 400 cm^{-1} a far–

Table 2–1. The results of elemental analysis for $[Cu(dieten)_2](BF_4)_2$.

	C%	H%	N%	Cu%
Obs.	30.78	6.84	11.91	13.55
Calc.	30.69	6.87	11.93	13.53

Table 2–2. The results of elemental analysis for $[Cu(dieten)_2](ClO_4)_2$.

	C%	H%	N%
Obs.	28.95	6.47	11.24
Calc.	29.13	6.52	11.32

Table 2–3. The results of elemental analysis for $[Ni(dieten)_2](BF_4)_2$.

	C%	H%	N%
Obs.	30.75	6.92	11.92
Calc.	31.02	6.94	12.06

Table 2–4. The results of elemental analysis for $[Ni(dieten)_2](ClO_4)_2$.

	C%	H%	N%
Obs.	29.47	6.55	11.44
Calc.	29.41	6.58	11.43

infrared spectrophotometer (Hitachi, Ltd., Model FIS-3). These spectra were used to estimate the normal heat capacities. The temperatures of the sample in the spectroscopic experiments were as follows:

$[Cu(dieten)_2](BF_4)_2$: 90, 220, 323 K,
$[Cu(dieten)_2](ClO_4)_2$: 90, 200, 300, 330 K,
$[Ni(dieten)_2](BF_4)_2$: 97, 300, 389 K,
$[Ni(dieten)_2](ClO_4)_2$: 92, 299, 393 K.

2-4-4. Heat Capacity Measurements

The two adiabatic calorimeters described in Chapter 1 [11-13] were used for the copper and nickel complexes. A small amounts of helium gas was sealed in a calorimeter cell to aid the heat transfer within the cell. The temperature ranges and the mass of samples were as follows:

$[Cu(dieten)_2](BF_4)_2$: 13-343 K, 10.3841 g (0.0221141 mol),
$[Cu(dieten)_2](ClO_4)_2$: 12-360 K, 10.0294 g (0.0202672 mol),
$[Ni(dieten)_2](BF_4)_2$: 14-413 K, 4.8949 g (0.0105332 mol),
$[Ni(dieten)_2](ClO_4)_2$: 14-420 K, 3.0303 g (0.0061842 mol).

The masses were corrected for the buoyancy using the density values from the crystal structure [7,8].

§2-5. Results and Discussion

2-5-1. DTA of $[M(dieten)_2]X_2$

A single endothermic peak occurred at 303.3 K in the first heating run

for $[Cu(dieten)_2](BF_4)_2$. A exothermic peak occurred at 295.2 K in the subsequent cooling run. Thus the transition temperature exhibited a thermal hysteresis of 8.1 K. The transition temperature was shifted to 301.7 K on the second heating run and remained at this temperature on further repetition of the measurement. The reason for this was not clear at that time, but during heat capacity measurements it was found that the virginal sample is somewhat strained. Once it is heated up to the high-temperature phase and cooled down slowly, the strain is released. Therefore the data obtained for the virginal sample are excluded from the analysis. Since no exothermic temperature drifts were observed during heat capacity measurements, there is no possibility that the low-temperature phase showing the transition at 301.7 K is metastable.

DTA measurements for the other samples were also carried out before heat capacity measurements. Each sample showed a single peak. The results of DTA are tabulated in Table 2-5.

2-5-2. Heat Capacity of $[M(dieten)_2]X_2$

To release the strain mentioned above, the samples were heated up to the high-temperature phase and cooled down slowly prior to heat capacity measurements. The molar heat capacity at constant pressure are listed in Tables 2-6 ~ 2-9 and plotted in Figs 2-3 ~ 2-6. Each compound exhibited a large heat capacity anomaly spreading over a wide temperature region from ~200 K to the phase transition point. In the vicinity of the phase transition temperature, the thermal relaxation time required for the thermal equilibration after an energy input was longer than 2 hours. This phenomenon is typically encountered for first-order phase transitions. For $[Ni(dieten)_2](ClO_4)_2$ an additional small peak centered at 400 K was found. The reason for the

Table 2–5. The results of DTA measurements.

Complexes	T_c / K for heating run	T_c / K for cooling run
$[Cu(dieten)_2](BF_4)_2$	301.7	295.2
$[Cu(dieten)_2](ClO_4)_2$	314.8	315.3
$[Ni(dieten)_2](BF_4)_2$	374.9	373.6
$[Ni(dieten)_2](ClO_4)_2$	380.0	382.0

Table 2–6. Molar heat capacity of $[Cu(dieten)_2](BF_4)_2$ (relative molecular mass: 469.568).

$\frac{T}{K}$	$\frac{Cp}{JK^{-1}mol^{-1}}$	$\frac{T}{K}$	$\frac{Cp}{JK^{-1}mol^{-1}}$	$\frac{T}{K}$	$\frac{Cp}{JK^{-1}mol^{-1}}$
		Series 1			
47.327	145.98	81.082	230.01	117.733	301.14
48.525	149.12	82.820	232.78	120.089	305.39
49.691	152.79	84.527	236.88	122.419	309.42
50.841	156.25	86.205	240.51	124.723	313.68
52.171	160.58	87.856	243.94	127.004	317.93
53.666	164.76	89.481	246.95	129.263	322.22
55.165	168.81	91.267	250.15	131.500	326.01
57.033	174.07	93.209	254.27	133.718	329.85
59.188	179.56	95.185	258.18	135.917	333.62
61.251	184.52	97.260	262.34	138.098	337.37
63.390	189.33	99.370	266.17	140.261	341.18
65.605	195.08	101.447	270.14	142.408	344.98
67.740	200.33	103.557	274.32	144.539	348.74
69.804	205.13	105.834	278.68	146.716	352.62
71.806	209.65	108.212	283.18	148.936	356.30
73.751	213.86	110.556	287.90	151.142	359.95
75.647	218.13	112.935	292.05	153.332	363.63
77.499	222.35	115.349	296.62	155.509	367.18
79.309	226.55				
		Series 2			
12.461	18.55	25.682	70.47	41.005	126.73
13.398	21.97	27.016	76.09	42.134	130.19
14.282	25.50	28.417	81.56	43.277	133.91
15.111	28.31	29.768	86.66	44.475	137.34
15.920	31.45	31.105	91.76	45.685	140.92
16.802	35.18	32.438	96.81	46.874	144.29
17.737	38.94	33.740	101.72	48.043	148.01
18.645	42.14	35.022	106.10	49.173	151.11
19.684	46.46	36.223	110.27	50.287	154.45
20.832	51.10	37.435	114.58	51.387	157.90
21.983	55.69	38.660	118.83	52.456	160.99
23.184	60.68	39.848	122.93	53.495	164.06
24.422	65.80				
		Series 3			
290.596	704.82	296.190	761.48	299.057	810.17
292.010	716.59	297.558	784.87	299.290	814.26
293.412	730.71	298.593	786.88	299.520	820.49
294.806	744.34	298.825	806.18	299.750	835.10

Table 2–6. (continued).

T / K	Cp / JK⁻¹mol⁻¹	T / K	Cp / JK⁻¹mol⁻¹	T / K	Cp / JK⁻¹mol⁻¹
299.978	843.61	302.556	9365.34	308.895	639.00
300.204	863.20	302.641	9637.20	309.411	641.63
300.429	884.27	302.726	9312.02	309.926	642.42
300.649	934.79	302.814	8779.13	310.440	643.71
300.865	1001.48	302.972	6893.42	310.955	644.27
301.070	1130.80	303.148	6019.24	311.469	645.63
301.258	1439.33	303.299	3989.14	311.983	645.32
301.418	1989.57	303.517	2367.04	313.244	649.34
301.548	2734.71	303.843	1168.91	315.748	652.81
301.656	3348.66	304.286	719.10	318.742	656.73
301.751	3849.60	304.785	672.80	321.727	660.42
301.837	4342.54	305.295	653.99	324.704	664.68
301.939	6248.39	305.807	645.92	327.673	669.50
302.060	6455.72	306.320	642.94	330.632	673.49
302.173	7216.63	306.834	642.74	333.583	677.39
302.277	7846.76	307.349	643.19	336.525	681.76
302.375	8286.33	307.865	643.08	339.455	686.54
302.468	8866.13	308.381	639.29	342.376	692.06
		Series 4			
298.231	791.36	302.557	9204.08	310.558	648.61
298.703	805.86	302.637	10965.30	311.563	649.12
299.168	821.63	302.715	9673.64	312.568	649.99
299.627	844.91	302.803	8467.24	313.572	651.41
300.082	861.10	302.906	6900.38	314.575	652.32
300.529	898.46	303.030	5461.75	315.577	653.84
300.956	1070.13	303.190	3735.44	316.579	655.16
301.311	1883.18	303.423	2059.92	317.579	656.36
301.557	3544.10	303.782	942.51	318.578	657.32
301.731	4566.88	304.252	662.86	319.577	658.21
301.877	5598.25	304.761	649.94	320.574	660.03
302.001	6656.23	305.520	646.77	321.571	661.32
302.110	7610.90	306.528	645.43	322.567	663.11
302.208	8468.75	307.536	645.99	324.059	664.61
302.299	8980.80	308.544	646.94	326.045	667.19
302.384	9632.63	309.551	647.87	328.026	670.38
302.470	9108.47				
		Series 5			
289.392	693.30	293.317	729.21	297.161	776.88
290.381	702.24	294.285	739.70	298.105	793.59
291.366	707.41	295.250	749.86	299.038	815.94
292.345	718.64	296.208	763.40	299.956	858.99

Table 2–6. (continued).

T / K	Cp / JK^{-1}mol^{-1}	T / K	Cp / JK^{-1}mol^{-1}	T / K	Cp / JK^{-1}mol^{-1}
300.827	1033.07	302.394	9972.43	304.179	690.82
301.457	3091.86	302.555	9997.53	305.185	647.05
301.801	5695.45	302.729	8477.86	306.206	643.66
302.036	7516.66	302.964	5195.56	307.227	643.73
302.227	9158.43	303.394	1992.09	308.247	644.51
		Series 6			
149.905	358.61	207.670	458.23	263.302	583.26
152.604	363.08	210.023	462.96	265.599	590.61
155.280	367.61	212.467	467.55	267.884	598.14
157.935	372.19	215.002	472.19	270.156	606.18
160.570	376.73	217.524	476.96	272.158	614.19
163.186	381.18	220.035	481.66	273.892	619.43
165.783	385.78	222.534	486.47	275.618	626.25
168.363	390.25	225.021	491.33	277.336	633.20
170.926	394.49	227.498	496.15	279.046	640.72
173.473	398.73	229.963	501.26	280.747	648.82
176.004	403.10	232.416	506.41	282.440	657.04
178.520	407.48	234.859	511.78	284.123	665.53
181.021	411.36	237.291	517.14	285.797	674.76
183.508	415.58	239.711	522.58	287.459	684.86
185.981	419.87	242.120	528.14	289.110	695.87
188.440	424.33	244.518	533.90	290.748	707.26
190.886	428.68	246.904	539.97	292.372	720.64
193.320	433.09	249.280	545.43	293.982	736.66
195.741	437.27	251.644	551.40	295.581	753.83
198.150	441.39	253.998	557.38	297.163	777.81
200.547	445.66	256.340	563.51	298.721	810.83
202.933	450.00	258.672	569.98	300.231	896.57
205.307	454.17	260.993	576.68	301.367	2623.76
		Series 7			
320.455	660.69	333.302	678.35	342.094	693.31
323.434	664.71	336.242	682.90	325.910	667.87
330.351	673.97	339.173	687.96	327.886	671.04

Table 2–7. Molar heat capacity of $[Cu(dieten)_2](ClO_4)_2$ (relative molecular mass: 494.860).

$\frac{T}{K}$	$\frac{Cp}{JK^{-1}mol^{-1}}$	$\frac{T}{K}$	$\frac{Cp}{JK^{-1}mol^{-1}}$	$\frac{T}{K}$	$\frac{Cp}{JK^{-1}mol^{-1}}$
		Series 1			
11.797	15.95	25.644	67.31	41.336	124.10
12.568	17.82	26.426	69.54	42.932	129.23
13.545	21.21	27.545	73.72	44.580	134.56
14.510	24.66	28.767	78.38	46.275	139.72
15.517	28.12	30.034	83.12	48.014	144.77
16.611	31.63	31.353	88.27	49.821	150.00
17.829	35.95	32.668	93.41	51.667	155.34
19.077	40.79	33.982	98.43	53.550	160.66
20.240	46.45	35.363	103.44	55.514	166.08
21.441	49.56	36.809	108.64	57.532	171.54
22.721	54.49	38.284	113.84	59.525	176.84
24.009	62.43	39.788	118.97		
		Series 2			
44.382	133.82	91.598	247.16	145.492	340.62
45.566	137.60	93.535	250.96	147.527	343.84
46.812	141.26	95.511	254.36	149.549	347.00
47.732	143.98	97.458	257.91	151.559	350.10
48.969	147.55	99.376	261.51	153.557	353.39
50.530	152.03	101.335	265.38	155.543	356.52
52.132	156.61	103.335	268.94	157.552	359.80
53.815	161.39	105.309	272.34	159.608	363.23
55.574	166.29	107.259	275.89	161.675	366.42
57.420	171.36	109.186	279.25	163.754	369.77
59.343	176.50	111.091	282.52	165.852	373.09
61.265	181.43	113.000	285.98	167.946	376.78
63.188	186.37	114.951	289.80	170.029	380.18
65.115	191.01	116.956	293.40	172.101	382.95
67.021	195.53	119.027	296.66	174.163	386.78
68.977	199.93	121.126	300.11	176.253	389.79
70.943	204.31	123.205	303.70	178.315	393.34
72.893	208.75	125.277	307.22	180.366	396.39
74.886	213.05	127.345	310.83	182.408	399.52
76.881	217.27	129.396	314.17	184.441	402.81
78.827	221.48	131.429	317.70	186.465	406.15
80.730	225.55	133.447	320.67	188.481	409.40
82.593	229.52	135.448	324.01	190.488	412.85
84.420	233.03	137.436	327.20	192.559	416.14
86.213	236.56	139.409	330.33	194.692	419.56
87.976	240.22	141.404	333.76	196.815	423.05
89.754	243.50	143.443	337.29	198.930	426.99

Table 2–7. (continued).

T / K	Cp / $JK^{-1}mol^{-1}$	T / K	Cp / $JK^{-1}mol^{-1}$	T / K	Cp / $JK^{-1}mol^{-1}$
201.037	429.88	270.277	570.21	317.285	5468.61
203.135	433.91	272.296	576.88	317.487	6785.33
205.224	437.24	274.341	582.27	317.644	10108.00
207.306	441.28	276.377	588.95	317.779	9213.68
209.380	444.79	278.410	596.29	317.941	6805.21
211.446	448.19	280.438	603.03	318.168	4223.28
213.504	451.76	282.455	610.25	318.597	1294.98
215.555	455.21	284.461	617.68	319.264	759.56
217.599	458.73	286.457	625.45	320.027	678.34
219.637	462.62	288.440	634.24	320.902	673.61
221.667	466.30	290.410	643.07	321.898	669.50
223.690	470.04	292.366	653.92	322.920	667.08
225.706	473.92	294.311	662.32	323.942	666.57
227.715	477.49	296.251	672.45	324.963	667.74
229.717	481.39	298.180	685.85	326.058	667.82
231.712	485.11	300.096	697.91	327.302	669.44
233.700	488.67	301.996	711.70	328.705	671.07
235.682	492.30	303.881	727.88	330.187	672.16
237.656	496.35	305.750	745.92	331.755	673.73
239.624	500.33	307.599	767.48	333.410	675.88
241.656	504.26	308.975	784.49	335.155	677.05
243.750	508.09	309.883	800.03	337.044	679.22
245.836	512.28	310.784	816.12	339.025	681.89
247.914	516.90	311.677	833.35	341.044	684.60
249.986	520.91	312.561	856.23	343.058	687.25
252.049	525.38	313.435	884.40	345.069	689.07
254.105	530.30	314.290	935.98	347.078	691.69
256.154	534.88	315.037	1068.05	349.082	694.71
258.194	539.57	315.635	1461.73	351.083	696.29
260.227	544.62	316.121	2288.88	353.081	699.62
262.253	548.89	316.496	3245.82	355.075	701.76
264.271	554.23	316.799	4123.03	357.082	703.84
266.281	559.85	317.056	4984.47	359.104	707.00
268.283	564.99				

Table 2–8. Molar heat capacity of $[Ni(dieten)_2](BF_4)_2$ (relative molecular mass: 464.712).

$\frac{T}{K}$	$\frac{Cp}{JK^{-1}mol^{-1}}$	$\frac{T}{K}$	$\frac{Cp}{JK^{-1}mol^{-1}}$	$\frac{T}{K}$	$\frac{Cp}{JK^{-1}mol^{-1}}$
		Series 1			
87.365	230.38	154.832	353.33	226.250	472.02
89.396	234.36	157.150	356.61	228.671	476.39
91.387	238.26	159.452	361.06	231.150	480.75
93.342	242.21	161.737	365.07	233.616	484.91
95.263	246.13	164.006	368.84	236.071	489.58
97.153	249.77	166.259	372.72	238.515	494.22
99.105	253.54	168.578	376.20	240.948	498.30
101.119	257.39	170.960	380.41	243.370	502.29
103.102	261.30	173.386	384.46	245.783	506.39
105.057	265.01	175.852	388.28	248.184	510.79
106.986	268.58	178.302	392.38	250.575	514.88
108.890	272.19	180.738	396.41	252.957	519.81
110.854	275.90	183.159	400.17	255.329	523.80
112.880	279.55	185.565	404.06	257.775	528.28
114.963	283.21	187.957	408.08	260.292	532.19
117.103	286.90	190.335	412.23	262.796	537.10
119.299	290.97	192.701	416.10	265.288	542.27
121.549	295.23	195.053	419.83	267.766	547.06
123.772	299.41	197.393	423.54	270.229	552.58
125.972	303.23	199.720	427.66	272.677	557.32
128.148	307.01	202.118	431.64	275.114	563.13
130.509	311.09	204.586	435.73	277.545	567.64
133.051	315.35	207.041	439.60	279.971	572.85
135.564	319.84	209.483	443.65	282.389	577.70
138.052	324.18	211.913	447.74	284.795	583.44
140.514	328.51	214.331	451.75	287.185	588.34
142.953	332.79	216.738	455.53	289.551	593.63
145.370	337.13	219.133	459.36	291.884	598.95
147.765	341.31	221.516	463.18	294.214	604.36
150.140	345.33	223.889	467.36	296.560	609.93
152.495	349.48				
		Series 2			
23.649	61.35	32.283	92.16	45.026	131.78
24.311	64.42	33.764	97.91	46.773	136.81
25.136	67.70	35.302	102.08	48.424	141.51
26.115	70.51	36.822	107.66	50.056	145.78
27.183	74.15	38.313	112.03	51.733	150.27
28.335	79.51	39.884	116.55	53.451	154.78
29.575	82.26	41.530	121.71	55.149	159.54
30.886	89.60	43.245	126.32	56.890	163.34

Table 2–8. (continued).

T / K	Cp / JK^{-1}mol^{-1}	T / K	Cp / JK^{-1}mol^{-1}	T / K	Cp / JK^{-1}mol^{-1}
58.728	168.05	75.507	206.42	89.642	235.03
60.618	172.39	77.537	210.77	91.565	238.81
62.602	176.86	79.514	214.81	93.454	242.46
64.713	182.17	81.549	219.06	95.311	246.20
66.849	187.11	83.640	223.38	97.139	249.71
69.033	192.21	85.683	227.14	98.939	253.26
71.263	197.05	87.683	231.17	100.715	256.67
73.418	201.89				
		Series 3			
13.680	22.72	19.820	49.37	26.152	70.03
14.579	26.15	20.499	51.88	27.182	72.85
15.433	30.22	21.191	55.48	28.282	77.53
16.242	33.44	21.900	56.74	29.454	80.66
17.033	37.00	22.640	59.77	30.688	86.35
17.792	39.09	23.434	62.54	32.000	89.65
18.489	44.25	24.279	63.79	33.379	95.63
19.152	46.79	25.182	66.68	34.818	101.49
		Series 4			
231.283	480.64	287.178	588.33	339.539	738.35
233.745	485.45	289.537	593.60	341.707	747.12
236.194	489.98	291.865	598.91	343.866	755.62
238.633	494.48	294.190	604.31	346.011	764.42
241.061	498.49	296.532	609.86	348.145	774.91
243.477	502.79	298.873	615.54	350.267	785.07
245.883	506.87	301.204	621.33	352.376	795.89
248.279	511.19	303.528	627.38	354.471	807.65
250.664	515.13	305.847	633.73	356.552	821.29
253.038	520.01	308.158	640.44	358.618	835.99
255.403	524.29	310.461	647.05	360.668	851.55
257.840	528.57	312.754	653.37	362.161	863.39
260.349	532.76	315.039	659.22	363.105	872.49
262.847	537.43	317.314	665.01	364.045	880.43
265.331	542.40	319.577	672.43	364.980	890.29
267.803	547.16	321.833	679.42	365.910	903.44
270.259	552.32	324.078	685.59	366.835	917.03
272.702	557.33	326.316	693.06	367.752	932.24
275.133	563.01	328.545	700.43	368.416	952.36
277.560	567.38	330.764	708.38	368.832	954.29
279.980	572.65	332.971	715.55	369.244	964.17
282.393	577.14	335.170	722.79	369.771	976.94
284.793	583.21	337.359	730.41	370.409	1001.39

Table 2–8. (continued).

T / K	Cp / JK^{-1}mol^{-1}	T / K	Cp / JK^{-1}mol^{-1}	T / K	Cp / JK^{-1}mol^{-1}
371.040	1030.20	375.083	7722.27	382.525	712.29
371.682	1056.95	375.344	2811.34	383.279	714.10
372.329	1125.47	375.843	1063.52	384.032	713.69
372.944	1270.13	376.520	817.65	385.403	717.29
373.501	1640.15	377.252	729.33	387.388	718.39
373.954	2531.93	378.001	720.96	389.369	720.28
374.286	4028.11	378.753	717.96	391.347	722.56
374.516	6665.78	379.507	714.35	393.323	724.56
374.668	10799.60	380.261	713.21	395.294	726.93
374.775	14360.20	381.016	713.16	397.263	729.34
374.863	16125.10	381.770	713.38	399.228	731.41
374.953	13743.70				
		Series 5			
302.479	624.16	361.285	855.24	378.060	717.45
304.805	629.88	362.234	862.67	378.810	718.02
307.124	636.10	363.179	872.53	379.563	713.63
309.436	642.60	364.119	882.05	380.317	711.90
311.739	649.03	365.054	892.97	381.071	711.68
314.032	654.81	365.984	904.79	381.826	710.55
316.316	660.95	366.909	918.77	382.580	711.26
318.590	667.96	367.827	933.66	383.334	712.27
320.854	675.13	368.737	953.64	384.087	712.85
323.107	681.94	369.639	974.86	385.216	712.75
325.350	689.31	370.529	1006.56	386.719	714.63
327.584	696.71	371.405	1052.20	388.222	716.23
329.807	704.47	372.256	1136.44	389.723	717.20
332.021	712.14	373.053	1377.68	391.221	718.86
334.224	720.17	373.703	2397.18	392.718	721.07
336.417	727.41	374.107	4887.52	394.213	722.33
338.599	735.32	374.319	7272.17	395.707	724.42
340.769	743.64	374.478	9396.33	397.199	725.05
342.929	752.32	374.604	12326.30	398.688	726.26
345.078	761.19	374.705	14932.10	400.416	729.44
347.216	770.38	374.798	14911.30	402.380	732.77
349.345	780.52	374.916	9186.57	404.342	735.98
351.461	790.20	375.214	2115.37	406.296	738.35
353.564	801.43	375.811	805.26	408.248	739.94
355.653	814.51	376.560	726.32	410.209	743.94
357.727	828.11	377.309	721.08	412.302	747.15
359.785	844.25				

Table 2–8. (continued).

T / K	Cp / JK^{-1}mol^{-1}	T / K	Cp / JK^{-1}mol^{-1}	T / K	Cp / JK^{-1}mol^{-1}
		Series 6			
383.383	714.91	393.290	723.25	403.122	733.68
385.866	716.61	395.756	725.33	405.566	737.06
388.345	718.14	398.216	728.39	408.004	740.61
390.819	720.15	400.672	731.12	410.436	743.14

Table 2-9. Molar heat capacity of $[Ni(dieten)_2](ClO_4)_2$ (relative molecular mass: 494.860).

$\frac{T}{K}$	$\frac{Cp}{JK^{-1}mol^{-1}}$	$\frac{T}{K}$	$\frac{Cp}{JK^{-1}mol^{-1}}$	$\frac{T}{K}$	$\frac{Cp}{JK^{-1}mol^{-1}}$
		Series 1			
15.672	26.47	34.407	96.31	58.489	168.34
16.431	27.23	35.735	100.83	60.340	172.78
17.285	30.62	37.067	105.30	62.121	177.10
18.134	34.10	38.433	109.86	63.841	181.34
18.997	39.26	39.816	114.14	65.508	185.14
20.978	46.44	41.212	119.46	67.192	188.67
22.067	50.94	42.640	123.56	68.956	193.26
23.208	54.25	44.122	128.11	70.735	197.86
24.383	58.97	45.681	132.67	72.467	201.72
25.579	63.66	47.336	137.81	74.155	204.71
26.832	68.67	49.076	142.94	75.862	208.31
28.033	73.06	50.883	148.02	77.662	211.76
29.178	76.97	52.740	153.06	79.547	215.31
30.397	82.01	54.624	158.24	81.499	219.67
31.701	86.46	56.559	163.20	83.462	223.43
33.052	91.66				
		Series 2			
85.386	227.67	108.805	271.11	130.213	307.69
87.271	231.19	110.544	273.97	131.772	309.83
89.120	234.65	112.264	276.97	133.404	312.47
90.937	238.13	113.968	280.01	135.110	315.50
92.724	241.45	115.655	282.92	136.908	318.36
94.483	244.89	117.326	285.80	138.795	321.36
96.264	248.55	118.983	288.60	140.719	324.56
98.067	251.79	120.625	291.36	142.683	327.69
99.845	255.26	122.253	294.19	144.633	330.87
101.646	258.33	123.869	296.72	146.570	333.82
103.468	261.84	125.473	299.23	148.493	337.09
105.269	265.70	127.064	302.13	150.404	340.26
107.047	268.40	128.644	304.92		
		Series 3			
152.304	342.87	165.234	364.11	178.366	384.50
154.185	346.50	167.040	366.81	180.301	388.19
156.053	348.63	168.837	369.36	182.227	390.86
157.911	351.46	170.624	372.84	184.143	393.63
159.756	355.29	172.501	375.71	186.050	397.02
161.592	358.39	174.466	378.81	187.949	399.96
163.418	361.42	176.421	381.60	189.838	402.68

Table 2–9. (continued).

T / K	Cp / JK^{-1}mol^{-1}	T / K	Cp / JK^{-1}mol^{-1}	T / K	Cp / JK^{-1}mol^{-1}
191.719	406.23	272.928	549.24	354.161	778.38
193.592	409.13	274.718	552.75	355.967	787.06
195.466	410.88	276.504	556.05	357.763	798.06
197.337	415.86	278.287	559.82	359.547	808.75
199.203	418.47	280.065	563.15	361.320	819.92
201.060	422.17	281.836	567.11	363.078	833.83
202.910	425.31	283.602	570.07	364.823	846.87
204.751	427.35	285.358	573.39	366.555	860.83
206.585	430.64	287.104	576.84	368.272	876.92
208.413	434.13	288.834	580.36	369.973	893.32
210.233	437.16	290.543	587.17	371.655	911.35
212.046	439.57	292.242	588.68	373.315	940.07
213.853	442.68	293.947	591.07	374.949	975.36
215.652	445.99	295.665	594.20	376.158	1007.21
217.446	448.80	297.386	598.64	376.951	1037.72
219.232	452.07	299.102	603.12	377.734	1076.10
221.059	455.06	300.814	606.78	378.501	1121.68
222.925	458.81	302.522	610.50	379.247	1206.70
224.787	461.35	304.227	613.78	379.951	1378.66
226.639	464.66	305.929	617.65	380.588	1742.98
228.486	467.91	307.628	621.57	381.027	2268.89
230.326	470.79	309.425	626.24	381.315	2803.55
232.160	473.67	311.323	632.14	381.575	3858.11
233.986	477.08	313.213	636.42	381.777	5428.68
235.806	480.59	315.096	641.89	381.932	7318.33
237.620	483.78	316.975	645.94	382.060	8475.08
239.427	486.68	318.845	650.97	382.186	7464.99
241.228	490.28	320.709	654.77	382.369	3810.61
243.023	492.98	322.567	659.94	382.668	1983.69
244.811	496.65	324.417	665.41	383.078	1413.39
246.599	500.46	326.261	671.02	383.554	1163.80
248.391	504.00	328.098	676.27	384.070	996.87
250.177	507.03	329.928	681.82	384.612	923.16
251.957	510.15	331.798	687.79	385.171	872.56
253.730	513.23	333.709	694.81	385.745	842.81
255.497	516.33	335.611	700.38	386.328	821.42
257.257	520.03	337.505	706.31	386.922	786.26
259.012	523.03	339.391	711.30	387.674	762.58
260.758	526.82	341.269	718.32	388.582	758.46
262.499	529.67	343.138	725.43	389.492	756.89
264.231	532.80	344.998	733.45	390.401	759.29
265.956	535.97	346.849	741.85	391.310	757.94
267.673	539.25	348.692	749.35	392.735	760.01
269.383	542.61	350.525	757.69	394.670	767.45
271.135	545.76	352.348	767.30	396.597	772.87

Table 2–9. (continued).

T / K	Cp / JK⁻¹mol⁻¹	T / K	Cp / JK⁻¹mol⁻¹	T / K	Cp / JK⁻¹mol⁻¹
398.518	781.94	404.261	765.86	410.050	769.99
400.430	787.13	406.190	762.96	411.976	773.37
402.340	780.43	408.122	764.33	413.898	777.20
		Series 4			
226.481	464.69	294.276	595.58	364.750	845.37
228.327	468.92	295.946	598.02	366.668	861.85
230.166	471.18	297.619	602.36	368.571	878.43
231.999	475.04	299.287	606.04	370.452	897.57
233.825	478.47	300.951	609.74	372.311	918.91
235.645	481.28	302.611	613.64	374.142	954.94
237.458	484.23	304.267	617.45	375.859	996.37
239.264	487.50	305.920	621.35	377.454	1057.40
241.064	490.73	307.569	625.39	378.621	1114.08
242.858	493.63	309.212	628.68	379.366	1199.73
244.646	497.12	310.854	631.39	380.067	1410.33
246.427	500.60	312.491	635.59	380.600	1781.68
248.203	504.05	314.125	638.87	380.971	2165.64
249.972	506.84	315.755	643.45	381.290	2833.35
251.735	510.26	317.429	647.82	381.548	3896.37
253.492	513.70	319.184	651.82	381.747	5603.66
255.242	517.22	320.973	656.89	381.896	7951.08
256.986	520.35	322.814	661.81	382.013	9307.98
258.724	523.87	324.706	667.70	382.124	9101.54
260.456	526.49	326.590	673.34	382.270	5215.14
262.179	530.07	328.466	678.70	382.539	2086.24
263.884	533.60	330.336	684.58	382.949	1353.77
265.568	537.38	332.198	690.44	383.446	1030.78
267.244	540.82	334.052	697.34	383.983	901.27
268.915	544.19	335.900	702.80	384.551	835.90
270.583	547.14	337.739	707.50	385.138	795.66
272.246	550.48	339.571	712.61	385.737	769.26
273.906	553.46	341.486	719.86	386.344	750.44
275.603	557.45	343.482	727.46	387.105	753.03
277.340	560.12	345.469	736.15	388.016	750.01
279.072	564.02	347.446	744.24	389.079	750.46
280.799	566.92	349.412	752.48	390.293	751.46
282.519	570.67	351.367	762.08	391.655	756.69
284.233	574.42	353.311	772.26	393.162	760.59
285.939	577.74	355.243	783.08	394.666	765.04
287.632	580.39	357.163	794.96	396.163	772.20
289.309	584.96	359.067	805.72	397.654	778.22
290.965	591.20	360.966	817.26	399.139	784.04
292.616	592.17	362.849	831.86	400.623	788.02

Table 2–9. (continued).

T / K	Cp / JK^{-1}mol^{-1}	T / K	Cp / JK^{-1}mol^{-1}	T / K	Cp / JK^{-1}mol^{-1}
402.106	785.47	409.591	764.99	415.580	771.46
403.595	770.40	411.090	765.89	417.075	772.26
405.092	764.35	412.588	767.55	418.568	776.76
406.592	763.55	414.085	769.68	420.036	778.99
408.092	764.03				
		Series 5			
390.896	754.61	401.385	789.55	411.882	768.82
392.410	758.68	402.874	776.40	413.383	768.09
393.918	763.80	404.372	764.86	414.887	769.80
395.419	770.20	405.875	762.34	416.389	772.08
396.917	775.40	407.379	762.64	417.892	771.36
398.411	782.33	408.882	763.76	419.390	778.13
399.900	788.06	410.385	764.45		

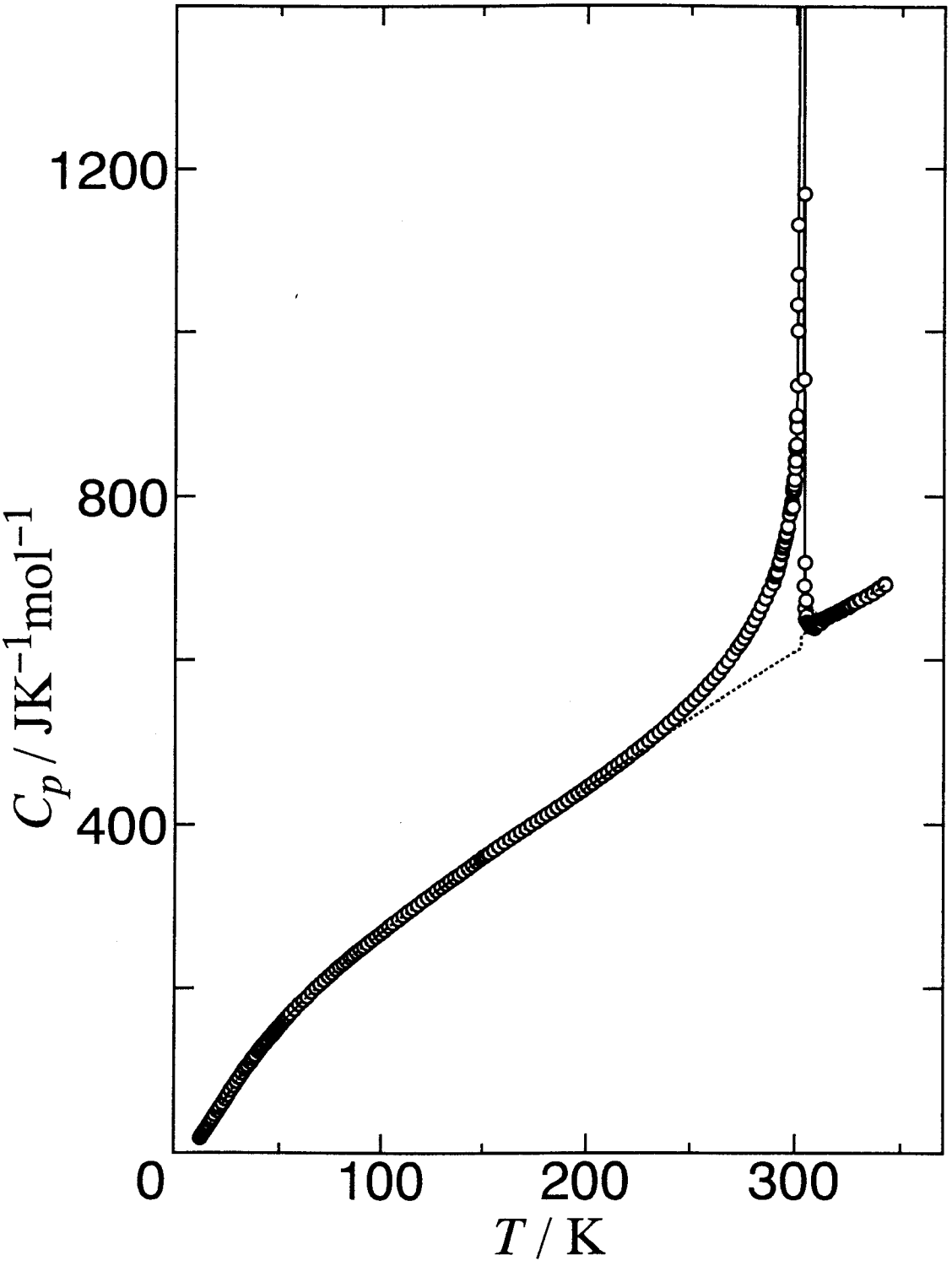

Fig. 2–3. Molar heat capacity of $[Cu(dieten)_2](BF_4)_2$ (relative molecular mass: 469.568). The doted curves indicate the calculated normal heat capacities.

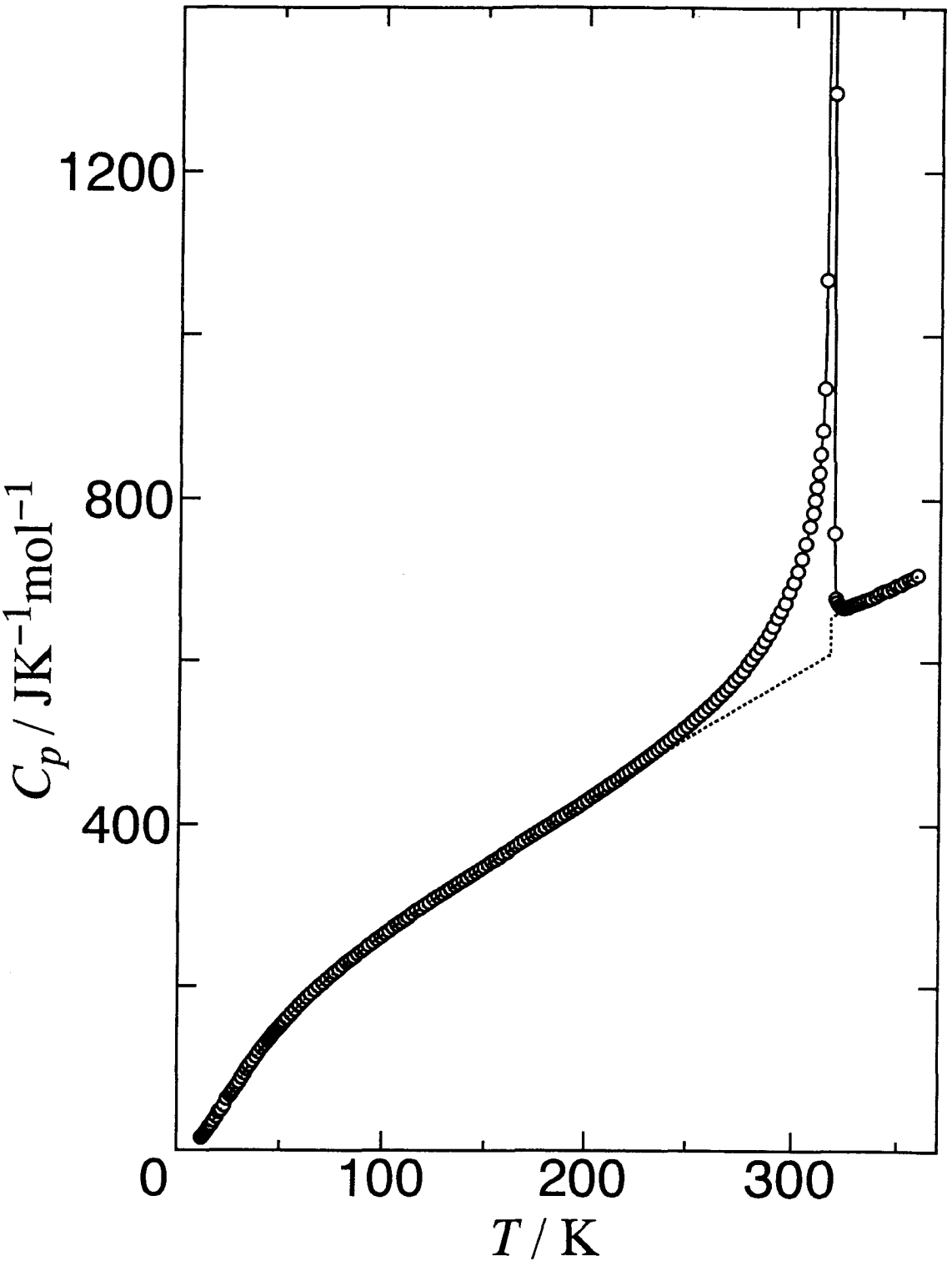

Fig. 2–4. Molar heat capacity of $[Cu(dieten)_2](ClO_4)_2$ (relative molecular mass: 494.860). The doted curves indicate the calculated normal heat capacities.

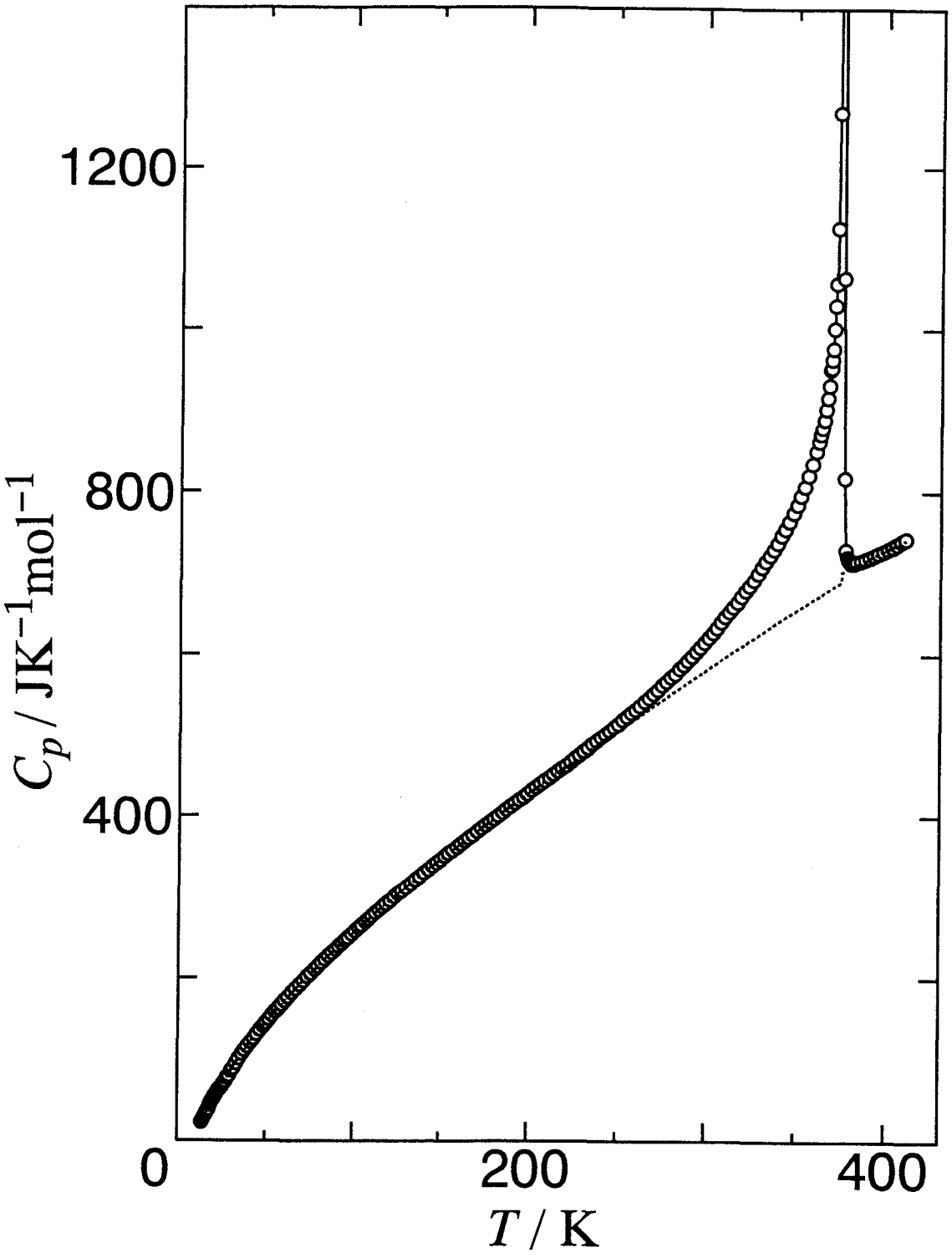

Fig. 2–5. Molar heat capacity of $[Ni(dieten)_2](BF_4)_2$ (relative molecular mass: 464.712). The doted curves indicate the calculated normal heat capacities.

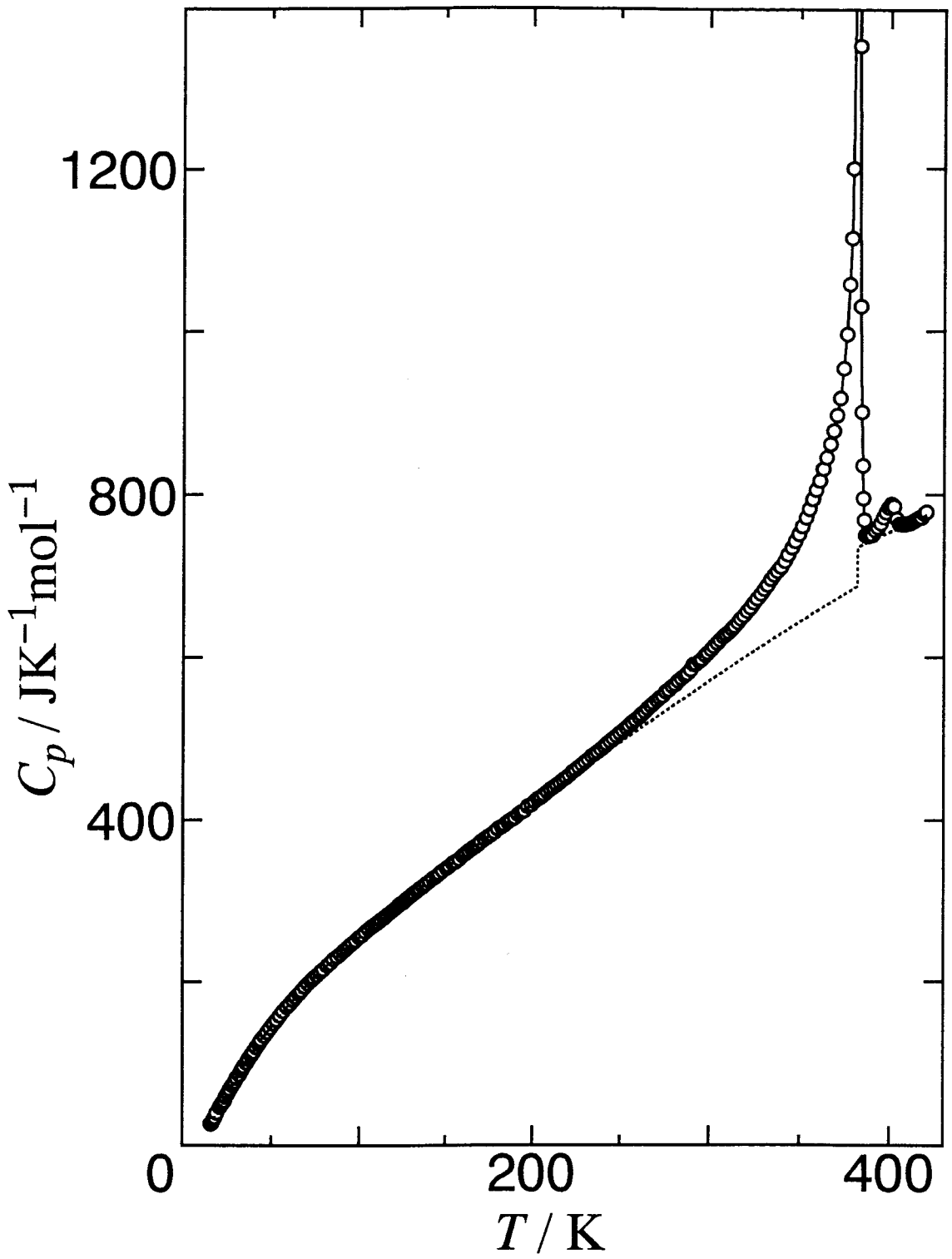

Fig. 2–6. Molar heat capacity of $[Ni(dieten)_2](ClO_4)_2$ (relative molecular mass: 494.860). The doted curves indicate the calculated normal heat capacities.

occurrence of this peak is not clear at present. An impurity effect is unlikely in view of the satisfactory chemical analysis. As this anomaly is very small, no discussion will be made on this anomaly in what follows (ΔH = 0.28 kJ mol^{-1} compared with 19.90 kJ mol^{-1} of the main peak).

The observed heat capacity is composed of two parts: one is the normal heat capacity due to the lattice and molecular vibrations and the other is the excess heat capacity due to the phase transition. In order to determine the thermodynamic quantities associated with the phase transition, normal heat capacities were estimated by using an effective frequency distribution method [14]. The intramolecular vibration frequencies necessary for this method were determined from the observed infrared spectra. The normal heat capacities of the low– and high–temperature phases were determined independently. The two curves did not meet at T_{trs}, resulting in a gap. The gaps of the normal heat capacities at T_{trs} are listed in Table 2–10. The normal heat capacities estimated by the procedure described above are shown by dotted curves in Figs 2–3 ~ 2–6. Subtraction of the normal heat capacities from the observed values gave the excess heat capacities, ΔC_p, due to the phase transition. The excess heat capacities are shown in Figs 2–7 ~ 2–10 as a function of temperature. A gradually increasing excess C_p tail extending below the transition temperature is clearly seen in these figures.

The enthalpy, $\Delta_{trs}H$, and the entropy of transition, $\Delta_{trs}S$, were determined by integration of ΔC_p with respect to T and ln T, respectively. The values of T_{trs}, $\Delta_{trs}H$ and $\Delta_{trs}S$ are listed in Table 2–11. There exist large differences in the transition temperatures from 302 to 382 K. However, the transition entropies are close to a constant values of 55 J K^{-1} mol^{-1}. This indicates that the same degree of disorder is involved in the process of phase transition from the low– to high–temperature phase in each complex.

DSC measurements have already been carried out by Fabbrizzi *et al.* [6].

Table 2–10. The gaps of the normal heat capacities at T_{trs}.

Complexes	T_{trs} / K	ΔC_p / J K^{-1} mol^{-1}
$[Cu(dieten)_2](BF_4)_2$	302.64	16
$[Cu(dieten)_2](ClO_4)_2$	317.64	46
$[Ni(dieten)_2](BF_4)_2$	374.86	12
$[Ni(dieten)_2](ClO_4)_2$	382.01	48

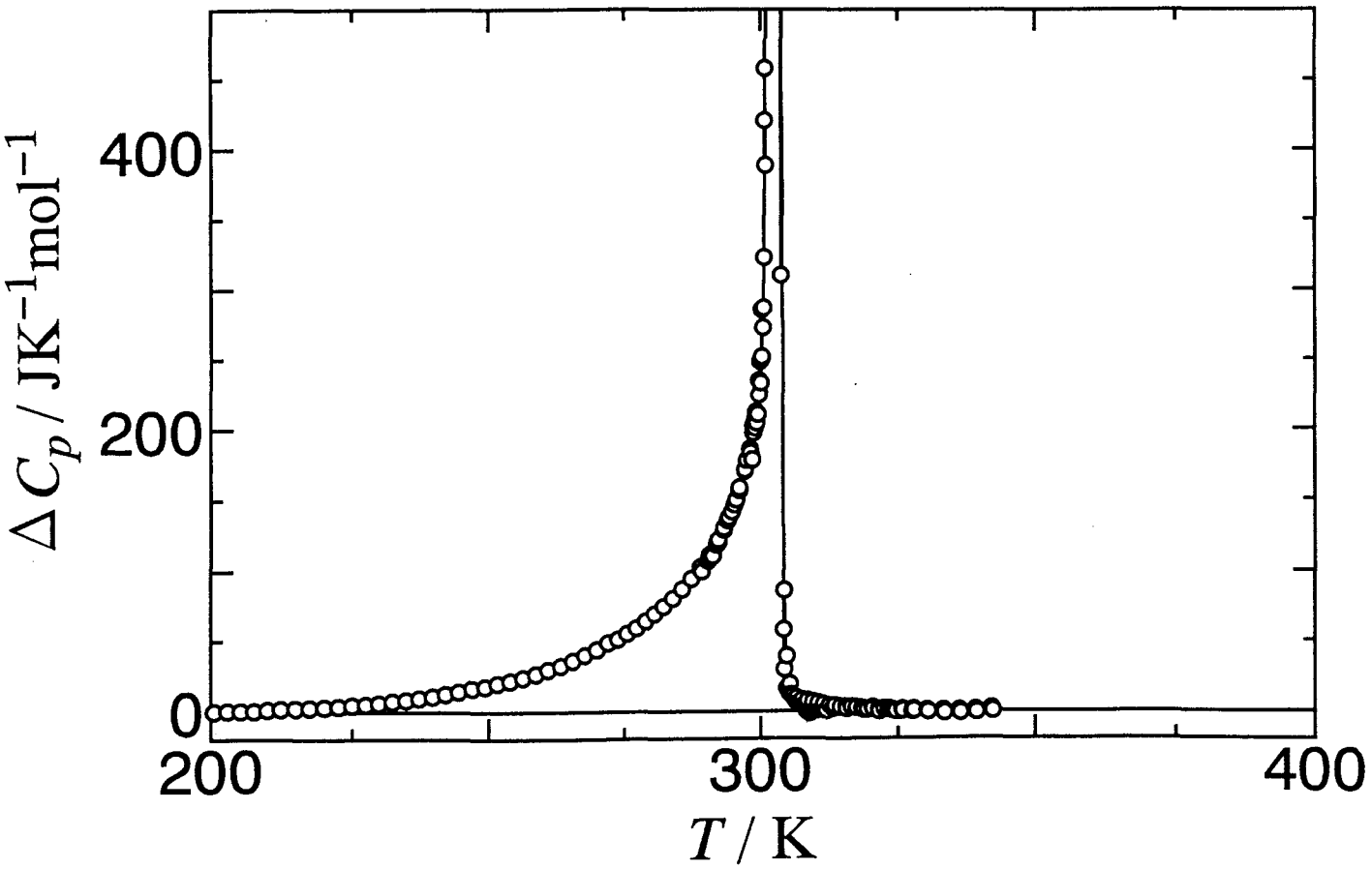

Fig. 2–7. Excess heat capacity of $[Cu(dieten)_2](BF_4)_2$.

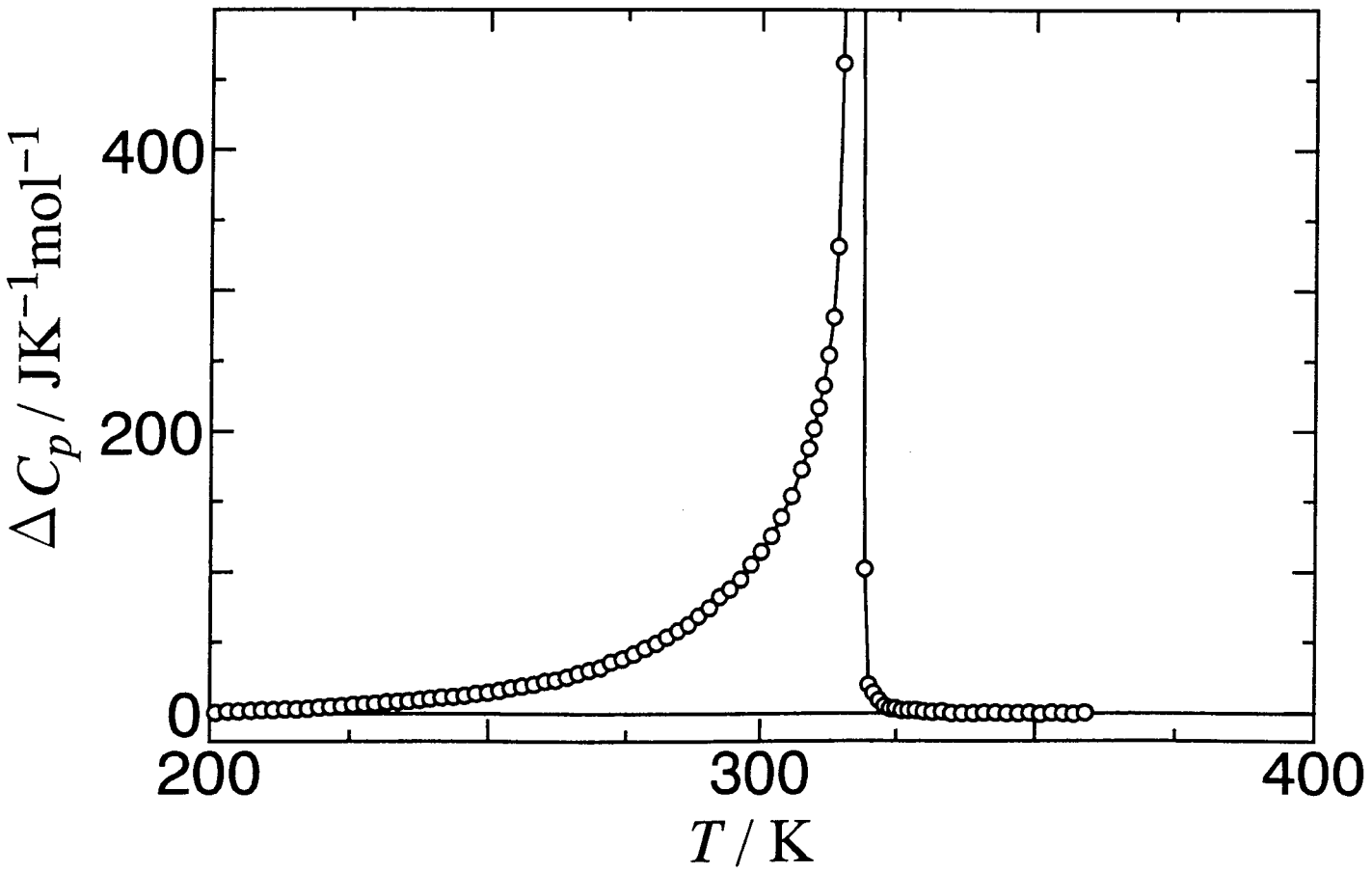

Fig. 2–8. Excess heat capacity of $[Cu(dieten)_2](ClO_4)_2$.

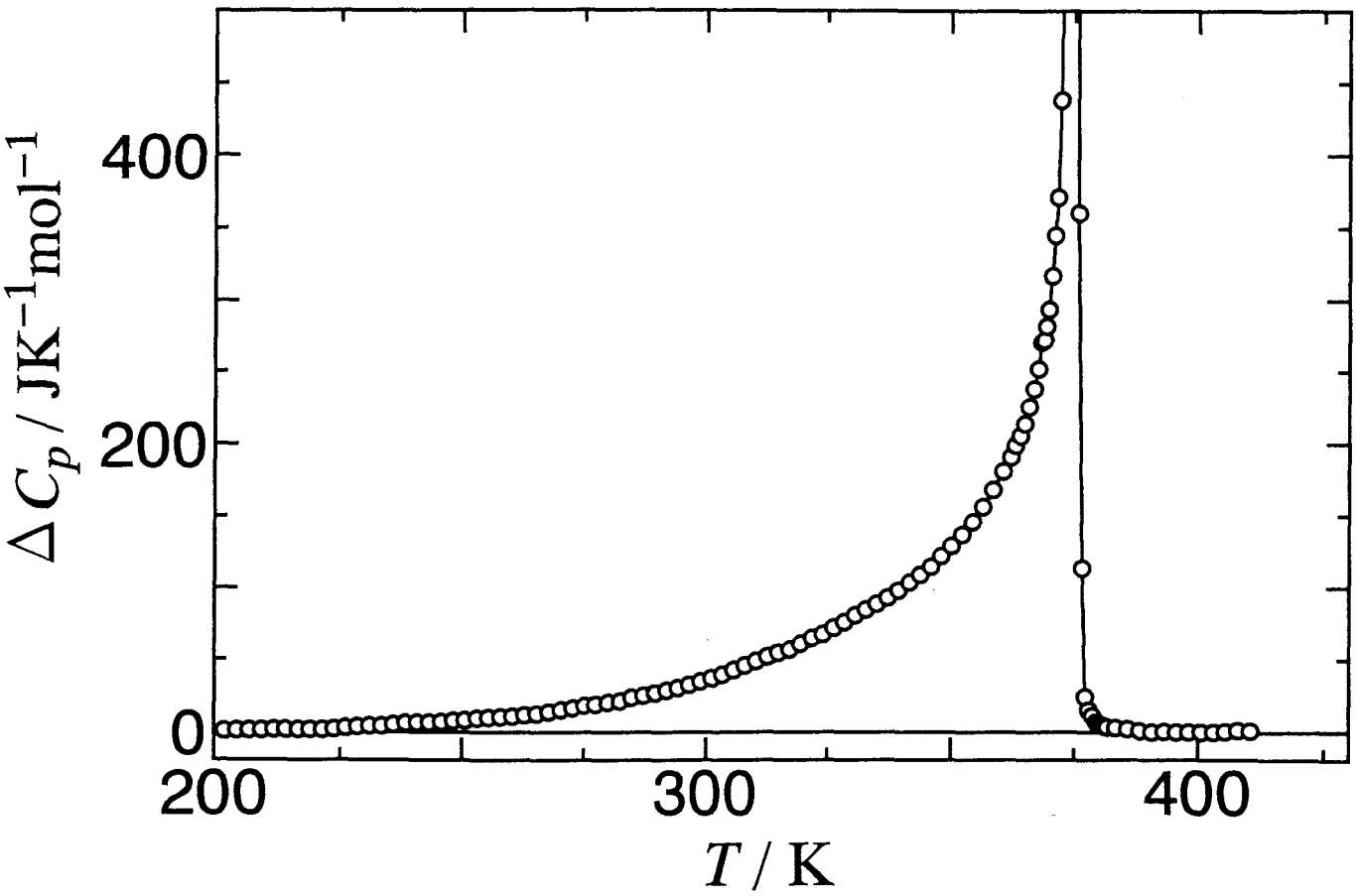

Fig. 2–9. Excess heat capacity of $[Ni(dieten)_2](BF_4)_2$.

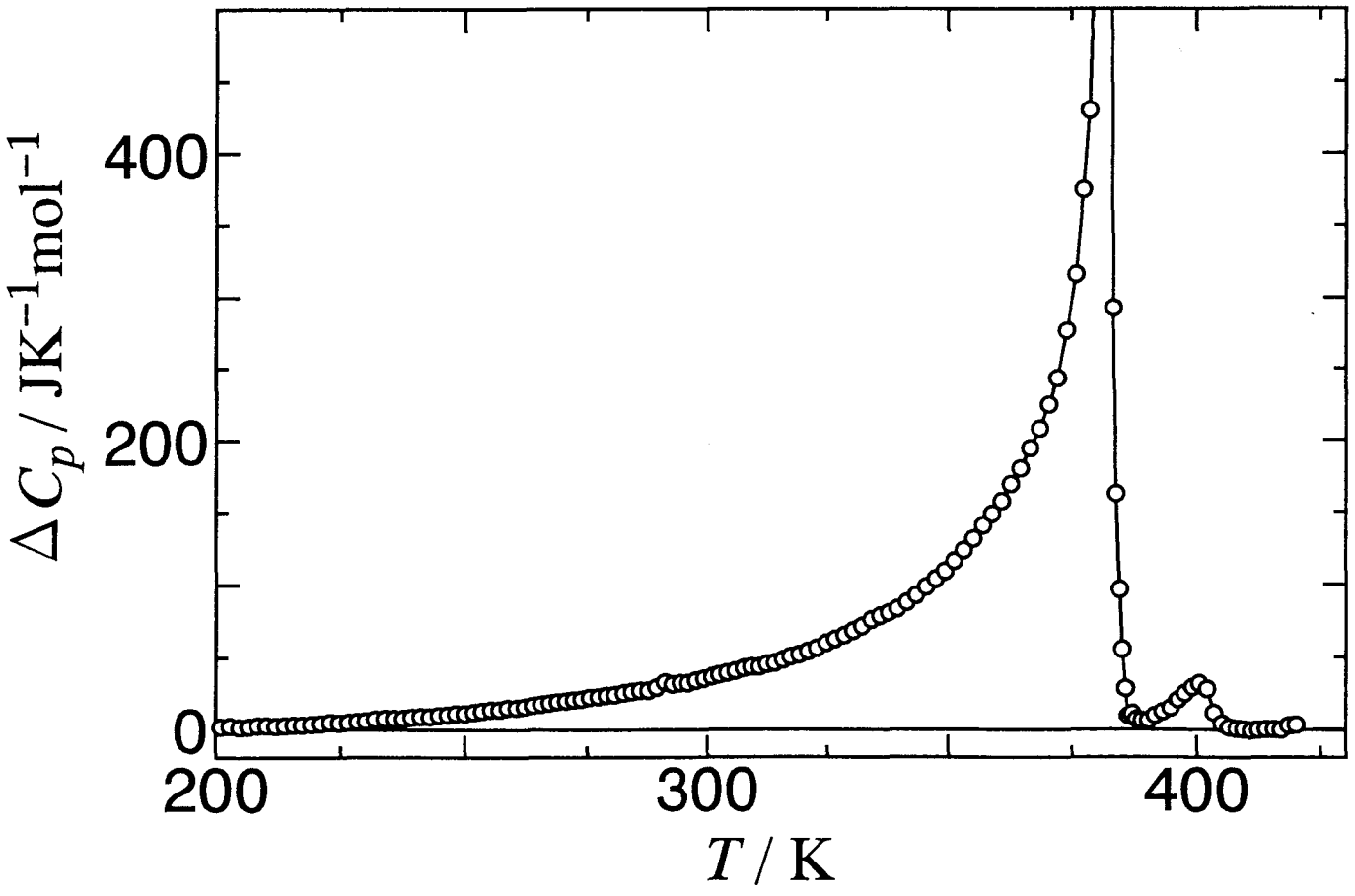

Fig. 2–10. Excess heat capacity of $[Ni(dieten)_2](ClO_4)_2$.

Table 2–11. Temperature, enthalpy and entropy of the phase transition of $[M(dieten)_2]X_2$ (M = Cu or Ni, X = BF_4 or ClO_4).

Complexes	T_{trs} / K	$\Delta_{trs}H$ / kJ mol^{-1}	$\Delta_{trs}S$ / J K^{-1} mol^{-1}
$[Cu(dieten)_2](BF_4)_2$	302.64	16.62	55.3
$[Cu(dieten)_2](ClO_4)_2$	317.64	17.43	55.2
$[Ni(dieten)_2](BF_4)_2$	374.86	20.85	57.4
$[Ni(dieten)_2](ClO_4)_2$	382.01	20.18	54.7

Their estimated values are given in Table 2–12. There are large differences between two sets of the data from DSC and the present adiabatic calorimetry. The difference between the results obtained by these two experiments may be attributed to the nature of this transition characterized by a long C_p tail at the low–temperature side of the phase transition. The DSC measurements seem to have failed in detecting the tail part.

Standard thermodynamic functions derived from the calorimetric data are given in the Table 2–13 ~ 2–16 for $[Cu(dieten)_2](BF_4)_2$, $[Cu(dieten)_2](ClO_4)_2$, $[Ni(dieten)_2](BF_4)_2$ and $[Ni(dieten)_2](ClO_4)_2$, respectively. For C_p values below 13 K, the effective frequency–distribution method was used for the extrapolation.

§2–5–3. Chelate Ring Puckering

Variable temperature crystal structures of $[Cu(dieten)_2](ClO_4)_2$ studied by Grenthe *et al.* [8] provide us with a useful clue to the molecular freedom responsible for the entropy gain. Their structural analysis has revealed that although there is no significant difference in the Cu–N distance, the conformation of the ligands is difference in the low– and high–temperature forms of the thermochromic compound. In the high–temperature form a thermally induced inversion of the conformation of the copper–ethylenediamine rings seems to be the origin of large atomic thermal parameters perpendicular to the ring system. The ring inversion also results in large atomic thermal parameters for the ethyl substituents. From these results it can be deduced that in each of the two different conformations of the Cu–dieten ring each ethyl group is interconverting between two or more positions. Thus, for $[Cu(dieten)_2]^{2+}$ each ethyl group gains two (or more) configurations for each of the two ring conformations for a total

Table 2–12. Comparison of the transition temperature and the enthalpy of transition measured between methods, differential scanning calorimeter [2] and adiabatic calorimeter [this work].

	DSC		Adiabatic Calorimeter	
Complexes	T_i / K	$\Delta_{trs}H$ / kJ mol^{-1}	T_{trs} / K	$\Delta_{trs}H$ / kJ mol^{-1}
$[Cu(dieten)_2](BF_4)_2$	288.15	10.04	302.64	16.62
$[Cu(dieten)_2](ClO_4)_2$	308.15	8.91	317.64	17.43
$[Ni(dieten)_2](BF_4)_2$	367.15	5.73	374.86	20.85
$[Ni(dieten)_2](ClO_4)_2$	383.15	6.65	382.01	20.18

T_i refers to the temperature at which the pen deflects from the base line.
T_{trs} refers to the temperature at which the ΔC_p takes the maximum value.

Table 2–13. Standard thermodynamic functions for $[Cu(dieten)_2](BF_4)_2$ in the unit of J K^{-1} mol^{-1}; the values in parentheses are extrapolated.

T/K	C_p°	S°	$(H^\circ-H_0^\circ)/T$	$-(G^\circ-H_0^\circ)/T$
5	(1.39)	(0.463)	(0.347)	(0.116)
10	(10.50)	(3.637)	(2.717)	(0.920)
15	27.94	11.012	8.071	2.941
20	47.74	21.765	15.530	6.235
30	87.55	48.735	32.983	15.752
40	123.43	78.944	51.203	27.741
50	153.65	109.790	68.718	41.073
60	181.52	140.371	85.297	55.075
70	205.57	170.154	100.768	69.386
80	227.90	199.068	115.257	83.811
90	247.88	227.058	128.879	98.179
100	267.37	254.192	141.766	112.426
110	286.78	280.582	154.068	126.515
120	305.23	306.326	165.898	140.428
130	323.47	331.472	177.306	154.166
140	340.72	356.071	188.361	167.709
150	358.71	380.180	199.099	181.081
160	375.75	403.838	209.581	194.256
170	392.96	427.137	219.861	207.276
180	409.78	450.076	229.945	220.131
190	427.10	472.685	239.857	232.829
200	444.68	495.042	249.663	245.379
210	462.91	517.171	259.377	257.794
220	481.60	539.137	269.054	270.083
230	501.34	560.974	278.718	282.256
240	523.25	582.767	288.443	294.324
250	547.25	604.611	298.310	306.301
260	573.81	626.577	308.379	318.198
270	605.62	648.804	318.778	330.026
280	645.27	671.508	329.689	341.819
290	698.79	695.064	341.473	353.591
300	847.31	720.753	355.365	365.388
		Phase transition at 302.64 K		
310	642.61	782.946	405.443	377.503
320	659.41	803.622	413.127	390.495
330	673.43	824.092	420.771	403.321
340	687.94	844.382	428.387	415.995
273.15	617.19	655.897	322.149	333.748
298.15	792.79	715.594	352.393	363.201

Table 2–14. Standard thermodynamic functions for $[Cu(dieten)_2](ClO_4)_2$ in the unit of J K^{-1} mol^{-1}; the values in parentheses are extrapolated.

T/K	C_p°	S°	$(H^\circ-H_0^\circ)/T$	$-(G^\circ-H_0^\circ)/T$
5	(1.46)	(0.488)	(0.366)	(0.122)
10	(10.48)	(3.746)	(2.787)	(0.959)
15	26.21	10.832	7.860	2.972
20	45.28	20.809	14.689	6.120
30	82.99	46.343	31.226	15.117
40	119.68	75.390	48.888	26.502
50	150.52	105.507	66.228	39.280
60	178.09	135.436	82.609	52.826
70	202.21	64.765	98.024	66.741
80	223.98	193.203	112.427	80.775
90	243.99	220.761	125.960	94.801
100	262.74	247.448	138.707	108.742
110	280.65	273.345	150.808	122.538
120	298.26	298.538	162.378	136.160
130	315.22	323.081	173.487	149.593
140	331.34	347.031	184.186	162.845
150	347.70	370.462	194.556	175.906
160	363.83	393.412	204.627	188.785
170	380.13	415.951	214.465	201.486
180	395.85	438.119	224.100	214.019
190	412.01	459.946	233.556	226.390
200	428.46	481.498	242.886	238.612
210	445.81	502.817	252.134	250.683
220	463.27	523.950	261.326	262.624
230	481.92	544.951	270.509	274.442
240	501.06	565.856	279.706	286.150
250	520.94	586.707	288.953	297.754
260	544.06	607.581	298.311	309.269
270	569.48	628.576	307.869	320.706
280	601.57	649.848	317.768	332.081
290	641.23	671.613	328.201	343.412
300	697.31	694.238	339.513	354.725
310	802.12	718.547	352.482	366.065
		Phase transition at 317.64 K		
320	681.22	778.412	401.886	376.526
330	672.03	799.019	410.002	389.017
340	683.20	819.237	417.862	401.375
350	695.43	839.219	425.620	413.600
273.15	579.13	635.238	310.941	324.297
298.15	685.64	689.960	337.329	352.632

Table 2–15. Standard thermodynamic functions for $[Ni(dieten)_2](BF_4)_2$ in the unit of J K^{-1} mol^{-1}; the values in parentheses are extrapolated.

T/K	C_p°	S°	$(H^\circ-H_0^\circ)/T$	$-(G^\circ-H_0^\circ)/T$
5	(1.46)	(0.488)	(0.366)	(0.122)
10	(11.04)	(3.831)	(2.862)	(0.970)
15	28.86	11.519	8.429	3.090
20	50.04	22.617	16.103	6.514
30	83.17	49.198	32.939	16.259
40	116.92	78.021	49.978	28.043
50	145.63	107.261	66.297	40.963
60	170.97	136.117	81.687	54.430
70	194.31	164.235	96.115	68.120
80	215.82	191.606	109.759	81.847
90	235.74	218.189	122.663	95.526
100	255.25	244.042	134.944	109.098
110	274.29	269.269	146.753	122.516
120	292.30	293.904	158.133	135.771
130	310.21	318.021	169.161	148.861
140	327.60	341.643	179.851	161.791
150	345.09	364.846	190.290	174.556
160	362.02	387.653	200.487	187.167
170	378.72	410.108	210.482	199.626
180	395.19	432.223	220.290	211.933
190	411.64	454.021	229.921	224.100
200	428.12	475.550	239.415	236.135
210	444.52	496.835	248.791	248.044
220	460.75	517.894	258.059	259.835
230	478.72	538.766	267.255	271.511
240	496.71	559.517	276.440	283.078
250	514.03	580.140	285.593	294.547
260	532.18	600.665	294.740	305.924
270	551.77	621.108	303.889	317.219
280	572.69	641.555	313.117	328.437
290	594.66	662.026	322.437	339.588
300	618.34	682.578	331.896	350.682
310	645.73	703.287	341.569	361.718
320	673.74	724.216	351.497	372.719
330	705.65	745.418	361.725	383.692
340	740.22	766.985	372.339	394.646
350	783.79	789.042	383.444	405.598
360	846.48	811.925	395.359	416.566
370	985.73	836.554	408.975	427.579
		Phase transition at 374.86 K		
380	713.61	886.729	448.826	437.903
390	719.48	905.325	455.676	449.649
400	730.37	923.675	462.405	461.270
410	742.69	941.859	469.089	472.770
273.15	558.37	626.546	306.784	320.761
298.15	613.79	678.768	330.136	348.635

Table 2-16. Standard thermodynamic functions for $[Ni(dieten)_2](ClO_4)_2$ in the unit of J K^{-1} mol^{-1}; the values in parentheses are extrapolated.

T/K	C_p°	S°	$(H^\circ-H_0^\circ)/T$	$-(G^\circ-H_0^\circ)/T$
5	(1.02)	(0.339)	(0.254)	(0.085)
10	(7.94)	(2.689)	(2.014)	(0.675)
15	(22.96)	(8.526)	(6.310)	(2.216)
20	42.89	17.743	12.909	4.834
30	80.37	42.147	29.074	13.073
40	114.84	70.129	46.336	23.793
50	145.53	99.161	63.192	35.970
60	171.96	128.085	79.182	48.903
70	195.96	156.383	94.128	62.254
80	216.32	183.922	108.178	75.744
90	236.34	210.592	121.329	89.263
100	255.52	236.484	133.797	102.687
110	273.07	261.691	145.686	116.005
120	290.31	286.195	157.022	129.173
130	307.31	310.093	167.921	142.172
140	323.36	333.446	178.442	155.004
150	339.59	356.305	188.642	167.663
160	355.70	378.714	198.558	180.155
170	371.62	400.757	208.269	192.488
180	387.61	422.446	217.785	204.660
190	402.98	443.812	227.126	216.686
200	420.06	464.908	236.333	228.574
210	436.78	485.803	245.479	240.324
220	453.32	506.492	254.536	251.956
230	470.85	527.024	263.556	263.467
240	488.82	547.456	272.579	274.877
250	506.90	567.777	281.593	286.184
260	525.80	588.036	290.630	297.406
270	546.11	608.263	299.718	308.545
280	565.58	628.476	308.865	319.611
290	587.56	648.676	318.067	330.609
300	607.62	668.924	327.374	341.549
310	629.98	689.224	336.787	352.437
320	654.13	709.591	346.311	363.280
330	683.52	730.162	356.079	374.083
340	714.24	751.038	366.176	384.862
350	755.37	772.317	376.690	395.627
360	811.38	794.351	387.955	406.396
370	892.97	817.616	400.425	417.190
380	1390.13	844.408	416.344	428.064
		Phase Transition at 382.01 K		
390	751.21	884.784	446.970	437.815
400	786.35	904.227	454.996	449.232
410	765.24	923.279	462.716	460.563
420	778.94	941.857	470.055	471.801
273.15	552.11	614.632	302.593	312.039
298.15	603.53	665.178	325.649	339.529

configurational count of $2^4 \cdot 2 \cdot 2 = 64$. The 2^4 factor reflects the fact that there are four ethyl groups, each being assumed to have two possible conformations to take at random, one 2 reflects the two conformations for each ring and the other 2 reflects the fact that there are two dieten groups on each $[Cu(dieten)_2]^{2+}$ cation. If this is the case, the entropy gain due to the $[Cu(dieten)_2]^{2+}$ cation amounts to R ln 64 = 34.58 J K^{-1} mol^{-1}. On the other hand, if the ethyl groups on each dieten ligand could gain access to more than two configurations per ring conformation, the entropy increment at the phase transition would become large. For example, if this member is 3, not 2, then the count for the cation is $3^4 \cdot 2 \cdot 2 = 324$ and the entropy gain is R ln 324 = 40.06 J K^{-1} mol^{-1}. Since the observed transition entropy (55 J K^{-1} mol^{-1}) is larger than these estimated values, additional sources contributing to the entropy gain are probably present. One possibility is the onset of motion of the counter anions. However, this possibility can be ruled out by the ^{19}F NMR data reported by Pylkki *et al.* [9]. For $[Cu(dieten)_2](BF_4)_2$, the second moment of ^{19}F NMR signal is 2.0 G^2 and shows no change at the transition. Thus the onset of dynamic disorder of BF_4^- anion is not involved in the phase transition.

The most striking change of structure through the phase transition is in the motion of the chelate rings. The chelate rings pucker up and down from the MN_4 plane in the high temperature phase. Assuming that this chelate ring puckering is a source of the large entropy of transition, we can estimate the enthalpy gain at the phase transition as follows. Let's assume that the chelate rings are static in the low-temperature phase but they begin to pucker at the transition point. There are two rings in a cation, and each of them consists of a five-membered ring, MN_2C_2 (M: metal ion). When the plane formed by MN_2 is fixed, the five-membered ring has four different configurations. Among them, two configurations in which two carbon atoms are tipped off to the same side of the plane and two configurations in which

two carbon atoms are tipped off to the opposite side of the plane. These modes are roughly approximated to the simple Einstein harmonic oscillator. The changes of thermodynamic quantities contributed by one oscillator at the transition point, T_{trs}, are evaluated by means of the following equations:

$$x = \frac{hc\tilde{\nu}}{kT_{trs}}, \tag{2-1}$$

$$\Delta C(x) = R\frac{x^2e^x}{(e^x - 1)^2}, \tag{2-2}$$

$$\Delta H(x) = RT_{trs}\frac{x}{e^x - 1}, \tag{2-3}$$

$$\Delta S(x) = R\{\frac{x}{e^x - 1} - \ln(1 - e^{-x})\}, \tag{2-4}$$

where, h, c, k and R are the Planck constant, speed of light, the Boltzmann constant and gas constant, respectively. $\tilde{\nu}$ is a wave number of the puckering motion. This puckering motion is assumed to be reasonable for the total entropy of transition. Then $\tilde{\nu}$ is calculated from the relation, $4\Delta S(x) = \Delta_{trs}S$. $\Delta_{trs}H$ and ΔC_p are similarly obtained from $\Delta H(x)$ and $\Delta C(x)$, respectively. The estimated values from the chelate ring puckering motion are shown in Table 2–17. $4\Delta C(x)$ corresponds to a heat capacity gap of between two base–lines at T_{trs}. The calculated gap, 33 J K^{-1} mol^{-1}, is nearly equal to the average value of the experimental data, about 30.3 J K^{-1} mol^{-1}. The contribution of the chelate ring puckering to the measured $\Delta_{trs}H$ is about 46 % for every sample.

Table 2–17. The estimated values, $\tilde{\nu}$, ΔH and ΔC_p, from the chelate ring puckering motion.

Complexes	$\tilde{\nu}$ / cm^{-1}	ΔC_p / J K^{-1} mol^{-1}	ΔH / kJ mol^{-1}
$[Cu(dieten)_2](BF_4)_2$	109	33	7.7
$[Cu(dieten)_2](ClO_4)_2$	115	33	8.0
$[Ni(dieten)_2](BF_4)_2$	127	33	9.9
$[Ni(dieten)_2](ClO_4)_2$	141	32	9.5

§2-5-4. Chesnut Model

As judged from the mean value of $\Delta_{trs}S$ (55.7 J K^{-1} mol^{-1} $\approx R$ ln 800), the present phase transitions involve a large change in the number of microscopic energy levels. This large phase transition effect can be divided into two parts; the discontinuous and gradual parts. The discontinuous part corresponds to the long the thermal relaxation time required for thermal equilibration after the energy input. The gradual part is characterized by the excess heat capacity and a normal relaxation time. The discontinuous region is easily determined from the temperature drift in the heat capacity measurement. The entropies due to the discontinuous and the gradual parts are given in Table 2-18. The higher the transition temperature, the smaller the discontinuous component in the entropy of transition is.

As discussed in the previous section, its main part obviously arises from the onset of motion in the cation involving the puckering of the copper-ligand ring and orientational disordering of the ethyl groups. In order to understand the transition behavior, the Chesnut exciton model [15] was applied to the present system. This simple phenomenological model was initially constructed to describe the gross aspects of the phase transition behavior in dense magnetic triplet exciton systems. The main feature of this model is a quadratic dependence of the free energy on the exciton density (exciton concentration); the presence of such a term is made plausible by considerations of exciton-exciton and exciton-lattice interactions. For the present non-magnetic system, the "exciton" may be replaced by the conformational excitation involved in the phase transition.

We assume that the excess entropy at T may be written as

$$\Delta S(\rho) = \rho\Delta_{trs}S - R\{\rho\ln\rho + (1-\rho)\ln(1-\rho)\}, \qquad (2\text{-}5)$$

Table 2–18. The comparison of the entropy of transition in terms of its thermal relaxation time. $\Delta_{trs}S$(dis) and $\Delta_{trs}S$(grad) indicate the discontinuous and gradual parts, respectively.

Complexes	T_{trs} / K	$\Delta_{trs}S$ / J K^{-1}mol^{-1}	$\Delta_{trs}S$(dis) / J K^{-1}mol^{-1}	$\Delta_{trs}S$(grad) / J K^{-1}mol^{-1}	$\Delta_{trs}S$(dis) / $\Delta_{trs}S$
$[Cu(dieten)_2](BF_4)_2$	302.64	55.3	40.2	15.1	0.73
$[Cu(dieten)_2](ClO_4)_2$	317.64	55.2	36.0	19.2	0.65
$[Ni(dieten)_2](BF_4)_2$	374.86	57.4	31.7	25.7	0.55
$[Ni(dieten)_2](ClO_4)_2$	382.01	54.7	19.6	35.1	0.36

where ρ represents the fraction of the molecules in the high–temperature phase at T. The free energy difference between the high– and low–temperature phase, ΔA, is written as

$$\Delta A = E_0\rho + E_1\rho^2/2 - T\Delta S(\rho), \qquad (2\text{–}6)$$

where E_0 represents the energy required to promote the system from the low– to high–temperature phase in the absence of any interactions and E_1 an effective interaction energy. At the transition temperature, T_{trs}, ρ changes isothermally from ρ_L to ρ_H. This model undergoes a phase transition occurring symmetrically about $\rho = ½$. ρ_L and ρ_H are related by $\rho_L + \rho_H = 1$ by definition. There exist some conditions at the phase transition point:

$$A(\rho_L) = A(\rho_H), \qquad (2\text{–}7)$$
$$\Delta A'(\rho_L) = \Delta A'(\rho_H) = 0, \qquad (2\text{–}8)$$
$$\Delta A''(\rho_L) > 0 \text{ and } \Delta A''(\rho_H) > 0, \qquad (2\text{–}9)$$

where $\Delta A'$ and $\Delta A''$ correspond to the first and second derivatives with respect to ρ. Then the following relations are obtained,

$$\Delta S(T_{trs}) = \Delta\rho\Delta_{trs}S, \qquad (2\text{–}10)$$
$$E_1 = -2(RT_{trs} / \Delta\rho)\ln\{(1 + \Delta\rho)/(1 - \Delta\rho)\}, \qquad (2\text{–}11)$$
$$T_{trs}\Delta_{trs}S = E_0 + E_1/2, \qquad (2\text{–}12)$$

where $\Delta\rho = \rho_H - \rho_L$. As described above, $\Delta S(T_{trs})$ is the first order component of the transition entropy. We calculated $\Delta\rho$, E_1 and E_0 from the experimental data. $\Delta\rho$, E_0 and E_1 are given in Table 2–19. ρ was determined by minimizing ΔA with respect to ρ. Assuming that the sample volume does not changes, we may neglect the PV term and equate the model values for $\Delta C_v(\rho)$, $\Delta S(\rho)$ and $\Delta U(\rho)$ to the experimental values of $\Delta C_p(T)$,

Table 2–19. The calculated Δρ, E_0 and E_1.

Complexes	T_{trs} / K	Δρ	E_0 / kJ mol^{-1}	E_1 / kJ mol^{-1}
$[Cu(dieten)_2](BF_4)_2$	302.64	0.73	23.13	−12.77
$[Cu(dieten)_2](ClO_4)_2$	317.64	0.65	23.85	−12.62
$[Ni(dieten)_2](BF_4)_2$	374.86	0.55	28.52	−14.04
$[Ni(dieten)_2](ClO_4)_2$	382.01	0.36	27.54	−13.29

$\Delta S(T)$ and $\Delta H(T)$ as follows:

$$\Delta C_p = \Delta C_v$$
$$= \frac{(E_0 + E_1\rho)^2}{T} \Big/ \left\{E_1 + \frac{RT}{\rho(1-\rho)}\right\}, \qquad (2\text{–}13)$$
$$\Delta S(T) = \Delta S(\rho), \qquad (2\text{–}14)$$
$$\Delta H(T) = \Delta U(\rho) = E_0\rho + E_1\rho^2/2, \qquad (2\text{–}15)$$

where Δ means the difference between the observed value and the estimated one which is determined from the base line of the low–temperature phase. The results are compared with the experimental values in Figs 2–11 ~ 2–14 for ΔC_p, Figs 2–15 ~ 2–18 for $\Delta_{trs}S$, Figs 2–19 ~ 2–22 for $\Delta_{trs}H$. In spite of the simplicity of the model, the Chesnut model accounts well for the thermochromic transition behavior of the present compounds, especially copper complexes. This fact implies that the attractive interaction term proportional to ρ^2 reasonably describes the present system and that the conformational change in the cation can be treated as "magnetic exciton".

§2–5–5. Angular Overlap Model (AOM)

According to the X–ray structural analysis of $[Cu(dieten)_2](ClO_4)_2$ [7,8], there is no significant change in the Cu–N distances, whereas the trans bond angles of N–Cu–N change slightly through the phase transition. In the low–temperature phase the angles are 180.0°, while in the high–temperature phase one is 178.0° and the other is 174.7°. The copper atom has a square–planar coordination geometry in the low–temperature phase. The geometry distorts slightly toward the tetrahedral coordination in the high–temperature phase. In spite of such a small geometrical change, the color of complexes changes

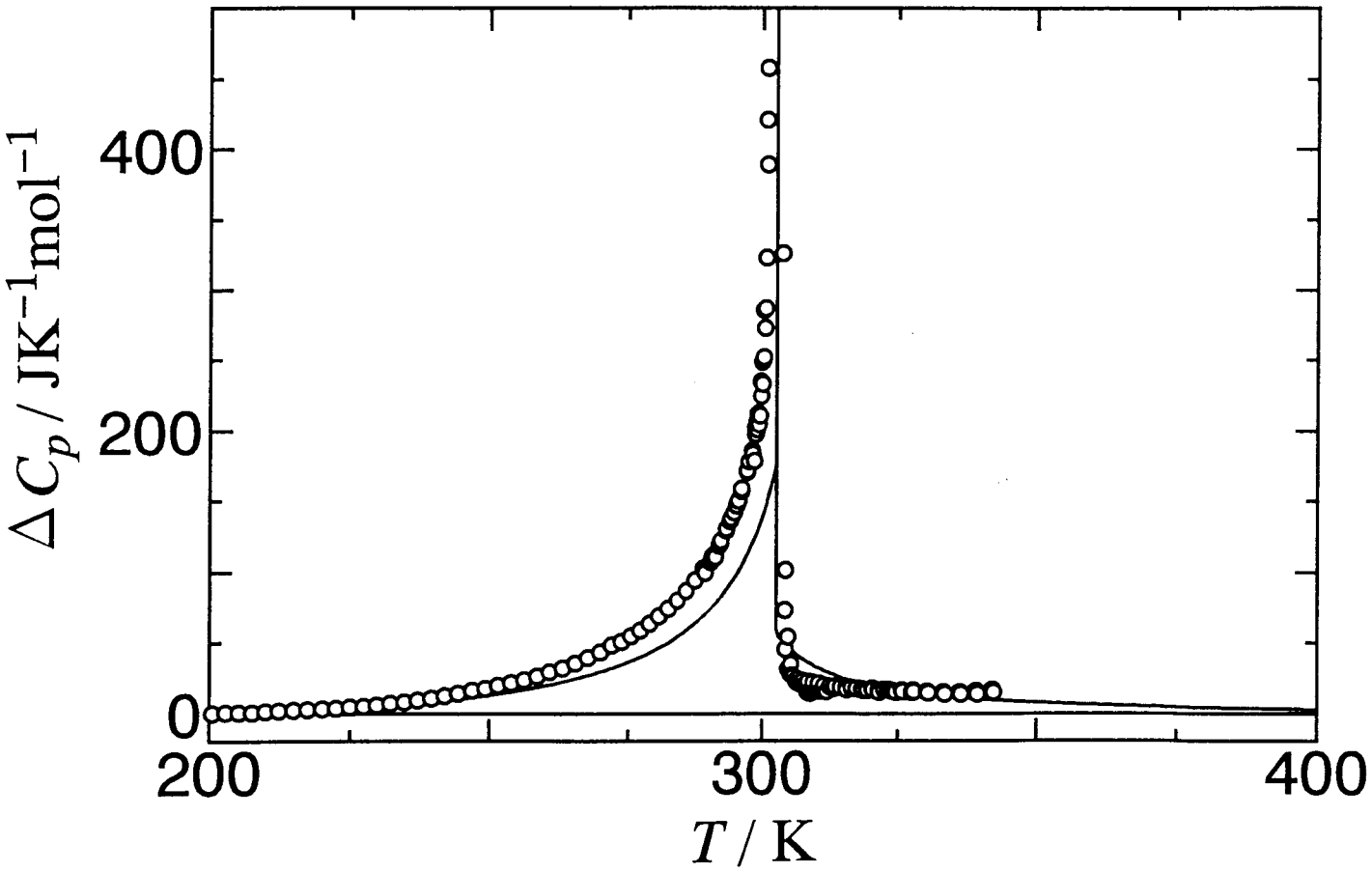

Fig. 2–11. Comparison of excess heat capacity of $[Cu(dieten)_2](BF_4)_2$. Open circles and solid line indicate the experimental and calculated values, respectively.

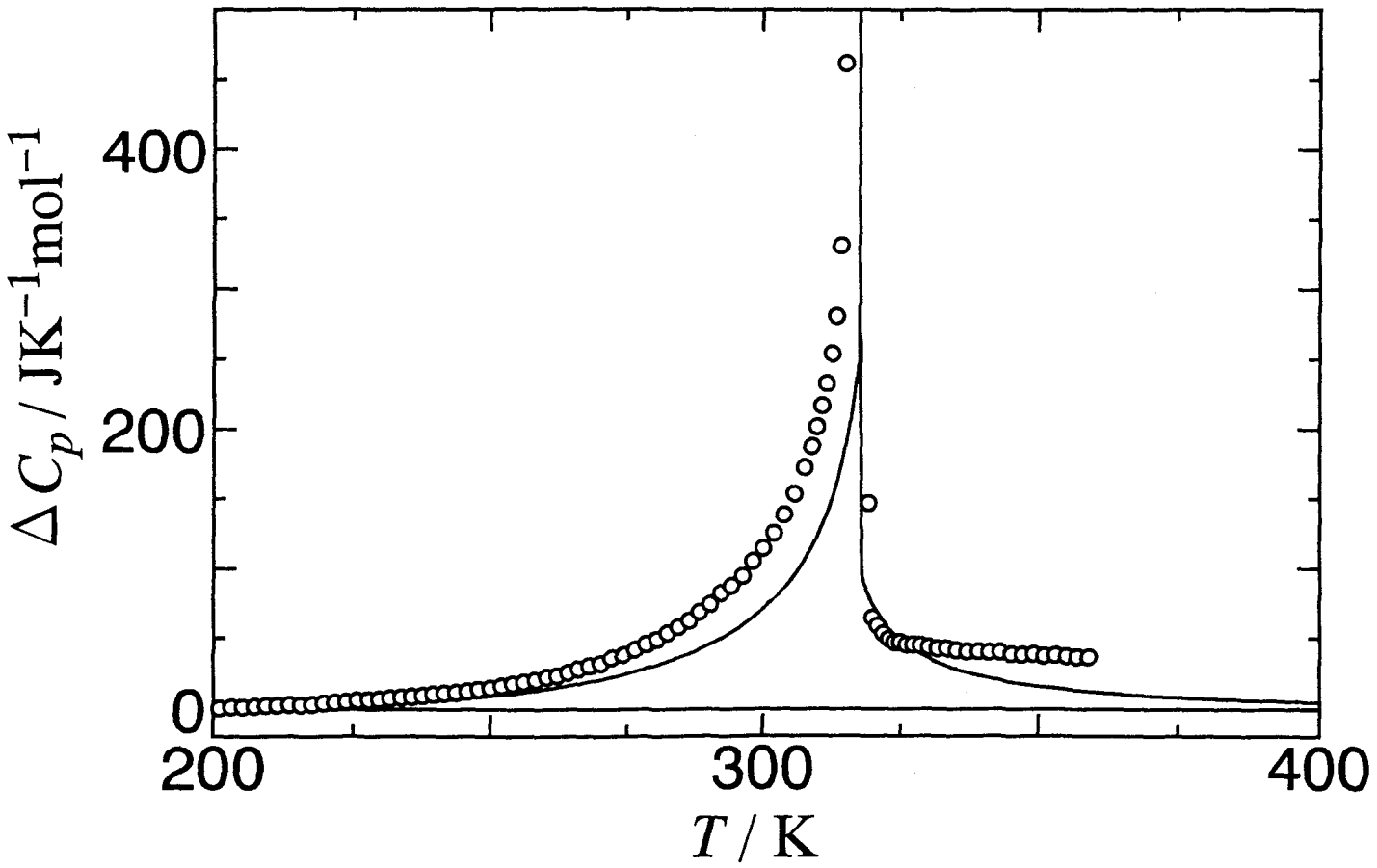

Fig. 2–12. Comparison of excess heat capacity of $[Cu(dieten)_2](ClO_4)_2$. Open circles and solid line indicate the experimental and calculated values, respectively.

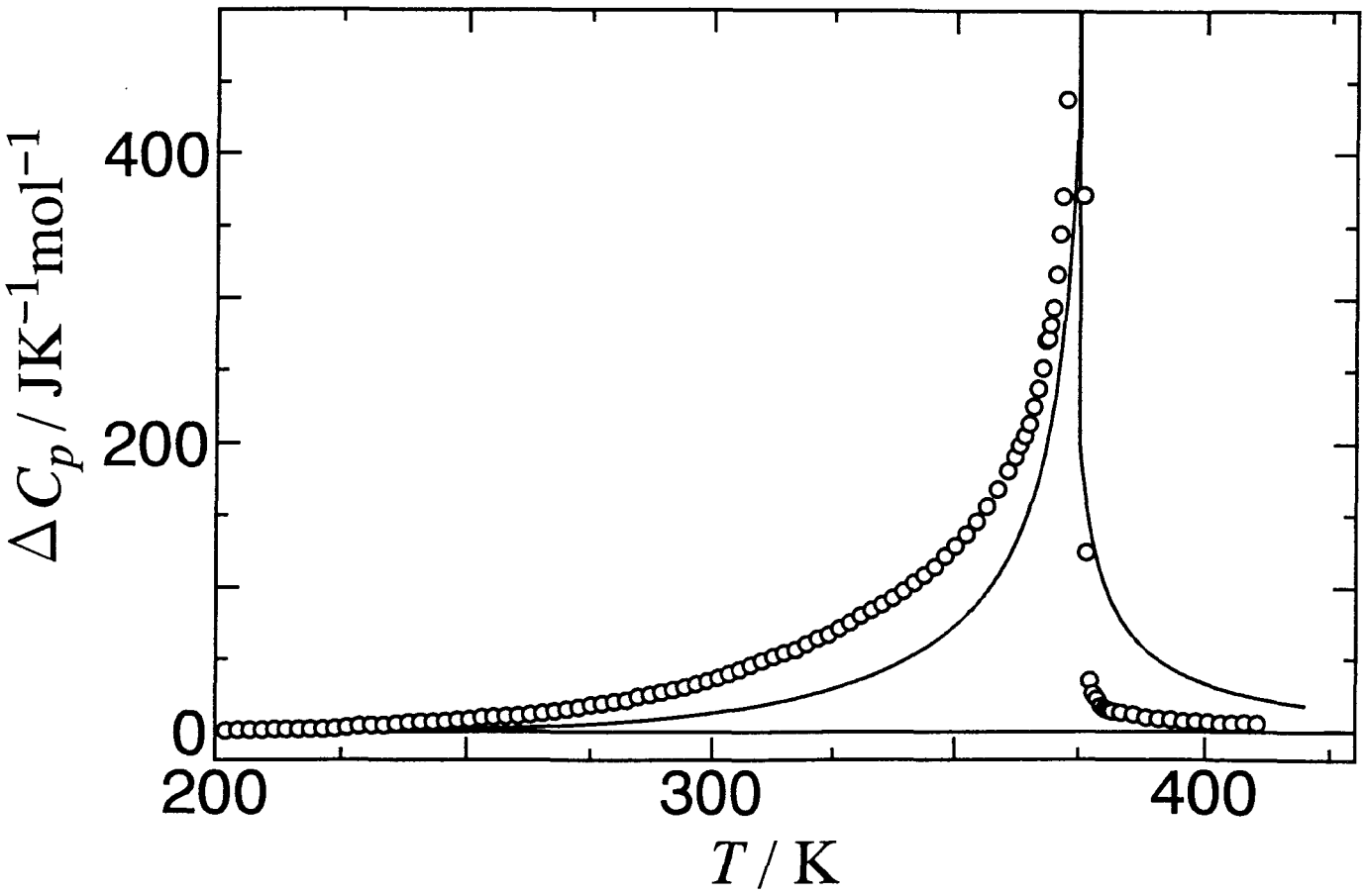

Fig. 2-13. Comparison of excess heat capacity of $[Ni(dieten)_2](BF_4)_2$. Open circles and solid line indicate the experimental and calculated values, respectively.

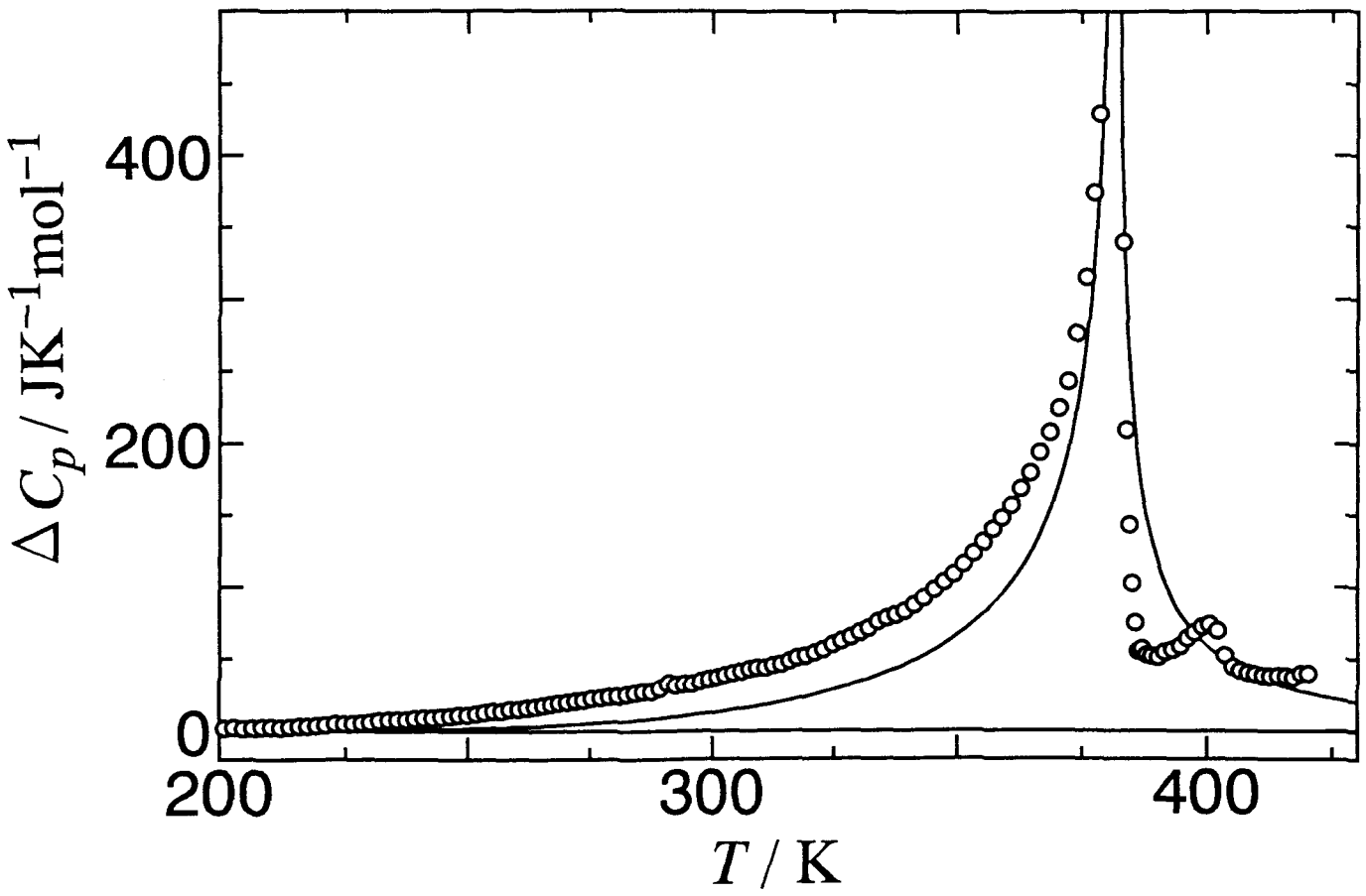

Fig. 2–14. Comparison of excess heat capacity of $[Ni(dieten)_2](ClO_4)_2$. Open circles and solid line indicate the experimental and calculated values, respectively.

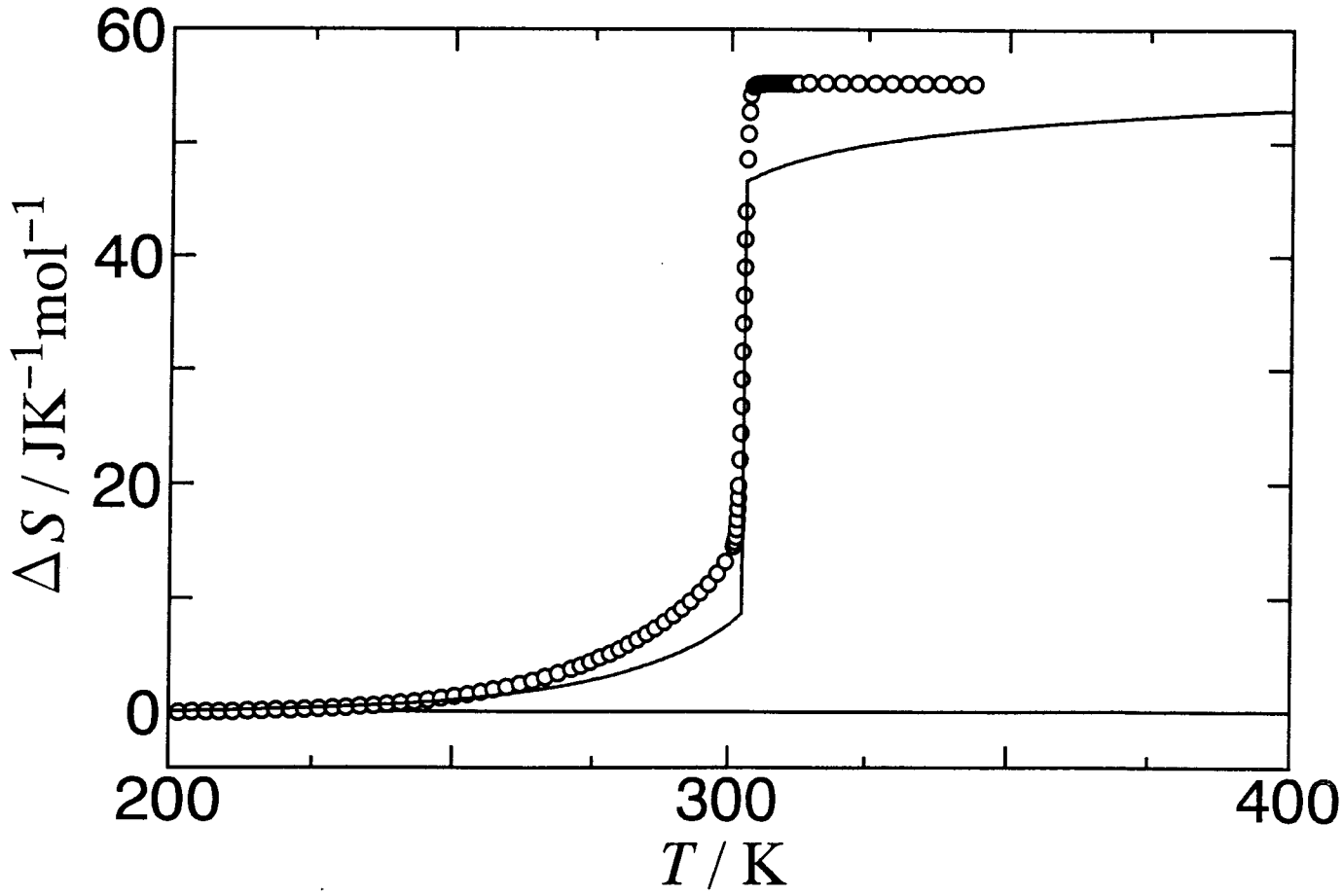

Fig. 2–15. Accumulated transition entropy of $[Cu(dieten)_2](BF_4)_2$ as a function of temperature. Open circles and solid line indicate the experimental and calculated values, respectively.

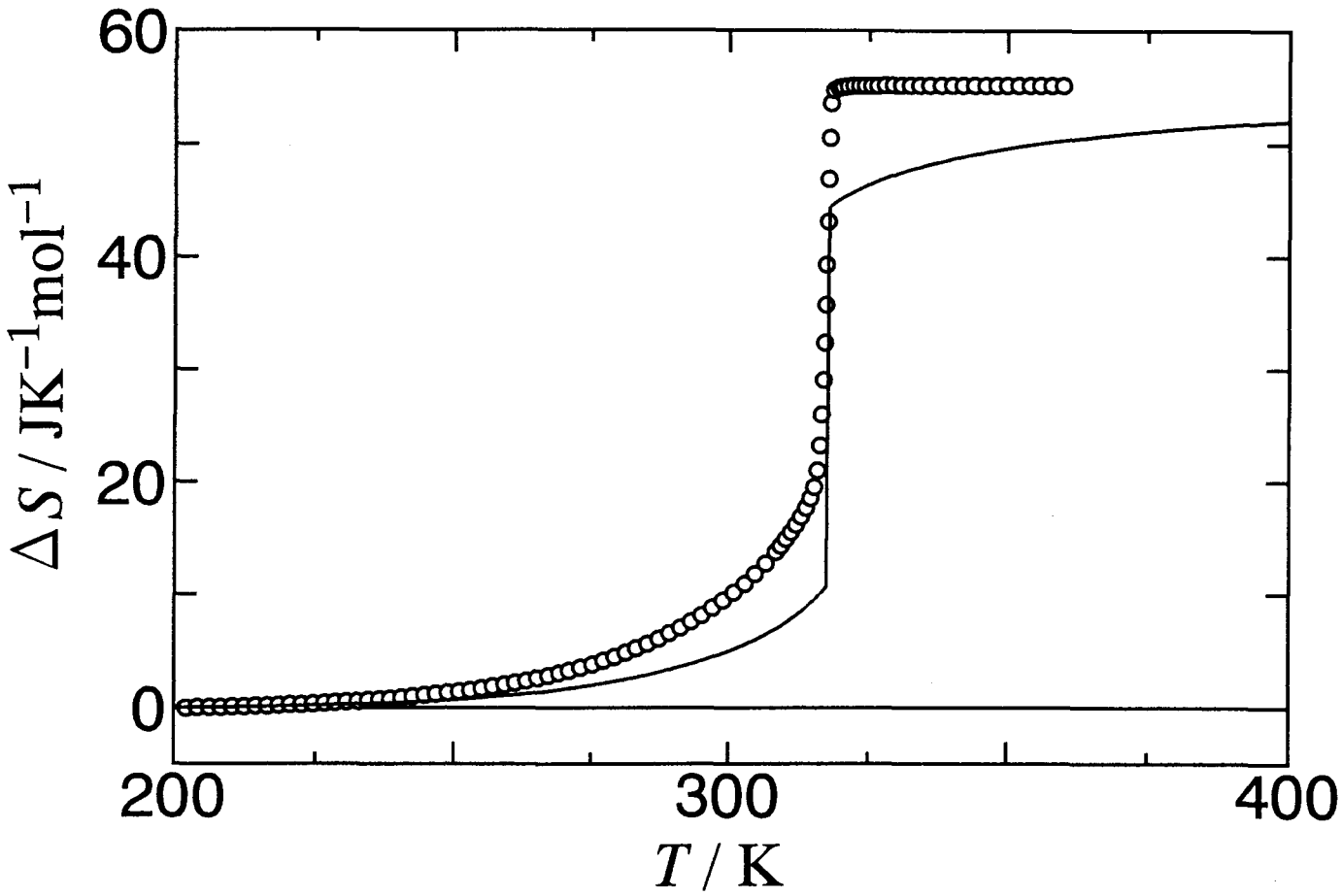

Fig. 2–16. Accumulated transition entropy of $[Cu(dieten)_2](ClO_4)_2$ as a function of temperature. Open circles and solid line indicate the experimental and calculated values, respectively.

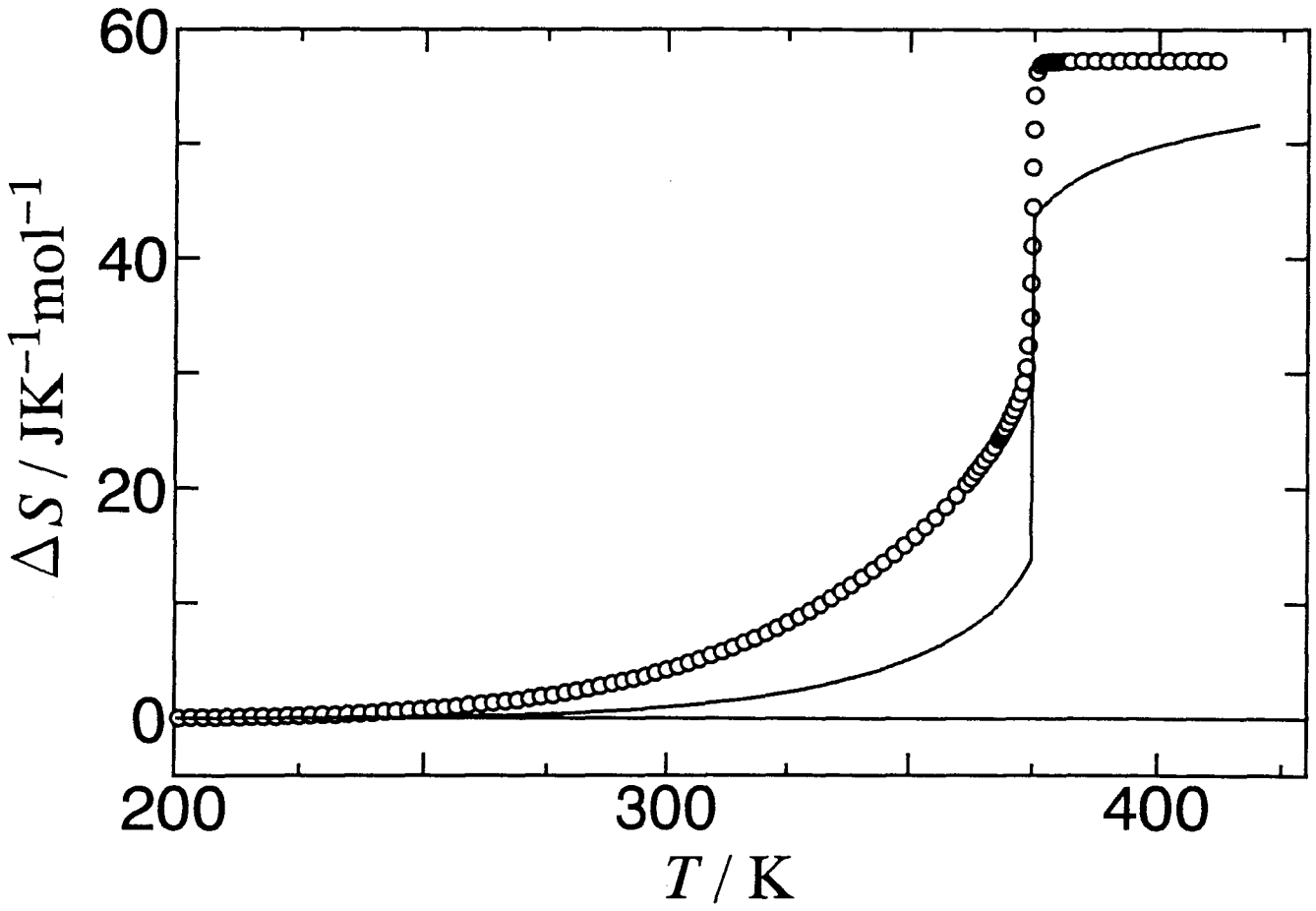

Fig. 2–17. Accumulated transition entropy of $[Ni(dieten)_2](BF_4)_2$ as a function of temperature. Open circles and solid line indicate the experimental and calculated values, respectively.

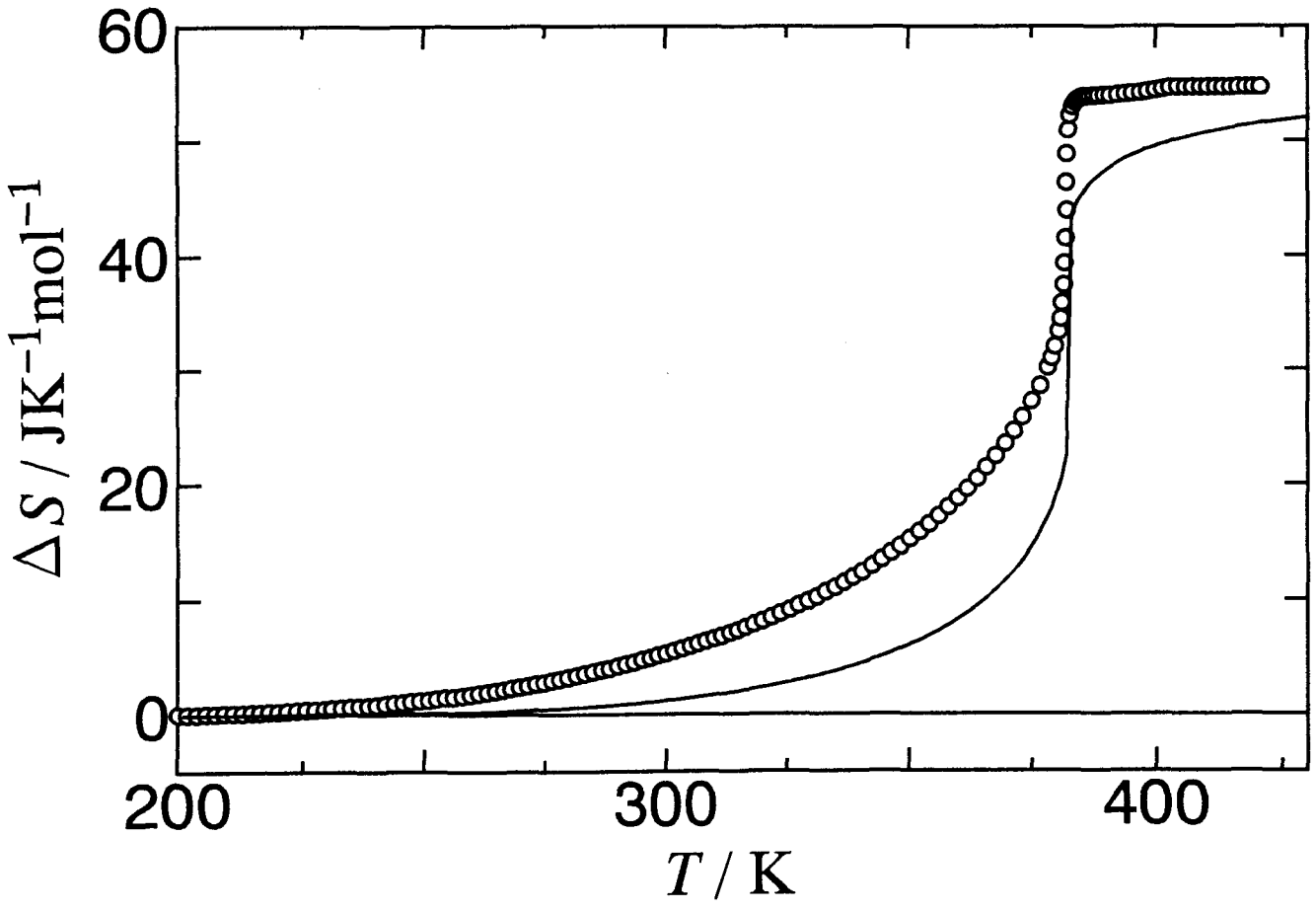

Fig. 2–18. Accumulated transition entropy of $[Ni(dieten)_2](ClO_4)_2$ as a function of temperature. Open circles and solid line indicate the experimental and calculated values, respectively.

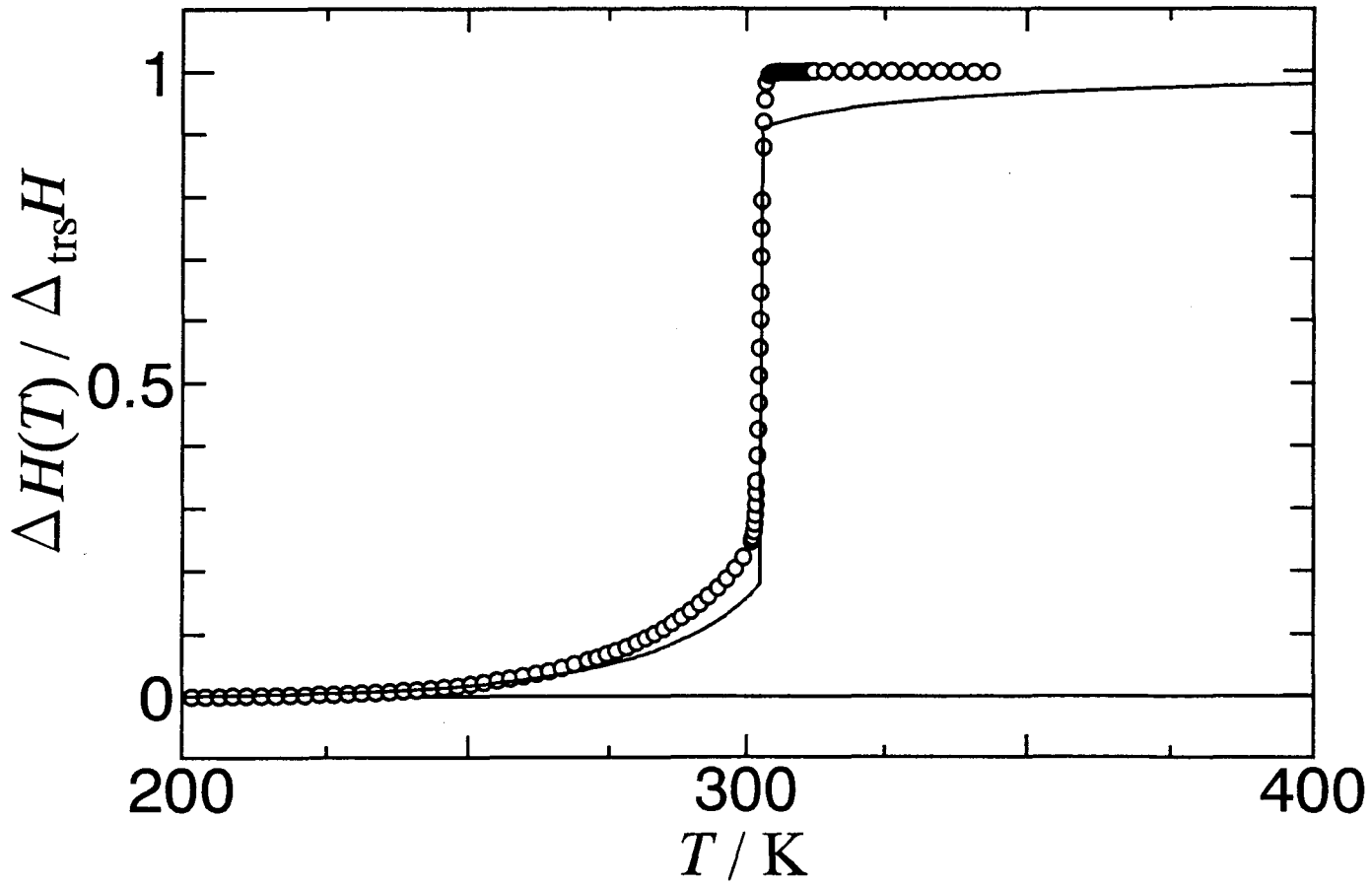

Fig. 2–19. Accumulated transition enthalpy of $[Cu(dieten)_2](BF_4)_2$ as a function of temperature. Open circles and solid line indicate the experimental and calculated values, respectively.

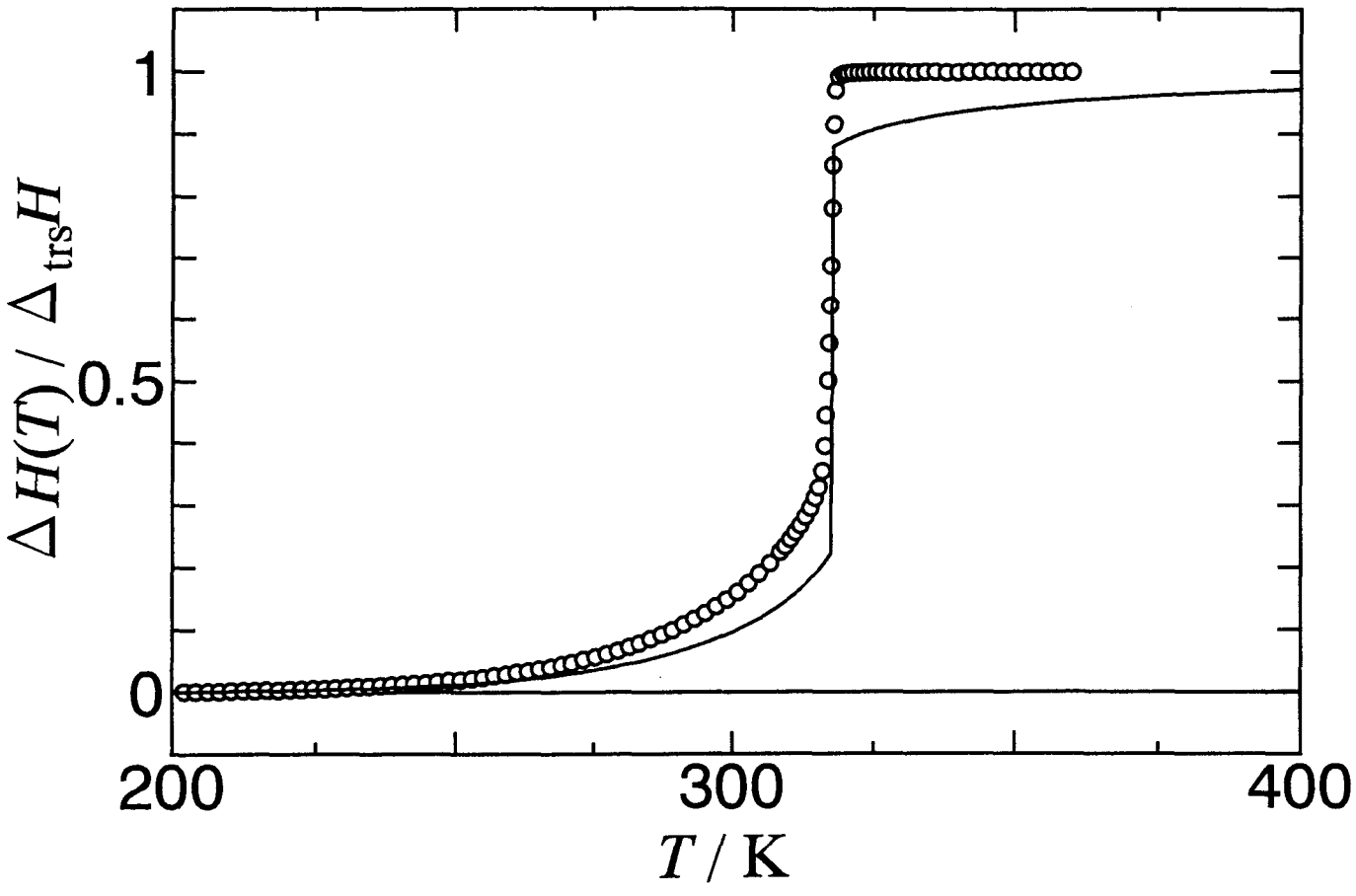

Fig. 2–20. Accumulated transition enthalpy of $[Cu(dieten)_2](ClO_4)_2$ as a function of temperature. Open circles and solid line indicate the experimental and calculated values, respectively.

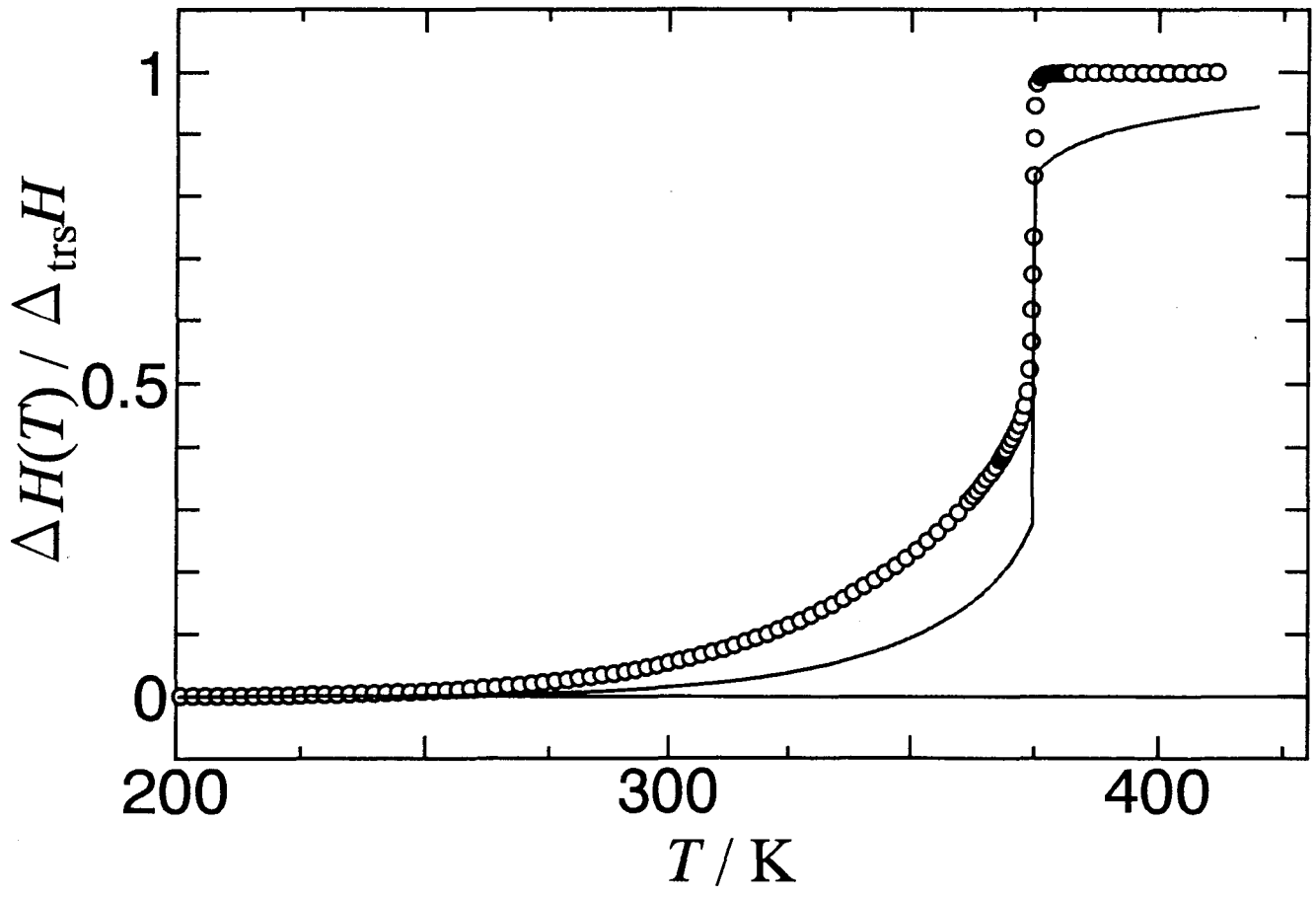

Fig. 2–21. Accumulated transition enthalpy of $[Ni(dieten)_2](BF_4)_2$ as a function of temperature. Open circles and solid line indicate the experimental and calculated values, respectively.

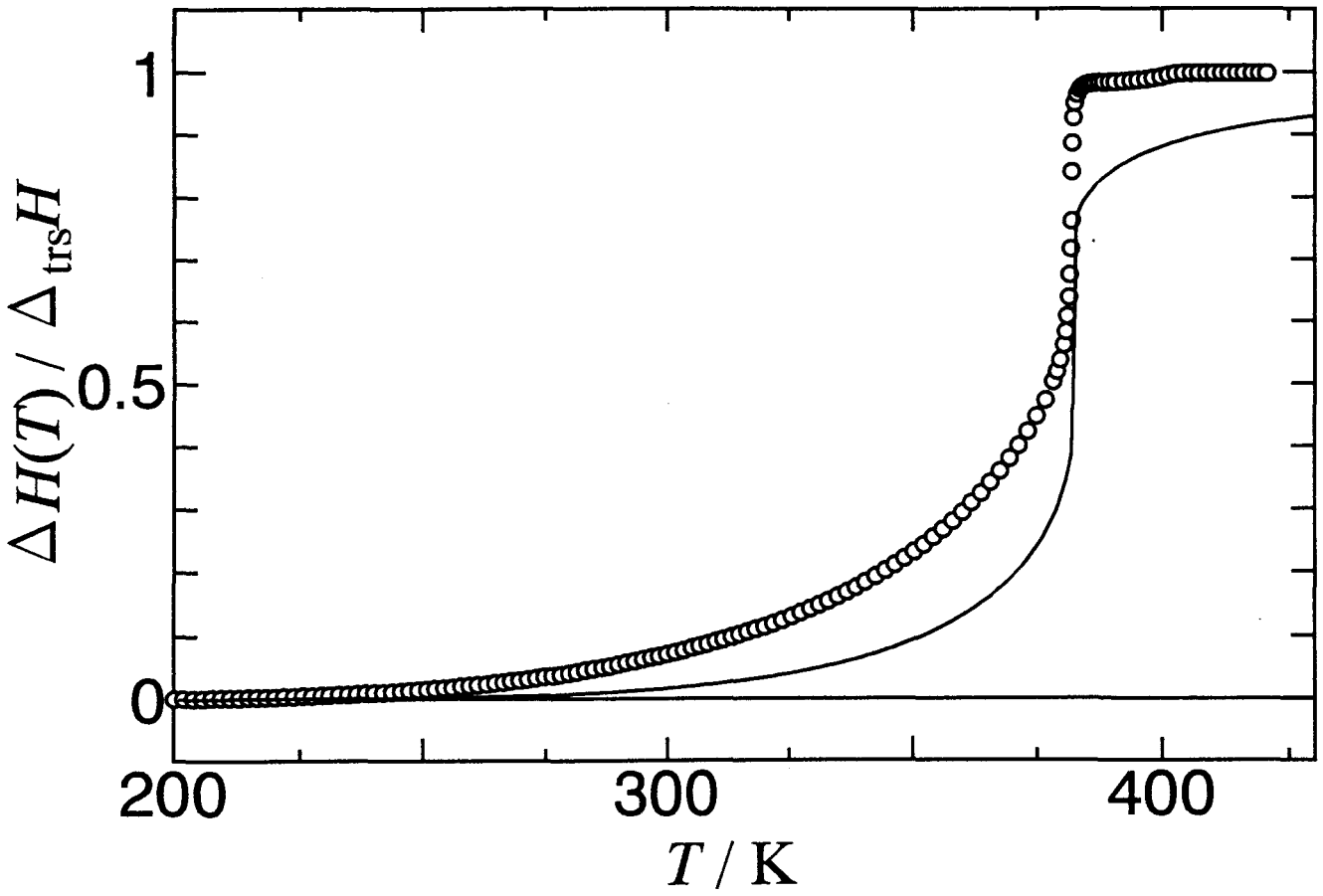

Fig. 2–22. Accumulated transition enthalpy of $[Ni(dieten)_2](ClO_4)_2$ as a function of temperature. Open circles and solid line indicate the experimental and calculated values, respectively.

dramatically when the phase transition occurs. The color of the complex depends on the absorption of visible light by the molecule. The absorption spectra in the visible region depends on the energy level splitting of d-orbitals. Temperature effects on the d-d transition of $[M(dieten)_2]X_2$ have been studied [4-6]. These complexes show a red shift in the d-d transition when they are heated. To investigate the relationship between the absorption spectra and the d-orbital energy levels, the angular overlap model, AOM [16-19], was adopted. In this model, the interactions between the d-orbitals of the central metal and the ligator orbitals are estimated by the coordination geometry. The relative energy levels of d-orbitals are calculated by solving the secular determinant which consists of the following matrix elements, E_{ij} $(i,j = 1\cdots5)$.

$$E_{ij} = e_\sigma \sum_{n=1}^{4} F(d_i,L_n)F(d_j,L_n), \qquad (2\text{-}6)$$

where e_σ is a energy unit describing σ-type interactions and F(d,L) indicates the angular overlap factors for the d-orbitals of the central metal atom and ligator orbitals. A ligand such as NH_3 is known to have very little π-bonding to metal ions. Then the only σ-type interactions are treated in this discussion. The angular dependence of these factors are given in Table 2-20. There are two types of N atoms in the present complexes: one with and the other without ethyl groups. Consequently there exists small differences in the Cu-N bond lengths. If the small differences in the Cu-N bond lengths are taken into account, the symmetry of the CuN_4 plane is D_{2h}. On the other hand, if these differences are negligible small, the symmetry of the CuN_4 plane is D_{4h}. The primary effect of lowering the symmetry from D_{4h} to D_{2h} is to remove the degeneracy of the two levels, d_{zx} and d_{yz}. Since this

Table 2–20. The angular overlap factors of the d–orbitals of a central atom as a function of the ligand position in polar coordinate, (θ,ϕ), with a ligand σ–type orbital.

d–orbital	$F(d,L(\theta,\phi))$
d_{z^2}	$(1 + 3\cos2\theta) / 4$
d_{yz}	$\sqrt{3}\sin\phi\sin2\theta / 2$
d_{zx}	$\sqrt{3}\cos\phi\sin2\theta / 2$
d_{xy}	$\sqrt{3}\sin2\phi(1 - \cos2\theta) / 4$
$d_{x^2-y^2}$	$\sqrt{3}\cos2\phi(1 - \cos2\theta) / 4$

splitting is expected to be small [20], four N atoms are treated to be equal for the sake of simplicity of the evolution of the matrix elements by (2–6).

The structure of $[Cu(dieten)_2](ClO_4)_2$ changes from square–planar in the low–temperature phase to slightly tetrahedrally distorted coordination in the high–temperature phase. The relative energies of the five d–orbitals can be calculated as a function of the polar angles (θ,ϕ) of the ligator position vectors. The central metal atom and ligand nitrogen atoms are arranged in the polar coordinate system as in Fig. 2–23. In the case of square–planar geometry, D_{4h}, the four nitrogen atoms are put on the positions, $L_1(90^\circ,0^\circ)$, $L_2(90^\circ,90^\circ)$, $L_3(90^\circ,180^\circ)$, $L_4(90^\circ,270^\circ)$, and in the case of tetrahedral geometry, T_d, they are put on the positions, $L_1(54.74^\circ,45^\circ)$, $L_2(125.26^\circ,135^\circ)$, $L_3(54.74^\circ,225^\circ)$, $L_4(125.26^\circ,315^\circ)$. Between these two coordination geometries, the positions of ligand nitrogens change as follows, $L_1(\theta,\phi)$, $L_2(180^\circ-\theta,\phi+90^\circ)$, $L_3(\theta,\phi+180^\circ)$, $L_4(180^\circ-\theta,\phi+270^\circ)$, where θ changes from 90° to 54.74° and ϕ changes from 0° to 45°. The relative energies of the d–orbitals are calculated from these parameters, (θ,ϕ), and AOM factors, F, in Table 2–20. The calculated energy levels are shown in Fig. 2–24 as a function of θ. The unit of the ordinate axis, e_σ, corresponds to $\Delta E(90)/3$ for each complex. The temperature effects on the absorption spectra in the visible region of the electronic spectrum of $[M(dieten)_2]X_2$ [4,5] are tabulated in Table 2–21. The absorption maximum in the electronic spectrum corresponds to the d_{yz}, $d_{zx} \rightarrow d_{x^2-y^2}$ transition. The transition energy, $h\tilde{\nu}_{max}$, corresponds to the energy difference between two orbitals, $\Delta E(\theta)$ in Fig. 2–24. In the low–temperature phase, D_{4h}, $\Delta E(90)$ is equal to $h\tilde{\nu}_{max}$ at lower temperature, and in the high–temperature phase $\Delta E(\theta)$ is equal to $h\tilde{\nu}_{max}$ at higher temperature. The relation is formulated as follows,

$$\frac{\Delta E(90)}{\Delta E(\theta)} = \frac{h\tilde{\nu}_{max} \text{ at lower temp.}}{h\tilde{\nu}_{max} \text{ at higher temp.}} \qquad (2\text{–}7)$$

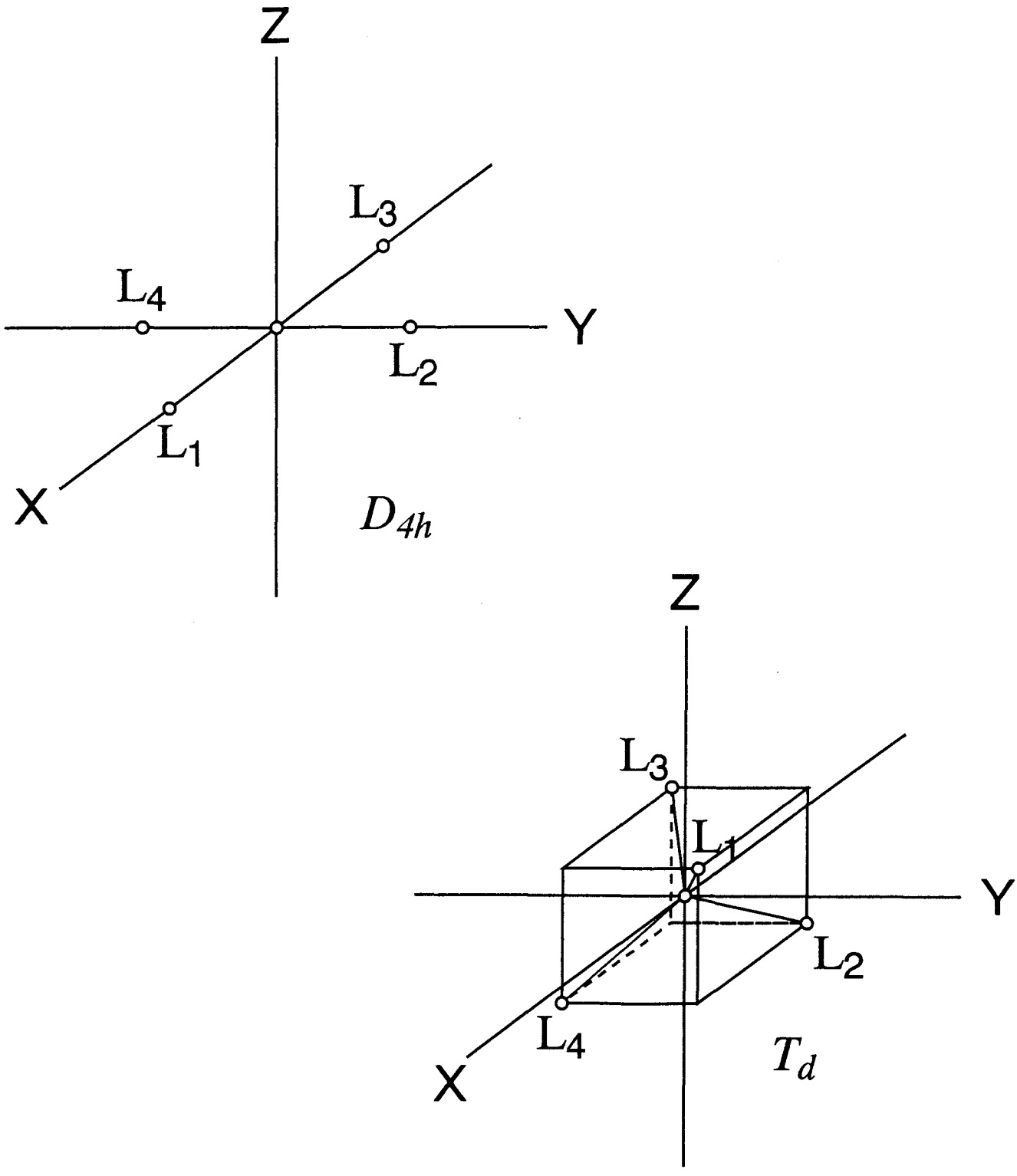

Fig. 2-23. The coordination geometry of the central metal atom and the ligand nitrogen atoms.

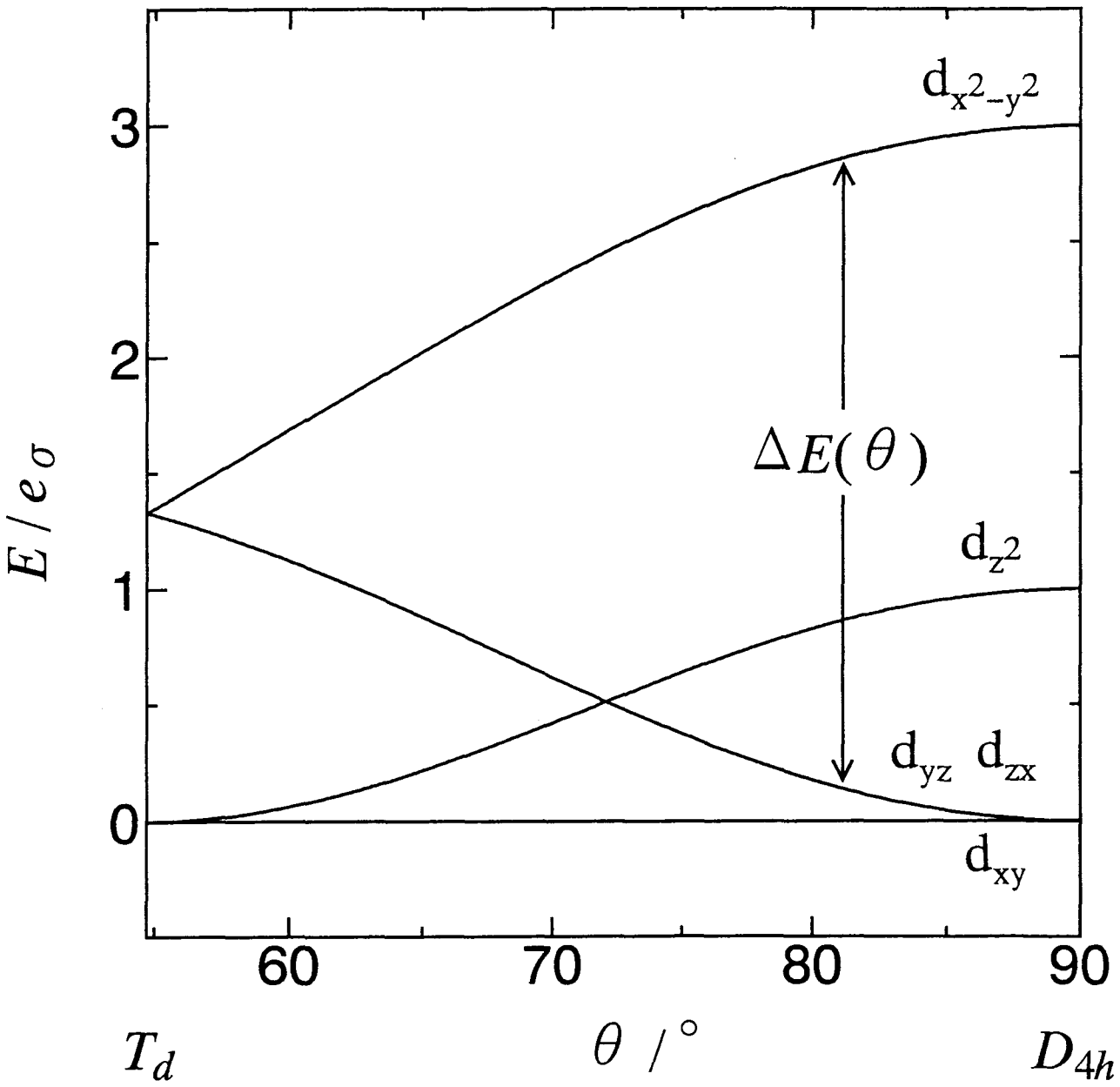

Fig. 2-24. The energy level diagram calculated from AOM.

Table 2–21. Temperature effects on the absorption in the visible region of the electronic spectrum of $[M(dieten)_2]X_2$ [3,5].

Complexes	t / °C ⇔ t / °C		$\tilde{\nu}_{max}$ / cm^{-1} ⇔ $\tilde{\nu}_{max}$ / cm^{-1}	
$[Cu(dieten)_2](BF_4)_2$	0	78	20750	19230
$[Cu(dieten)_2](ClO_4)_2$	25	78	20700	19305
$[Ni(dieten)_2](BF_4)_2$	25	94	21505	20200
$[Ni(dieten)_2](ClO_4)_2$	25	110	21622	20619

The trans bond angles, ∠N–Cu–N = 2θ, are estimated from $\Delta E(\theta)$ in the above equation and $h\tilde{\nu}_{max}$ in Table 2–21.

The enthalpy (actually the internal energy) of the d–orbitals is the sum of each electron's energy. The d–electrons are placed from bottom to upper orbitals in the energy level diagram in Fig. 2–24. There are nine and eight d–electrons in the copper and nickel complexes, respectively. The enthalpy of the d–orbitals in the low–temperature phase is calculated from the diagram at θ = 90°. And the enthalpy of d–orbitals in the high–temperature phase is calculated from the diagram at the estimated θ by equation (2–7). Consequently, the enthalpy change of the d–orbitals arising from deformation of the coordination geometry is the difference in two sums, in the low– and the high–temperature phase. Trans bond angles of the high–temperature phase, 2θ, and the enthalpy difference due to the d–orbitals, $\Delta H_{orbital}$, are given in Table 2–22. The trans bond angles, ∠N–Cu–N, of $[Cu(dieten)_2](ClO_4)_2$ change from 180.0° in the low–temperature phase to 164.4° in the high–temperature phase by the calculation of AOM, while the bond angles change from 180.0° to 178.0° and 174.7° by the X–ray structural analyses [7,8]. In the case of other complexes, the calculated bond angles are 165.0°, 165.8° and 167.6°, but the X–ray structural analyses have not been carried out. The enthalpy of transition due to the d–orbital for $[Cu(dieten)_2](BF_4)_2$, $[Cu(dieten)_2](ClO_4)_2$, $[Ni(dieten)_2](BF_4)_2$ and $[Ni(dieten)_2](ClO_4)_2$ are 9.06, 8.37, 15.6 and 12.0 kJ mol^{-1}, respectively. These values are about a half of $\Delta_{trs}H$.

§2–6. Conclusion

Thermal properties of four thermochromic complexes, $[M(dieten)_2]X_2$, have been studied by means of the adiabatic calorimeters. Phase transitions due to the thermochromism were observed and the thermodynamic quantities,

Table 2–22. The energy unit of σ–type interaction, e_σ, the trans bond angle ∠N–Cu–N, 2θ in the high–temperature phase and the enthalpy of transition due to the change of the d–orbitals.

Complexes	e_σ / kJ mol^{-1}	2θ / °	$\Delta H_{orbital}$ / kJ mol^{-1}
$[Cu(dieten)_2](BF_4)_2$	82.74	164.4	9.06
$[Cu(dieten)_2](ClO_4)_2$	82.54	165.0	8.37
$[Ni(dieten)_2](BF_4)_2$	85.75	165.8	15.6
$[Ni(dieten)_2](ClO_4)_2$	86.22	167.6	12.0

T_{trs}, $\Delta_{trs}H$ and $\Delta_{trs}S$ were determined by the present heat capacity measurements. There are large differences in the transition temperatures, from 302.64 K for $[Cu(dieten)_2](BF_4)_2$ to 382.01 K for $[Ni(dieten)_2](ClO_4)_2$. However, the transition entropies, $\Delta_{trs}S$, are approximately equal to the same value of 55 J K^{-1} mol^{-1}. This fact indicates that the same degrees of disorder take place in the thermochromic transitions. The transition enthalpies, $\Delta_{trs}H$, observed in the present study are quite different from those of DSC measurements. The comparison of observed values are shown in Table 2–23. The enthalpies detected by DSC are less than 60 per cent of the transition enthalpies. In the case of this type of transition, it is difficult to get highly accurate value by DSC. Because the transition has a long C_p tail extending below the transition temperature, DSC measurement appears to have failed to detect the gradual part extending below T_{trs} and could measure only the discontinuous part (see Table 2–18).

The Chesnut model was applied to reproduce the observed thermodynamic quantities, ΔC_p, $\Delta_{trs}S$ and $\Delta_{trs}H$. In spite of the simplicity of this model, the Chesnut model accounts well for the thermochromic transition behavior of the present compounds, especially the copper complexes.

The transition enthalpies were discussed by means of the chelate ring puckering and the angular overlap model. The estimated ΔH are tabulated in Table 2–24 with observed transition enthalpies, $\Delta_{trs}H$. These values are in good agreement with the experimental values. More than half of transition enthalpy is attributed to the change of d–electron energy levels and the rest is attributed to the ring motions. The sources of $\Delta_{trs}H$ are successfully explained. The result of the heat capacity measurement is often discussed in terms of transition entropy, $\Delta_{trs}S$. However, not only the transition entropy but also the transition enthalpy is discussed in this thesis.

The present thesis did not treat the effect of different counter anions, BF_4^- and ClO_4^-. For a further understanding of the nature of

Table 2-23. Comparison of the observed enthalpies measured by different method, adiabatic calorimeter and differential scanning calorimeter.

Complexes	Adiabatic Calorimeter $\Delta_{trs}H$ / kJ mol^{-1}	DSC $\Delta_{trs}H$ / kJ mol^{-1}	ratio of two values
$[Cu(dieten)_2](BF_4)_2$	16.62	10.04	0.60
$[Cu(dieten)_2](ClO_4)_2$	17.43	8.91	0.51
$[Ni(dieten)_2](BF_4)_2$	20.85	5.73	0.27
$[Ni(dieten)_2](ClO_4)_2$	20.18	6.65	0.33

Table 2–24. Comparison of the theoretical and observed transition enthalpies. ΔH(puckering), ΔH(AOM) indicate the enthalpies estimated from the chelate ring puckering and AOM, respectively. ΔH(sum) means a sum of these two values. $\Delta_{trs}H$ indicates an experimental transition enthalpy.

Complexes	ΔH(puckering) kJ mol^{-1}	ΔH(AOM) kJ mol^{-1}	ΔH(sum) kJ mol^{-1}	$\Delta_{trs}H$ kJ mol^{-1}
$[Cu(dieten)_2](BF_4)_2$	7.7	9.06	16.76	16.62
$[Cu(dieten)_2](ClO_4)_2$	8.0	8.37	16.37	17.43
$[Ni(dieten)_2](BF_4)_2$	9.9	15.6	25.50	20.85
$[Ni(dieten)_2](ClO_4)_2$	9.5	12.0	21.50	20.18

thermochromism in the complexes, it will be valuable to study that effect and some similar complexes which do not exhibit the thermochromic phase transition.

References to Chapter 2.

[1] K. Sone and Y. Fukuda, "*Inorganic Thermochromism*", (Inorganic Chemistry Concepts, Vol. 10) Springer–Verlag, Berlin (1987).

[2] D. R. Bloomquist and R. D. Willett, *Coord. Chem. Rev.*, **47**, 125 (1982).

[3] P. Pfeiffer and H. Glaser, *J. Prakt. Chem.*, **151**, 134 (1938).

[4] J. R. Ferraro, L. J. Basile, L. R. Gracia–Ineguez, P. Paoletti and L. Fabbrizzi, *Inorg. Chem.*, **15**, 2342 (1976).

[5] A. B. P. Lever, E. Mantovani and J. C. Donini, *Inorg. Chem.*, **10**, 2424 (1971).

[6] L. Fabbrizzi, M. Micheloni and P. Paoletti, *Inorg. Chem.*, **13**, 3019 (1974).

[7] M. M. Andino, J. D. Curet and M. M. Muir, *Acta Crystallogr.*, **B32**, 3185 (1976).

[8] I. Grenthe, P. Paoletti, M. Sandström and S. Glikberg, *Inorg. Chem.*, **18**, 2687 (1979).

[9] R. J. Pylkki, R. D. Willett and H. W. Dodgen, *Inorg. Chem.*, **23**, 594 (1984).

[10] D. M. L. Goodgame and L. M. Venanzi, *J. Chem. Soc.*, 616 (1963).

[11] M. Yoshikawa, M Sorai, H. Suga and S. Seki, *J. Phys. Chem. Solids,* **44**, 311 (1983).

[12] A. Nishimori, Y. Nagano and M. Sorai *unpublished result.*

[13] M. Sorai, K. Kaji and Y. Kaneko, *J. Chem. Thermodyn.*, **24**, 167 (1992).

[14] M. Sorai and S. Seki, *J. Phys. Soc. Jpn.*, **32**, 382 (1972).

[15] D. B. Chesnut, *J. Chem. Phys.*, **40**, 405 (1964).

[16] J. K. Burdett, *Adv. Inorg. Chem. Radiochem.*, **21**, 113 (1978).

[17] E. Larsen and G. N. La Mar, *J. Chem. Educ.*, **51**, 633 (1974).

[18] W. Smith and D. W. Clark, *Rev. Roum. Chim.*, **20**, 1243 (1975).

[19] A. B. P. Lever, "*Inorganic Electronic Spectroscopy* (second ediditon)",

(Studies in Physical and theoretical Chemistry, Vol.33) Elsevier, Amsterdam, (1984)

[20] K. L. Bray, H. G. Drickamer, E. A. Schmitt and D. N. Hendrickson, *J. Am. Chem. Soc.*, **111**, 2849 (1989).

Chapter 3. Thermochromic Phase Transition in $(IPA)CuCl_3$

§3-1. Introduction

The thermochromic phenomena are classified in various ways. For example, a gradual color change over a wide temperature range or an abrupt color change with a phase transition, reversible color change or irreversible, and so on. A number of copper(Ⅱ) and nickel(Ⅱ) halide complexes are known to show the thermochromism [3-5]. $(IPA)CuCl_3$ and $(IPA)_2CuCl_4$ exhibit a reversible thermochromic phase transition in the solid state, where IPA stands for isopropylammonium ion. In the case of $(IPA)CuCl_3$, the color of the solid changes from brown to orange when it is heated. This complex was first prepared by Remy and Laves in 1933 and they described its thermochromism [6]. There had been practically no study on this complex until 1981. Roberts *et al.* studied this complex by use of X-ray structure analysis, NMR, EPR, DSC and magnetic susceptibility [7].

The low-temperature phase of $(IPA)CuCl_3$ is triclinic space group $P\bar{1}$ with a = 11.692 Å, b = 7.804 Å, c = 6.106 Å, α = 79.00°, β = 122.60°, γ = 116.47° and Z = 2. The high-temperature phase is orthorhombic Pcan with a = 17.589 Å, b = 7.296 Å , c = 6.365 Å and Z = 4. The structures of low- and high-temperature phases are shown in Figs 3-1 and 3-2, respectively. The coordination geometry of $(IPA)CuCl_3$ changes grossly through the thermochromic transition, namely, the coordination number of copper atom changes from five at low temperatures to six at high temperatures. The IPA cation is linked by a hydrogen bond to a terminal chloride ion, which does not bridge coppers, in the low-temperature phase. In the high-temperature phase, the hydrogen bond is weakened and the terminal chloride ion coordinates to copper. Thus there are bibridged linear

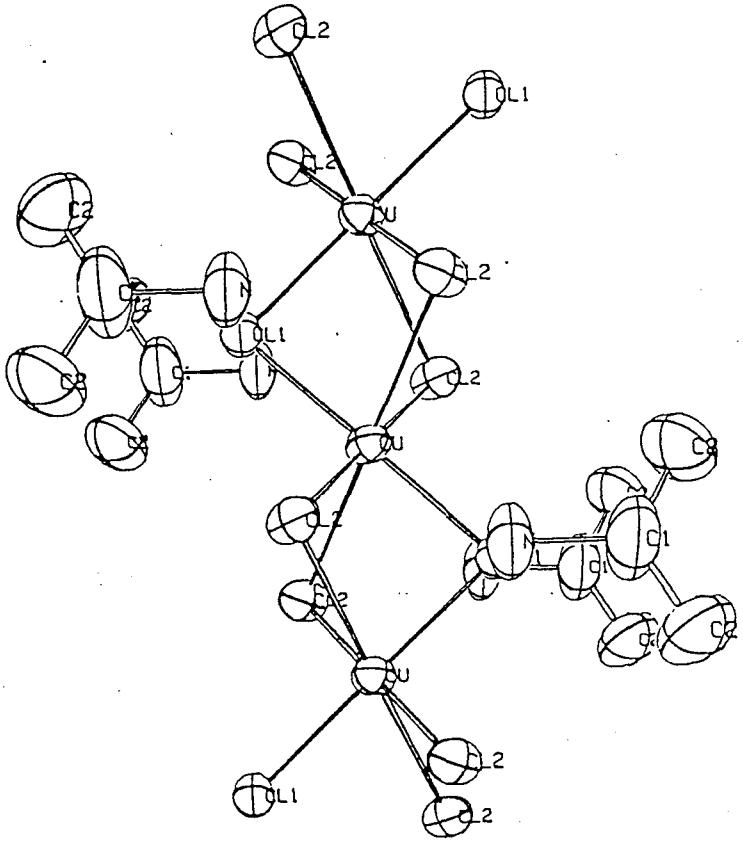

Fig. 3–1. The structure of high–temperature phase (after ref. 7)

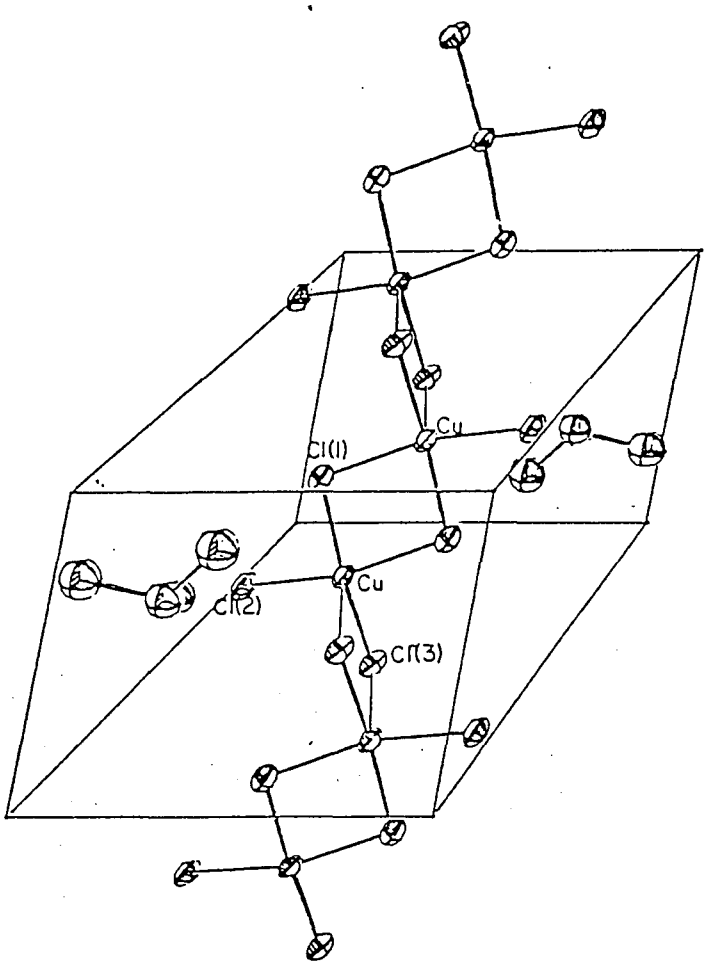

Fig. 3–2. The structure of low–temperature phase (after ref. 7).

chains of $[(CuCl_3)_2^{2-}]_n$ and tribridged linear chains of $[(CuCl_3)_n]^{n-}$ in the low- and high-temperature phase, respectively. Proton NMR spectra and magnetic susceptibility also change their values at T_{trs}. The NMR line width narrows at T_{trs}. The magnitude of the NMR line width above T_{trs} corresponds to a twofold rotation of IPA cation. This fact is consistent with the disorder of IPA cation seen in the X-ray structural analysis at the high-temperature phase. DTA and DSC measurements were carried out to give $\Delta_{trs}H$ = 1.4 kcal mol^{-1} and $\Delta_{trs}S$ = 4.3 cal K^{-1} mol^{-1}.

Mechanism of the thermochromic phase transition of $(IPA)CuCl_3$ is different from that of $[M(dieten)_2]X_2$ described in Chapter 2. The coordination number of $(IPA)CuCl_3$ changes through the thermochromic phase transition, while that of $[M(dieten)_2]X_2$ remains constant throughout the thermochromic phase transition. How this difference will be reflected on thermodynamic properties? This is the subject of the present Chapter.

§3-2. Experimental

3-2-1. Preparation of Sample

This sample was prepared according to the method of Remy *et al.* [6]. $CuCl_2$ was prepared by the dehydration of $CuCl_2 \cdot 2H_2O$ by heating. $(CH_3)_2CHNH_2 \cdot HCl$ was added to an ethanolic solution of $CuCl_2$. $(IPA)CuCl_3$ crystallized out when ether was added dropwise to the ethanolic solution. The crystallization was continued further in a refrigerator. A brown precipitates were filtered and washed with ethanol and ether and then dried in a vacuum desiccator. The total yield of product was 13.6 %. The elemental analysis for the complex was good. *Anal.* Calcd. for

$C_3H_{10}NCuCl_3$: C, 15.66; H, 4.38; N, 6.09. Found: C, 15.76; N, 4.42; N, 6.06.

3-2-2. Differential Thermal Analysis (DTA)

Qualitative nature of the thermal properties of $(IPA)CuCl_3$ was preliminarily examined by use of a home-built DTA apparatus in the temperature range from 80 to 473 K.

3-2-3. Heat Capacity Measurements

The heat capacity were measured with an adiabatic calorimeter [8] in the 13-360 K range. A calorimeter cell made of gold-plated beryllium-copper alloy and oxygen-free copper contained 4.9340 g (0.0214498 mol) of the sample after buoyancy correction using the density of 1.82 g cm^{-3} [7]. A small amount oh helium gas was sealed in the cell to aid the heat transfer.

3-2-4. Infrared Absorption Spectra

Variable temperature infrared spectra were recorded for Nujol mulls in the 4000-400 cm^{-1} range with an infrared spectrophotometer (Japan Spectroscopic Co., Ltd., Model DS-402G) and far-infrared spectra in the 400-30 cm^{-1} range with a far-infrared spectrophotometer (Hitachi, Ltd., Model FIS-3). The temperature at which the spectra were recorded are as follows:

stable phase: 90, 300, 373 K,

metastable phase: 90, 173, 223, 300, 373 K.

These spectra were used to estimate the normal heat capacity by means of the effective frequency distribution method [9].

§3–3. Results and Discussion

The first cooling DTA run for (IPA)$CuCl_3$ from 280 K to 79 K showed no peak. The subsequent heating run showed a broad endothermic peak spanning from 330 K to 367 K. The second cooling run showed no peak at that temperature region but gave an exothermic peak at 211 K. The next heating run showed an endothermic peak at 210 K and exothermic peak at 285 K. This complex exhibits a complicated phase relation. To get the stable phase, this sample was annealed for one day at about 300 K. The heating DTA run from 79 K for the annealed sample showed no endothermic peak at 211 K but a single peak at 346 K. During one day annealing at about 300 K, the metastable phase relaxed to the stable phase. This indicates that the sample precipitated from a solution is a metastable and the high–temperature phase of (IPA)$CuCl_3$ is easily quenched to another metastable phase. The typical DTA curves of both heating and cooling runs are shown in Fig. 3–3.

(IPA)$CuCl_3$ decomposed on heating to the high–temperature phase even in helium atmosphere when the specimen was in contacts with copper. In order to avoid the decomposition and to get the stable phase, the precipitate was heated up about 373 K in a glass tube and cooled down slowly. The color of (IPA)$CuCl_3$ changed from brown to orange and from orange to brown in this procedure. The crystals were loaded in a calorimeter sample cell after this heat treatment. It was confirmed by the heat capacity measurement in the temperature range 190 K to 220 K that the sample was in the stable phase. If the sample is a mixture of the stable and metastable

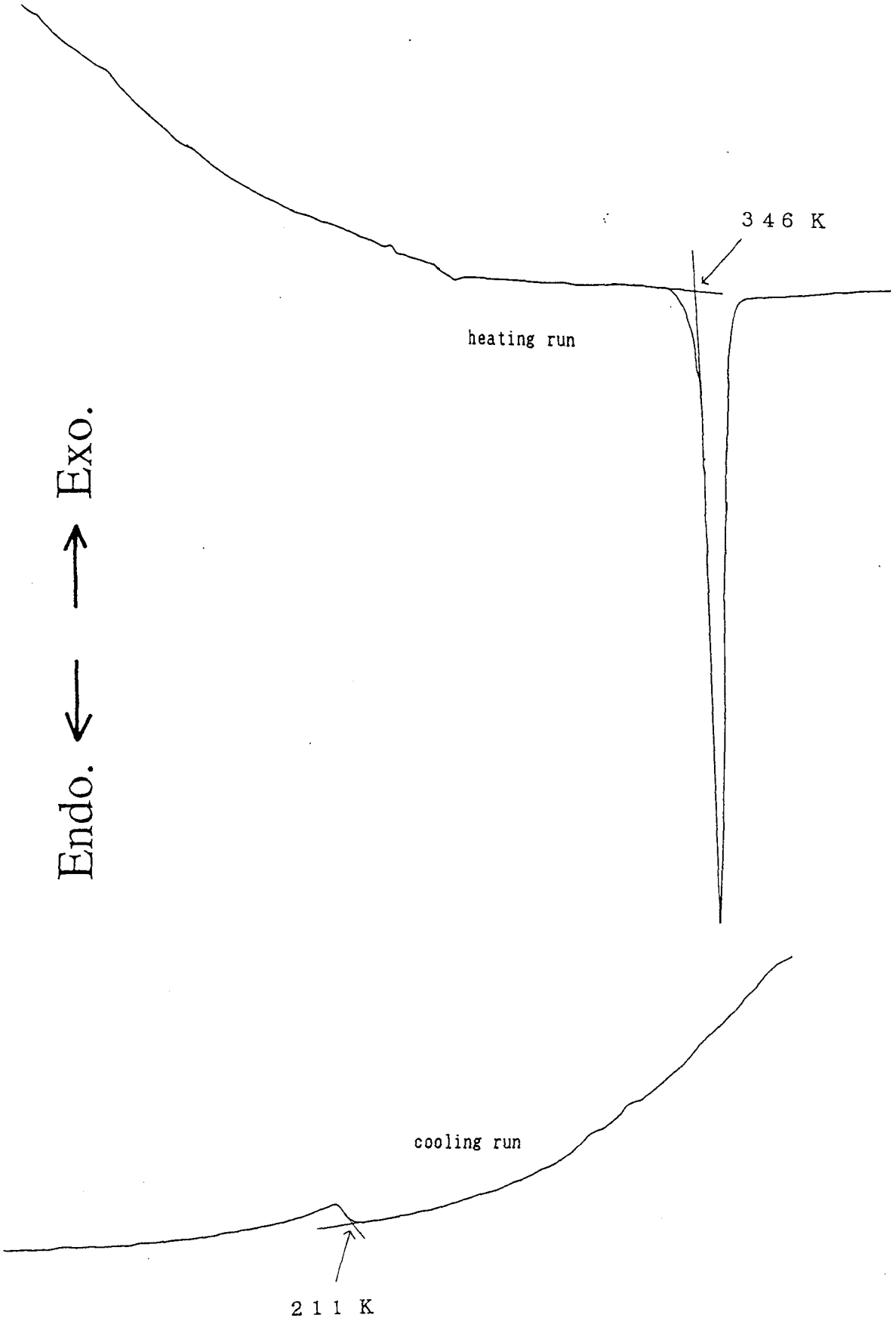

Fig. 3–3. The heating and cooling DTA curves of (IPA)$CuCl_3$.

phases, there should exist the heat capacity anomaly at about 210 K, which is a phase transition characteristic of the metastable phase.

Heat capacity measurements of the stable phase were carried out from 13 K to 315 K. As mentioned above, this sample decomposes easily when it is exposed to high temperature. Since it takes long time to measure the heat capacity, especially in the region of phase transition, we used the calorimeter as an adiabatic scanning calorimeter in the high temperature region. The calorimeter cell containing the sample was heated up continuously from 307.6 K to 361.4 K in 76 minutes, and during that period the supplied Joule–energy and the temperature were recorded every one minute. The ratio of the input energy to the temperature increment was regarded as the heat capacity. The sample in the high temperature phase was cooled down quickly from 362 K to 80 K after one point heat capacity measurement at 362 K. The cooling rate passing over the temperature region of thermochromic phase transition was −4.5 K min^{-1} and no exothermic phenomena was detected. Heat capacity measurements of this quenched metastable phase were successfully carried out from 13 K to 258 K, whereas it was impossible to measure the heat capacity above that temperature because of exothermic temperature drift due to stabilization of the metastable state to the stable one. The quenched metastable sample relaxed to the stable phase with an enthalpy relaxation. Heat capacities of both stable and metastable phases are shown in Fig. 3–4 and tabulated in Table 3–1.

As can be seen in Fig. 3–4, a single phase transition was observed at 335.63 K in the stable phase. Normal heat capacities of both the low– and high–temperature phases were independently calculated by means of polynomial expressions. Temperature ranges where the fitting was made are from 310 K to 325 K and from 350 K to 360 K for the low– and high–temperature phases, respectively. Subtraction of the normal heat capacities from the observed values gives the excess heat capacities due to the phase

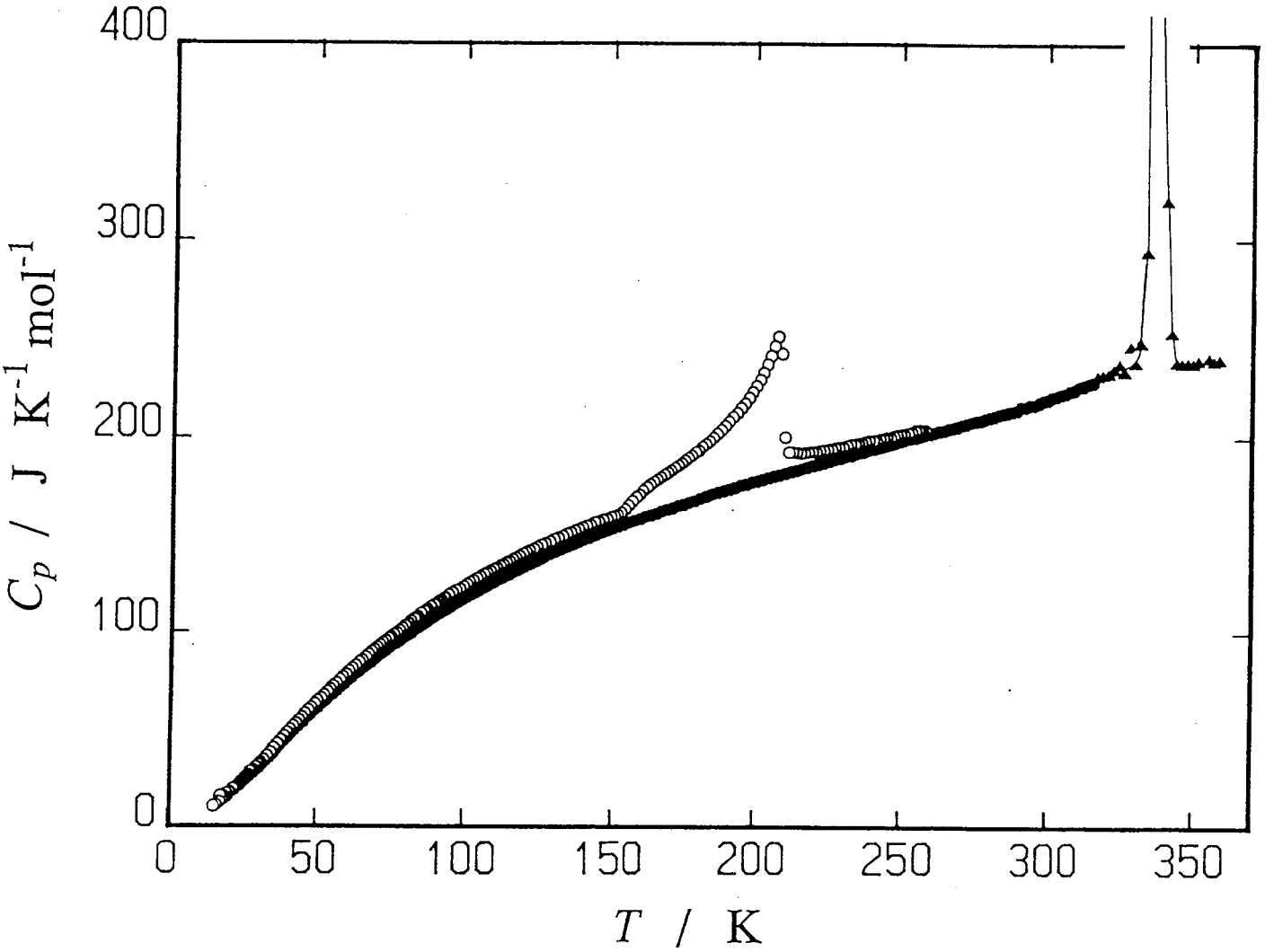

Fig. 3–4. Molar heat capacity of (IPA)$CuCl_3$ (relative molecular mass: 230.023). Full and open circles indicate the stable and metastable phases, respectively. Full triangles also indicate the stable phase.

Table 3-1. Molar heat capacity of (IPA)$CuCl_3$ (relative molecular mass: 230.023)

$\frac{T}{K}$	$\frac{Cp}{JK^{-1}mol^{-1}}$	$\frac{T}{K}$	$\frac{Cp}{JK^{-1}mol^{-1}}$	$\frac{T}{K}$	$\frac{Cp}{JK^{-1}mol^{-1}}$
		Series 1			
95.693	114.09	155.869	156.73	212.313	183.27
98.104	116.40	157.829	157.78	214.220	183.77
100.468	118.52	159.777	158.78	216.121	184.72
102.788	120.52	161.714	159.84	218.016	185.61
105.068	122.45	163.641	160.79	219.904	186.44
107.312	124.39	165.557	161.67	221.787	187.12
109.523	126.20	167.463	162.65	223.665	187.98
111.702	127.92	169.360	163.45	225.537	188.70
113.851	129.60	171.247	164.48	227.403	189.47
115.974	131.21	173.125	165.44	229.264	190.12
118.071	132.77	174.998	166.22	231.120	190.90
120.144	134.31	176.866	167.16	232.970	191.61
122.195	135.77	178.817	168.24	234.815	192.46
124.224	137.31	180.853	169.28	236.655	193.38
126.234	138.60	182.880	170.32	238.490	194.08
128.224	140.03	184.897	171.48	240.321	194.91
130.197	141.33	186.905	172.37	242.146	195.49
132.152	142.60	188.905	173.41	243.967	196.45
134.091	143.91	190.897	174.21	245.783	197.16
136.015	145.13	192.880	175.14	247.594	197.99
137.924	146.32	194.855	176.04	249.401	198.78
139.818	147.55	196.823	176.84	251.202	199.55
141.792	148.72	198.783	177.72	253.000	200.30
143.845	149.94	200.737	178.39	254.791	201.05
145.883	151.14	202.683	179.26	256.579	201.78
147.907	152.29	204.622	180.03	258.443	202.61
149.917	153.50	206.555	180.86	260.383	203.29
151.913	154.64	208.481	181.64	262.317	204.05
153.897	155.66	210.400	182.34		
		Series 2			
16.568	21.47	26.348	25.19	37.232	41.80
17.285	16.01	27.214	26.45	38.515	43.80
18.263	15.72	28.092	27.51	39.724	45.67
19.333	17.21	29.023	28.90	40.869	47.53
20.397	17.96	30.016	30.24	41.958	49.30
21.422	19.48	31.096	31.77	43.056	50.93
22.394	20.32	32.240	33.46	44.162	52.62
23.405	21.01	33.444	35.36	45.273	53.75
24.439	22.69	34.688	37.41	46.438	56.02
25.421	24.07	35.941	39.70	47.605	57.54

Table 3–1. (continued).

T/K	Cp/JK^{-1}mol^{-1}	T/K	Cp/JK^{-1}mol^{-1}	T/K	Cp/JK^{-1}mol^{-1}
48.797	59.47	74.506	92.10	99.046	116.87
50.061	61.25	75.556	93.22	100.427	118.11
51.324	63.08	76.591	94.32	101.792	119.28
52.588	64.84	77.611	95.41	103.144	120.46
53.853	66.58	78.617	96.44	104.482	121.63
55.156	68.23	79.609	97.52	105.807	122.76
56.499	69.97	80.633	98.58	107.120	123.81
57.796	71.67	81.753	99.64	108.421	124.92
59.053	73.34	82.923	101.18	109.711	125.96
60.274	74.94	84.077	102.45	110.991	126.93
61.545	76.63	85.215	103.63	112.260	128.00
62.864	78.30	86.339	104.85	113.519	128.99
64.147	79.91	87.449	105.92	114.769	129.91
65.398	81.50	88.604	107.11	116.010	130.90
66.619	82.99	89.801	108.29	117.242	131.81
67.813	84.45	91.050	109.47	118.466	132.69
68.981	85.81	92.348	110.73	119.681	133.64
70.127	87.17	93.630	111.98	120.970	134.59
71.251	88.49	94.898	113.14	122.332	135.59
72.354	89.76	96.238	114.32	123.685	136.52
73.439	90.95	97.651	115.64	125.029	137.53
		Series 3			
241.233	195.79	267.268	205.91	292.261	216.54
242.892	196.07	268.860	206.56	293.773	217.30
244.544	196.59	270.447	207.24	295.298	217.25
246.192	197.24	272.029	207.84	296.832	218.39
247.836	198.11	273.606	208.69	298.367	219.44
249.477	198.88	275.181	209.20	299.899	220.28
251.114	199.48	276.755	209.70	301.428	221.21
252.747	200.20	278.328	210.40	302.956	221.81
254.376	200.69	279.901	211.04	304.483	222.61
256.001	201.37	281.470	211.69	306.011	223.19
257.623	202.05	283.036	212.41	307.537	224.30
259.240	202.81	284.598	212.99	309.060	224.97
260.854	203.34	286.155	213.60	310.658	226.36
262.464	203.97	287.705	214.01	312.329	227.09
264.070	204.54	289.241	214.61	313.996	228.17
265.671	205.29	290.758	216.33	315.662	228.83
		Series 4			

Table 3–1. (continued).

T / K	Cp / JK^{-1}mol^{-1}	T / K	Cp / JK^{-1}mol^{-1}	T / K	Cp / JK^{-1}mol^{-1}
308.750	217.11	328.574	233.29	341.795	240.94
309.376	237.59	329.187	241.23	342.397	253.57
309.997	228.85	329.799	236.64	342.998	244.94
310.625	219.10	330.413	235.37	343.605	236.01
311.256	222.45	331.022	248.20	344.215	234.65
311.881	233.59	331.627	248.23	344.826	234.11
312.502	231.09	332.232	247.19	345.433	242.95
313.128	223.26	332.835	255.73	346.039	237.07
313.759	214.24	333.426	278.67	346.647	237.71
314.388	230.29	333.988	352.58	347.251	250.28
315.004	247.56	334.490	507.37	347.858	226.74
315.621	229.00	334.903	831.49	348.468	240.80
316.244	228.86	335.196	1716.37	349.075	235.88
316.864	237.17	335.384	2829.26	349.683	237.18
317.484	227.83	335.519	3841.96	350.289	239.08
318.105	233.35	335.632	4195.07	350.895	239.25
318.727	227.21	335.749	3603.43	351.501	239.45
319.347	235.50	335.880	3196.22	352.108	234.42
319.968	227.54	336.033	2473.61	352.715	237.90
320.591	226.57	336.218	1998.76	353.324	228.93
321.208	243.21	336.437	1592.49	353.931	241.14
321.826	225.51	336.688	1363.72	354.539	227.55
322.442	245.95	336.972	1106.42	355.143	254.01
323.056	233.05	337.295	907.82	355.740	243.89
323.672	237.78	337.656	761.18	356.344	236.87
324.286	240.68	338.058	614.20	356.950	236.26
324.900	233.49	338.501	514.37	357.557	233.85
325.516	238.96	338.982	429.76	358.161	242.25
326.128	239.51	339.495	369.41	358.762	243.83
326.747	221.84	340.038	319.79	359.366	235.43
327.357	264.59	340.609	274.93	359.972	234.76
327.960	241.51	341.196	265.43		
		Series 5			
361.835	238.38				
		Series 6			
79.943	103.70	86.711	111.50	91.474	116.40
81.687	105.83	88.325	113.18	93.014	117.72
83.394	107.96	89.912	114.84	94.530	119.19
85.068	109.75				

Table 3–1. (continued).

$\frac{T}{K}$	$\frac{Cp}{JK^{-1}mol^{-1}}$	$\frac{T}{K}$	$\frac{Cp}{JK^{-1}mol^{-1}}$	$\frac{T}{K}$	$\frac{Cp}{JK^{-1}mol^{-1}}$
		Series 7			
13.928	12.65	56.575	73.86	101.647	125.74
14.885	10.80	57.691	75.44	102.791	126.73
15.939	11.67	58.777	76.99	103.925	127.76
16.977	13.04	59.836	78.46	105.051	128.80
17.973	14.10	60.942	80.04	106.167	129.73
18.906	15.41	62.093	81.57	107.274	130.59
19.851	16.53	63.216	83.10	108.374	131.58
20.813	17.93	64.314	84.58	109.465	132.47
21.781	18.90	65.389	85.99	110.549	133.37
22.741	20.61	66.441	87.39	111.626	134.26
23.718	22.28	67.473	88.72	112.695	135.08
24.713	23.83	68.487	90.02	113.758	135.93
25.659	25.36	69.482	91.24	114.814	136.70
26.552	26.83	70.461	92.48	115.917	137.46
27.450	28.38	71.424	93.58	117.067	138.29
28.362	28.81	72.372	94.80	118.209	139.24
29.266	30.58	73.306	95.83	119.390	140.29
30.188	31.89	74.228	96.94	120.608	141.18
31.127	33.03	75.136	97.92	121.819	142.04
32.117	34.47	76.033	98.95	123.090	142.99
33.183	36.41	76.961	99.95	124.420	143.81
34.312	38.16	77.919	101.04	125.742	144.88
35.431	40.36	78.886	102.13	127.122	145.86
36.529	42.40	79.862	103.25	128.557	146.85
37.674	44.39	80.826	104.40	129.984	147.80
38.821	46.41	81.829	105.60	131.402	148.71
39.910	48.22	82.870	106.96	132.811	149.68
40.946	49.94	83.962	108.14	134.212	150.57
41.937	51.64	85.104	109.49	135.605	151.44
42.888	53.14	86.231	110.72	136.991	152.29
43.853	54.78	87.344	111.83	138.370	153.18
44.871	56.27	88.479	113.06	139.743	154.08
45.939	58.11	89.634	114.25	141.109	154.99
47.015	59.77	90.839	115.46	142.470	155.69
48.098	61.42	92.092	116.72	143.825	156.66
49.187	63.10	93.331	117.97	145.176	157.42
50.239	64.69	94.556	119.13	146.524	158.09
51.257	66.20	95.767	120.33	147.867	158.75
52.283	67.70	96.966	121.47	149.207	159.49
53.358	69.26	98.153	122.56	150.541	160.11
54.440	70.81	99.329	123.66	151.868	160.82
55.491	72.32	100.493	124.71	153.184	161.94

Table 3–1. (continued).

T / K	Cp / JK^{-1}mol^{-1}	T / K	Cp / JK^{-1}mol^{-1}	T / K	Cp / JK^{-1}mol^{-1}
154.487	163.70	189.452	206.54	226.296	195.11
155.776	165.65	190.805	208.62	227.614	195.56
157.053	167.80	192.152	210.86	228.931	195.94
158.323	169.79	193.492	213.04	230.245	196.14
159.587	171.34	194.826	215.61	231.556	196.72
160.846	173.39	196.153	218.00	232.865	197.34
162.101	175.12	197.473	220.73	234.123	197.50
163.351	176.48	198.787	223.60	235.327	197.76
164.596	177.85	200.092	226.78	236.529	198.24
165.836	178.97	201.390	229.84	237.730	198.59
167.070	180.22	202.681	233.35	238.928	199.16
168.301	181.23	203.962	237.50	240.125	199.25
169.526	182.51	205.235	241.79	241.321	199.71
170.746	183.61	206.498	246.68	242.514	200.04
171.962	184.93	207.752	251.64	243.706	200.52
173.173	186.20	209.007	242.90	244.896	200.87
174.379	187.36	210.302	201.06	246.084	201.11
175.581	188.83	211.639	193.39	247.270	201.55
176.778	190.04	212.981	193.29	248.454	202.04
177.971	191.34	214.323	192.91	249.637	202.30
179.160	192.90	215.661	192.82	250.819	202.80
180.344	193.92	216.999	192.94	251.999	202.94
181.525	195.75	218.334	193.19	253.179	203.68
182.753	197.15	219.667	193.45	254.359	204.33
184.030	198.79	220.997	193.69	255.540	204.74
185.355	200.54	222.325	194.09	256.728	204.81
186.727	202.42	223.651	194.49	257.922	204.33
188.093	204.34	224.974	194.70		
		Series 8			
180.013	168.42	207.666	181.24	234.025	191.79
182.042	169.48	209.586	182.07	235.868	192.40
184.061	170.52	211.501	182.76	237.706	193.34
186.072	171.49	213.409	183.51	239.539	194.10
188.074	172.52	215.311	184.23	241.367	194.86
190.067	173.49	217.207	185.13	243.190	195.62
192.053	174.46	219.098	185.88	245.009	196.38
194.030	175.34	220.982	186.51	246.823	197.10
195.999	176.25	222.861	187.27	248.632	198.03
197.961	177.12	224.735	188.08	250.436	198.66
199.916	178.00	226.603	188.78	252.236	199.58
201.864	178.72	228.465	189.41	254.032	200.24
203.805	179.52	230.324	190.21	255.823	200.98
205.738	180.38	232.177	191.04	257.609	201.63

Table 3–1. (continued).

$\frac{T}{K}$	$\frac{Cp}{JK^{-1}mol^{-1}}$	$\frac{T}{K}$	$\frac{Cp}{JK^{-1}mol^{-1}}$	$\frac{T}{K}$	$\frac{Cp}{JK^{-1}mol^{-1}}$
259.390	202.37	307.820	223.46	327.605	1621.52
261.167	203.06	309.347	224.60	327.899	1203.83
262.939	203.76	310.872	225.52	328.264	837.03
264.706	204.31	312.394	226.44	328.726	521.58
266.467	205.12	313.913	227.13	329.287	363.48
268.224	205.44	315.430	228.20	329.913	288.27
269.974	206.31	316.717	228.15	330.575	260.50
271.718	207.50	317.773	229.86	331.250	252.76
273.456	208.32	318.818	240.08	331.929	250.49
275.191	208.65	319.649	330.49	332.614	234.58
276.925	209.19	320.272	339.18	333.291	230.13
278.657	209.81	320.902	305.88	333.970	231.09
280.389	210.60	321.551	287.12	334.650	230.18
282.116	211.43	322.207	281.31	335.329	230.66
283.839	212.01	322.864	287.73	336.009	231.21
285.557	212.85	323.513	301.78	336.858	232.53
287.266	213.48	324.149	323.68	337.875	231.62
288.963	213.83	324.764	366.84	338.892	232.18
290.637	215.50	325.325	518.12	339.909	231.55
292.294	216.78	325.762	1050.87	341.153	232.71
293.957	217.94	326.106	1152.51	342.627	233.18
295.560	216.85	326.428	1289.01	344.098	233.67
297.097	218.12	326.692	2089.57	345.568	234.17
298.634	218.96	326.815	20656.90	347.036	234.85
300.166	219.64	326.879	5302.72	348.504	236.09
301.698	220.55	326.995	3847.08	349.970	237.40
303.229	221.42	327.151	2643.77	351.436	237.40
304.760	221.97	327.358	1936.94	352.897	237.48
306.291	222.50				

transition. Figure 3–5 illustrates a plot of ΔC_p as a function of T for the thermochromic phase transition. The enthalpy of transition is 5.54 kJ mol^{-1} and the entropy of transition is 16.5 J K^{-1} mol^{-1} ($\approx R$ ln 7.3). The temperature dependence of the transition entropy of $(IPA)CuCl_3$ is shown in Fig. 3–6. DSC measurement has also been carried out [7,10]. Their values are T_{trs} = 358.15 K, ΔH = 5.95 kJ mol^{-1} and ΔS = 18.3 J K^{-1} mol^{-1}. These values are about 10 % larger than those of the present work.

X–ray diffraction analysis [7] has shown that a drastic change in crystal structure is involved at the thermochromic phase transition. The low–temperature phase contains bibridged linear chains of $Cu_2Cl_6^{2-}$ dimers. The IPA cation is bound to a terminal chloride ion with a hydrogen bonding, N–H···Cl. On the other hand, the hydrogen bonding is weakened in the high–temperature phase, and thereby the terminal chloride ion bonded to IPA changes its bonding partner from IPA to Cu atom. The high–temperature phase contains tribridged linear chains of $(CuCl_3)_n^{n-}$. Each copper atom is coordinated by five and six chloride ions in the low– and high–temperature phases, respectively. The coordination geometry changes from a nearly square–pyramidal arrangement to an octahedral arrangement. The schematic structures of both the phases are drawn in Fig. 3–7. Furthermore the IPA cations are disordered in the high–temperature phase. The NMR data [7] support the disorder of the IPA cations. The origin of thermodynamic quantities of this phase transition, $\Delta_{trs}H$ and $\Delta_{trs}S$, is the sum of a change in the hydrogen bonding, a change in the coordination geometry, order–disorder of the IPA cations. The contribution of each factor is not clear at present time. ΔH and ΔS are only one third of the values observed in the case of $[M(dieten)_2]X_2$ described in Chapter 2.

Two anomalies are seen in the heat capacity of the quenched metastable phase in Fig. 3–4: one is a heat capacity jump at 155 K and the other is a higher order transition at 207.75 K. Figure 3–8 shows the spontaneous

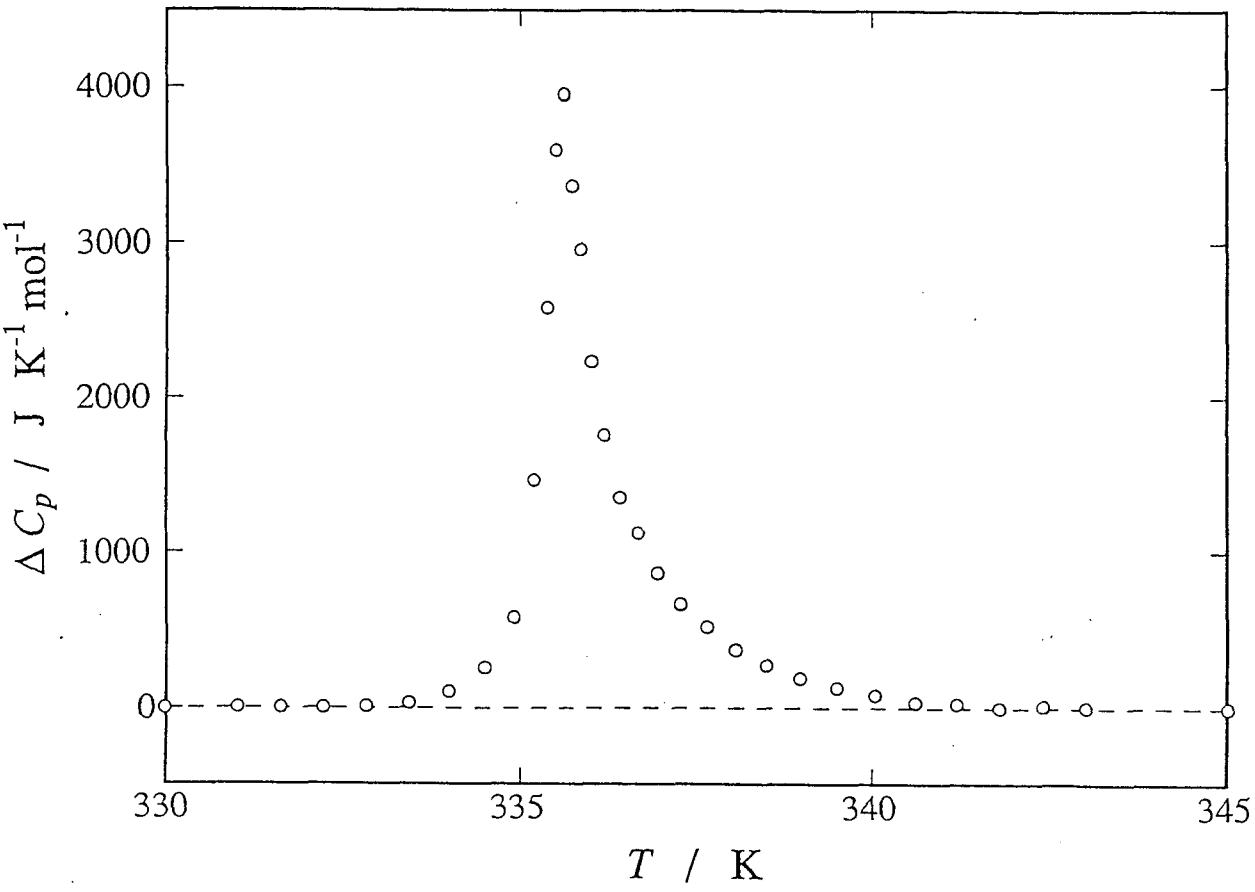

Fig. 3–5. Excess heat capacity of (IPA)$CuCl_3$ as a function of temperature.

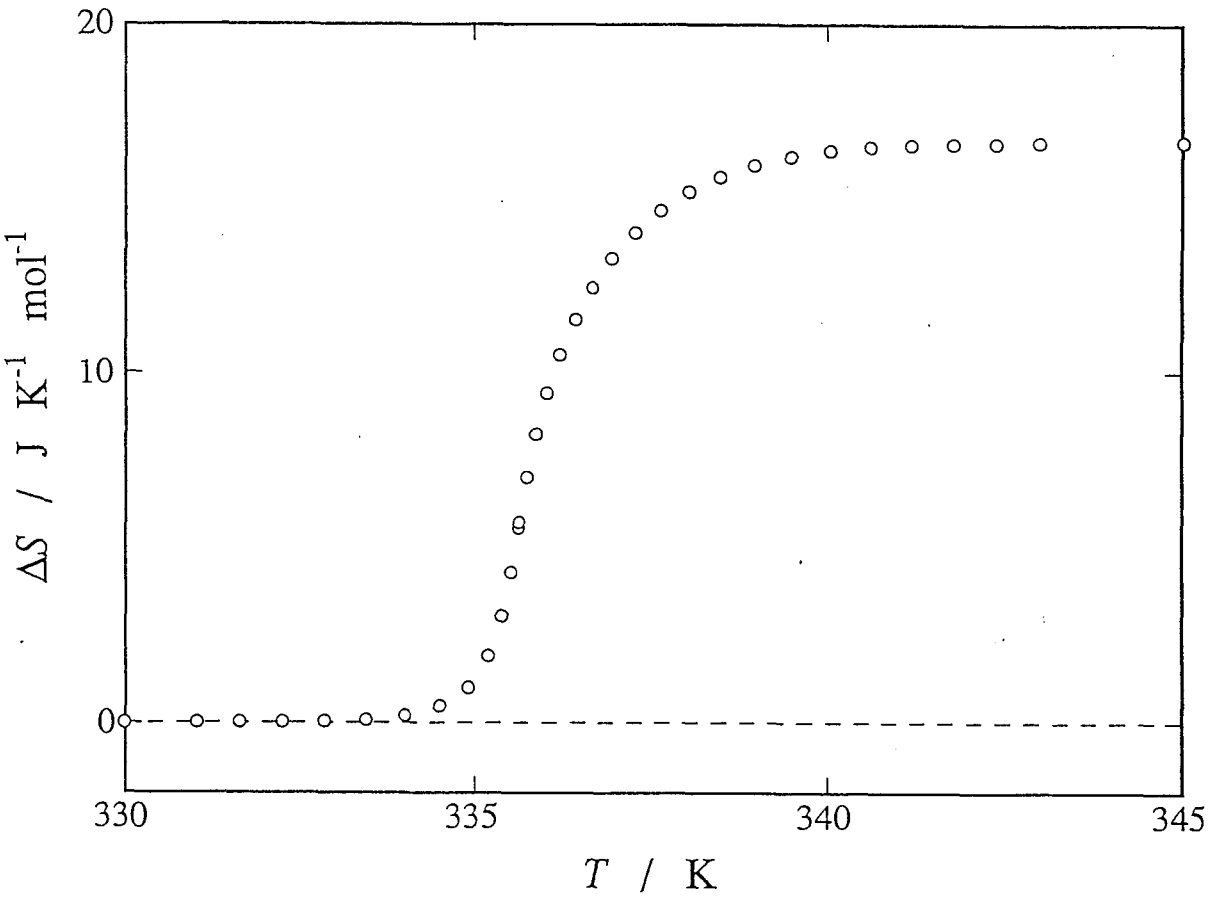

Fig. 3–6. Temperature dependence of the transition entropy of (IPA)$CuCl_3$.

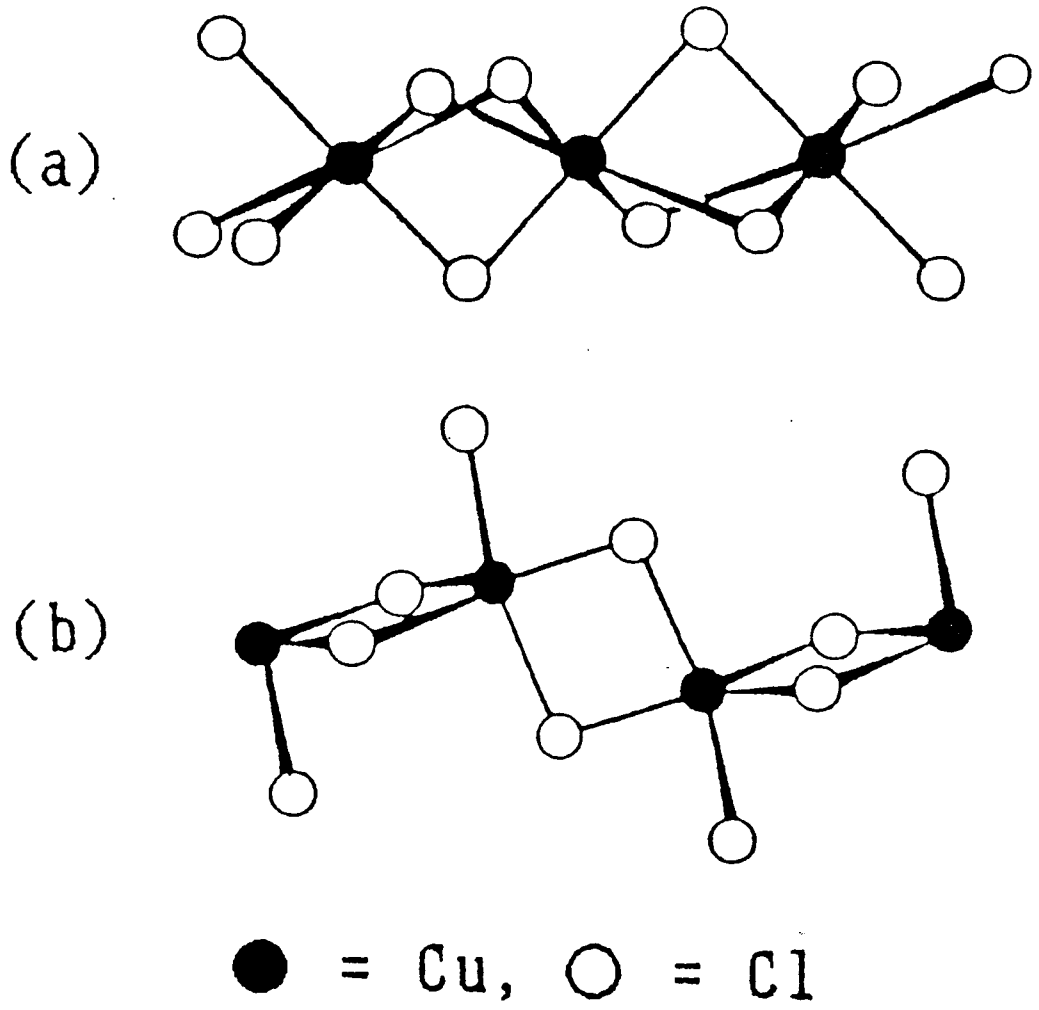

Fig. 3–7. Part of the schematic coordination geometry of the copper–chloride chains. (a) and (b) indicate the high– and low–temperature phase, respectively.

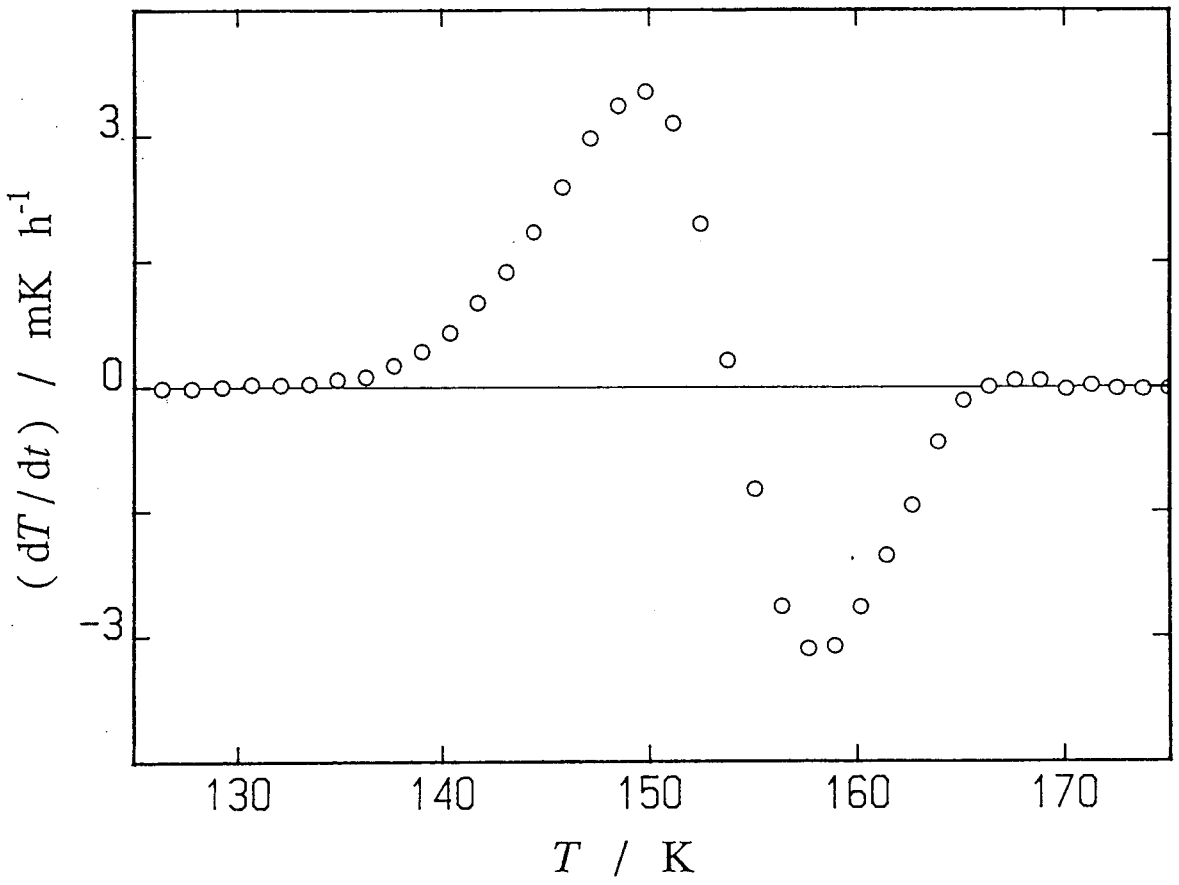

Fig. 3–8. Spontaneous temperature drift rates of (IPA)$CuCl_3$ observed at 25 minutes after each energy input of the heat capacity measurement.

temperature drift rates observed at 25 minutes after each energy input of the heat capacity measurement. Exothermic and endothermic drifts appeared in the temperature range 130 K to 170 K. The temperature drift rates changed from positive to negative at 154 K. This type of temperature drift and the heat capacity jump are characteristic of the glass transition [11].

In order to compare the molar enthalpy and the molar entropy at 0 K of the two phases, the effective frequency distribution method [9] was used to extrapolate the experimental values. We shall regard the highest temperature of the heat capacity measurements, 362.188 K, as a reference temperature. In the case of the stable phase, the values below 18.8 K were extrapolated and above that point the experimental values were integrated. In the case of the quenched phase, the values below 16.5 K were extrapolated, in the region from 16.5 K to 247.9 K the experimental values were integrated, and above that point the extrapolation was used again. Table 3–2 shows the calculated enthalpy and entropy. The residual entropy and the enthalpy difference at 0 K can be estimated from Table 3–2, because the reference states for both the phases are the identical one at 362.188 K.

$$\Delta S(0\ \mathrm{K}) = S(\text{stable}) - S(\text{quenched}) = -5.53\ \mathrm{J\ K^{-1}\ mol^{-1}} \qquad (3\text{–}1)$$

$$\Delta H(0\ \mathrm{K}) = H(\text{stable}) - H(\text{quenched}) = -3.55\ \mathrm{kJ\ mol^{-1}} \qquad (3\text{–}2)$$

The residual entropy due to the glass transition at 154 K is 5.53 J K^{-1} mol^{-1}, and this estimated value is close to R ln 2 ($\approx$ 5.76 J K^{-1} mol^{-1}).

The infrared spectra of the high–temperature phase and quenched metastable phase were measured at various temperatures. The results are shown in Fig. 3–9. No remarkable change can be seen in the spectra.

The glass transition and the higher order transition in the quenched phase were founded for the first time in this complex.

Table 3–2. Molar enthalpy and entropy of (IPA)$CuCl_3$ at 362.188 K.

phase	S(362.188 K) / J K^{-1} mol^{-1}	H(362.188 K) / kJ mol^{-1}
stable	352.198	61.525
quenched	346.655	57.978

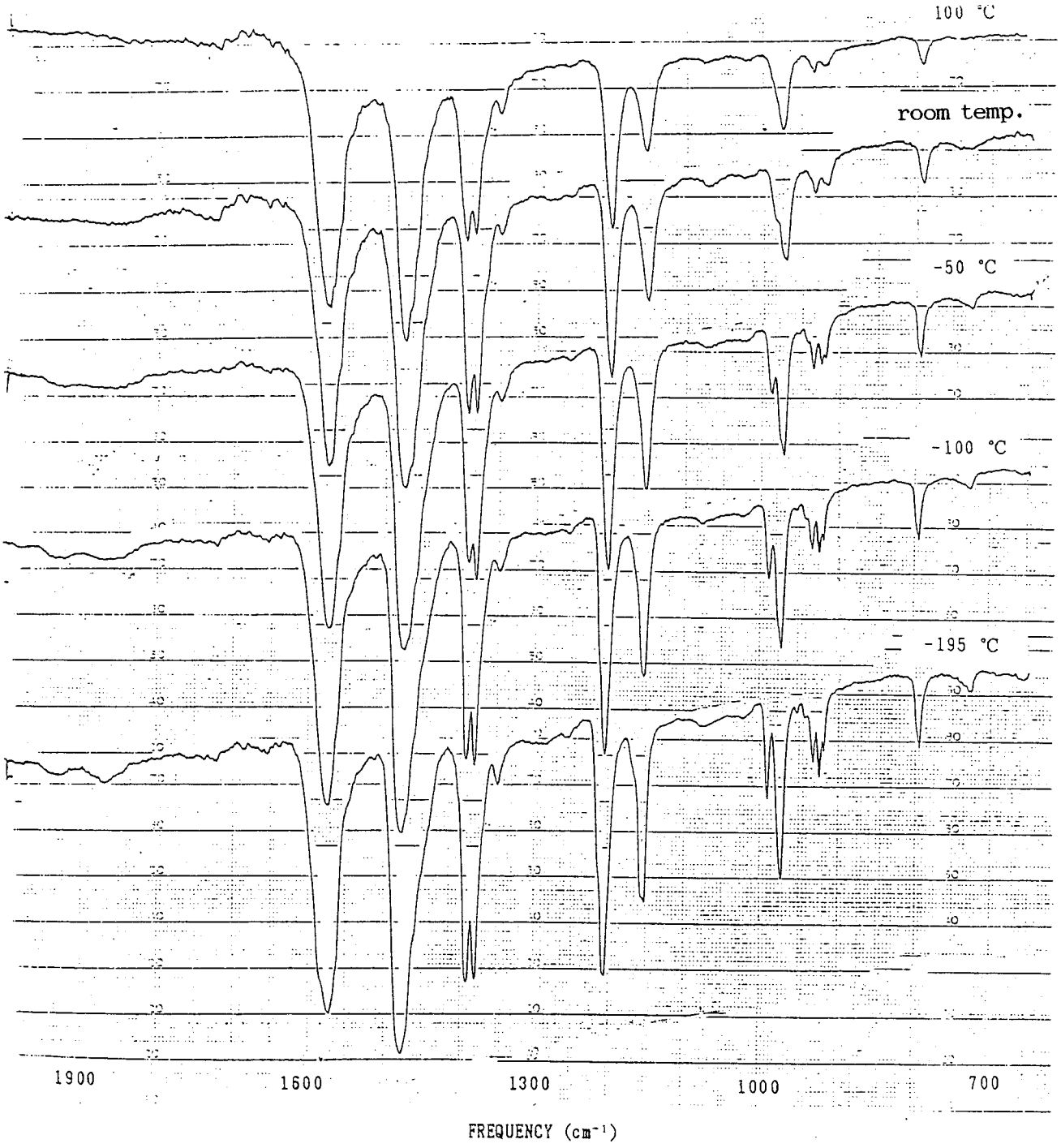

Fig. 3–9. Infrared spectra of the high–temperature phase and quenched metastable phase measured at various temperatures.

Standard thermodynamic functions derived from the calorimetric data are given in Table 3–3. For C_p values below 16 K, the effective frequency distribution method was used for the extrapolation.

Table 3–3. Standard thermodynamic functions for (IPA)$CuCl_3$ in the unit of J K^{-1} mol^{-1}; the values in parentheses are extrapolated.

T/K	C_p°	S°	$(H^\circ-H_0^\circ)/T$	$-(G^\circ-H_0^\circ)/T$
5	(3.64)	(1.475)	(1.077)	(0.398)
10	(9.21)	(5.883)	(3.880)	(2.004)
15	(13.06)	(10.353)	(6.304)	(4.049)
20	17.68	14.714	8.549	6.165
30	30.21	24.111	13.569	10.542
40	46.12	34.946	19.690	15.256
50	61.16	46.874	26.500	20.373
60	74.58	59.232	33.413	25.819
70	87.02	71.683	40.202	31.481
80	97.93	84.030	46.748	37.282
90	108.47	96.185	53.034	43.152
100	117.73	108.101	59.048	49.053
110	126.18	119.725	64.773	54.952
120	133.88	131.038	70.215	60.823
130	141.20	142.053	75.405	66.647
140	147.66	152.755	80.337	72.418
150	153.55	163.144	85.022	78.121
160	158.90	173.227	89.475	83.752
170	163.80	183.012	93.705	89.306
180	168.84	192.516	97.738	94.778
190	173.85	201.784	101.617	100.167
200	178.14	210.813	105.339	105.474
210	182.19	219.603	108.903	110.700
220	186.48	228.175	112.330	115.845
230	190.43	236.553	115.640	120.913
240	194.76	244.747	118.845	125.902
250	199.03	252.783	121.965	130.817
260	203.06	260.667	125.006	135.661
270	207.05	268.403	127.969	140.434
280	211.08	276.006	130.866	145.140
290	215.47	283.483	133.700	149.783
300	220.34	290.865	136.503	154.362
310	225.79	298.174	139.289	158.884
273.15	208.44	270.812	128.888	141.924
298.15	219.29	289.505	135.986	153.520

References to Chapter 3.

[1] K. Sone and Y. Fukuda, *Inorganic Thermochromism.* (Inorganic Chemistry Concepts, Vol. 10) Springer-Verlag, Berlin (1987).

[2] D. R. Bloomquist and R. D. Willett, *Coord. Chem. Rev.*, **47**, 125 (1982).

[3] R. L. Harlow, W. J. Wells, Ⅲ, G. W. Watt and S. H. Simonsen, *Inorg. Chem.*, **13**, 2106 (1974).

[4] R. D. Willett, J. A. Haugen, J. Lebsack and J. Morrey, *Inorg. Chem.*, **13**, 2510 (1974).

[5] J. R. Ferraro and A. T. Sherren, *Inorg. Chem.*, **17**, 2498 (1978).

[6] H. Remy and G. Laves, *Ber. Dtsch. Chem. A*, **66**, 401 (1933).

[7] S. A. Roberts, D. R. Bloomquist, R. D. Willett and H. W. Dodgen, *J. Am. Chem. Soc.*, **103**, 2603 (1981).

[8] M. Sorai, K. Kaji and Y. Kaneko, *J. Chem. Thermodyn.*, 24, 167 (1992).

[9] M. Sorai and S. Seki, *J. Phys. Soc. Jpn.*, **32**, 382 (1972).

[10] D. B. Bloomquist and R. D. Willett, *J. Am. Chem. Soc.*, **103**, 2615 (1981).

[11] H. Suga and S. Seki, *J. Non-Crystalline Solids*, **16**, 171 (1974).

Chapter 4. Thermochromic Phase Transition in $(IPA)_2CuCl_4$

§4-1. Introduction

The thermochromic complex, $(IPA)_2CuCl_4$ was first prepared by Remy and Laves in 1933 [1]. This sample exhibits a reversible color change with a phase transition in the solid state. Remy and Laves noted that the green crystals crystallized at room temperature change their color to yellow at about 330 K. $(IPA)_2CuCl_4$ shows a first-order phase transition at that temperature. Phase transitions are also induced by application of high pressure [2]. The crystal structures of both the green and the yellow phases were determined by Willett *et al.* [3-5]. The low-temperature phase is the triclinic of space group P1 with lattice constants of a = 7.245 Å, b = 14.588 Å, c = 21.738 Å, α = 87.08°, β = 103.59° and γ = 104.73° with Z = 6. The high-temperature phase is the orthorhombic of space group Pnma with lattice constants of a = 16.007 Å, b = 12.262 Å and c = 7.784 Å with Z = 4. Tetrachlorocuprate(Ⅱ) salts of a primary ammonium ion tend to crystallize in a two-dimensional layer structure with layers separated by the organic cations [6]. However, neither the green low-temperature phase [3] nor the yellow high-temperature phase [4] take such a two-dimensional sheets. In the green low-temperature phase, the reported structure is entirely complex. It is formed by two varieties of $CuCl_4^{2-}$ ribbons. These ribbons are illustrated in Fig. 4-1. Four unique copper atoms can be seen in Fig. 4-1. Each ribbon is sheathed by a layer of IPA cations with hydrogen bonding, N-H···Cl. One third of the $CuCl_4^{2-}$ anions has a square planar geometry and the other two thirds have a distorted tetrahedral configuration. On the other hand, in the yellow high-temperature phase, all copper atoms become equivalent and are isolated. The structure of $(IPA)_2CuCl_4$ in the high-

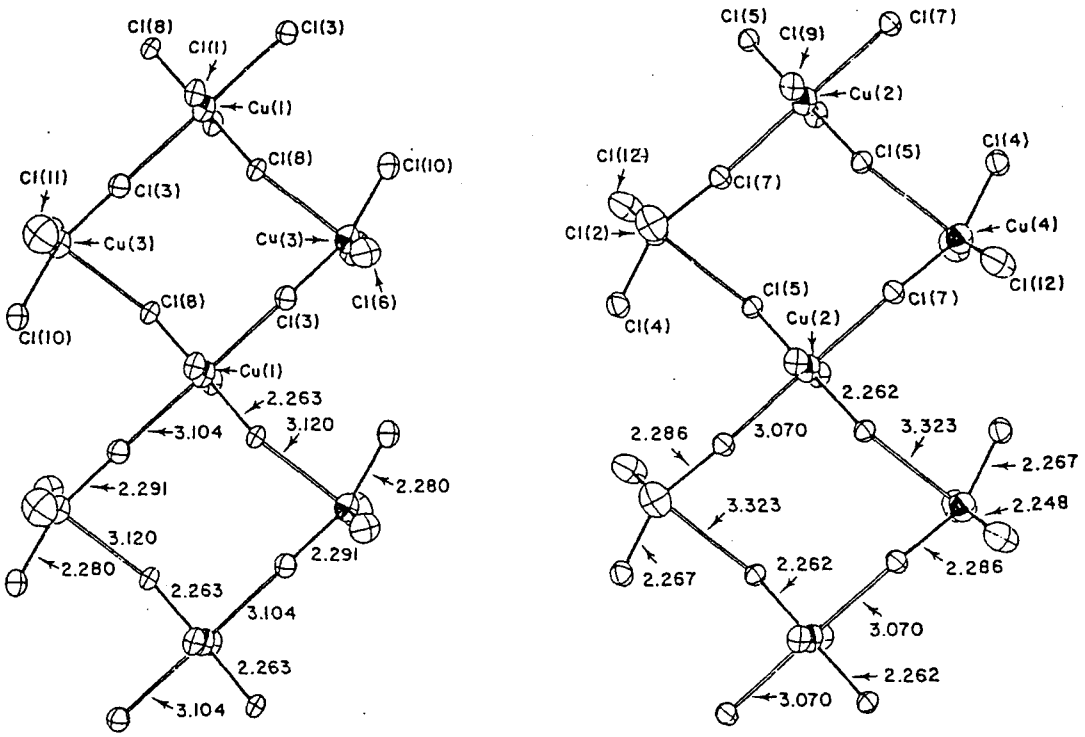

Fig. 4–1. An illustration of the two varieties of $CuCl_4^{2-}$ ribbons in $(IPA)_2CuCl_4$ (after ref. 4).

temperature phase is illustrated in Fig. 4–2. Two types IPA disordered in different ways can be seen in Fig. 4–2. One is a twofold hindered rotation of the IPA cations about the N–C bond axis and the other is a 135° flipping motion of the IPA cations about the N–C axis. The dynamic motions of the IPA cations are supported by the NMR studies [4]. As described above, the $CuCl_4^{2-}$ anions change the coordination geometries and the IPA cations show the onset of disordering through the thermochromic phase transition. The position of the absorption band for the d–d transitions is sensitive to the coordination geometry of $CuCl_4^{2-}$ [7]. The change of geometries in complex, $(IPA)_2CuCl_4$, is reflected on the color change. DSC studies [4] have revealed $\Delta_{trs}H$ = 2.9 kcal / mol and $\Delta_{trs}S$ = 9.0 cal / (mol deg).

§4–2. Experimental

4–2–1. Preparation of Sample

The complex $(IPA)_2CuCl_4$ was prepared according to the method of Remy *et al.* [1]. Stoichiometric amounts of isopropylammonium chloride and $CuCl_2$ were dissolved in ethanol. Ether was added to this solution until polycrystals were precipitated, then it was cooled down in the refrigerator. The green product was filtered and washed with ether three times and dried in vacuo at 360 K. The total yield of product was 42.05 %. The elemental analysis for the complex was good. *Anal.* Calcd. for $C_6H_{20}N_2CuCl_4$: C, 22.13; H, 6.19; N, 8.60. Found: C, 22.19; H, 6.20; N,8.56.

4–2–2. Differential Thermal Analysis (DTA)

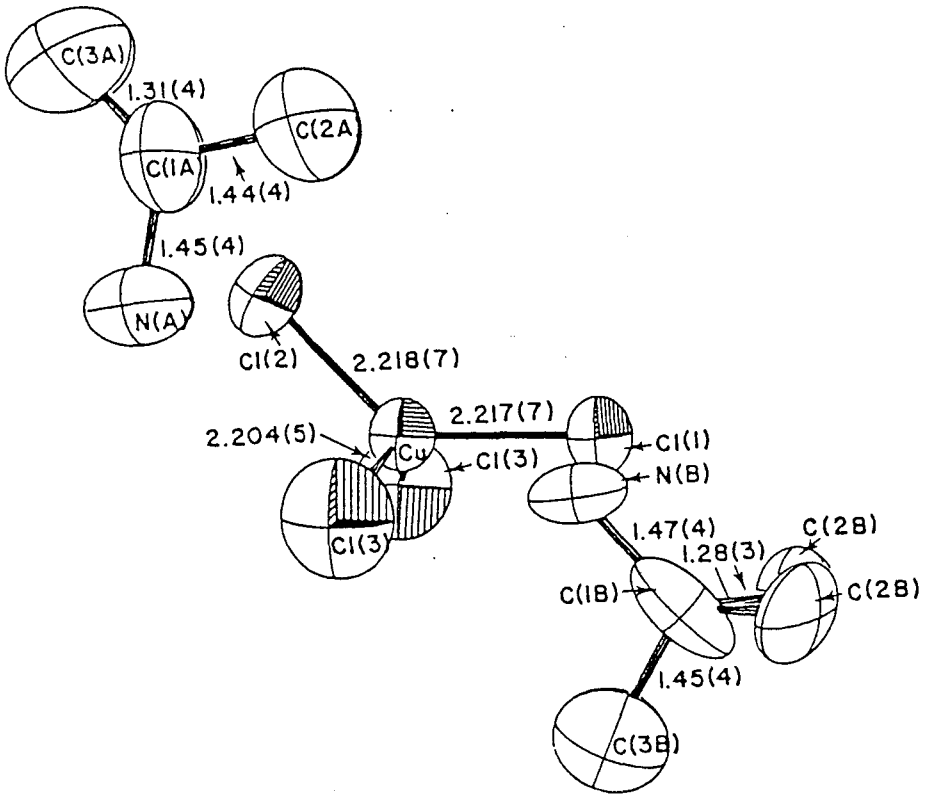

Fig. 4–2. An illustration of the isolated $CuCl_4^{2-}$ anion with IPA cations (after ref. 3).

Preliminary observation of the thermal properties of $(IPA)_2CuCl_4$ for heat capacity measurements was made with a home-built DTA apparatus.

4-2-3. Heat Capacity Measurements

Heat capacity measurements were carried out with an adiabatic calorimeter [8,9] in the 13-365 K range. The mass of sample loaded in a calorimeter cell made of gold-plated beryllium-copper alloy was 5.1401 g (0.015787 mol). A small amount of helium gas was sealed in the cell to aid the heat transfer.

4-2-4. Infrared Absorption Spectra

Variable temperature infrared spectra in the 3950-400 cm^{-1} range were recorded for Nujol mulls with an infrared spectrophotometer (Japan Spectroscopic Co. Ltd., FT/IR-3).

4-2-5. Visible and Ultraviolet Spectra

Visible and ultraviolet spectra were recorded in the 200-900 nm range with a uv-vis recording spectrophotometer (Shimadzu, UV-2000). Powdered sample on a filter paper was used to record spectra. Green stable and quenched yellow metastable powders were measured at room temperature.

§4-3 Results and Discussion

When the green sample was dried in vacuo at about 360 K, its color changed: upper part in a bottle was orange and the rest was yellow. While the warm sample was loaded in a DTA glass tube, the orange part changed its color to yellow. Color of the specimen in the DTA tube remained yellow when it was cooled down to room temperature. This fact indicates that the yellow high-temperature phase of $(IPA)_2CuCl_4$ is easily undercooled. The first cooling DTA run from 280 K to 81 K showed a peak at 249 K, and the subsequent heating run showed four endothermic peaks at 250, 287, 329 and 353 K. Furthermore the second cooling run showed three exothermic peaks at 345, 290 and 239 K, but no peak could be found at 330 K. The second heating run showed a complicated result: four endothermic peaks at 249, 285, 323 and 352 K and one exothermic anomaly at 270 K were found. The peak at about 330 K corresponds to the reported thermochromic phase transition temperature [1,10], and the other peaks have not been reported. It is considered that the peak at 330 K is a thermochromic phase transition, the peak at 352 K is a transition to other high-temperature phase, the peaks at 249 K and 285 K are transitions occurring between metastable phases, and an exothermic anomaly at 270 K is an enthalpy relaxation from a metastable phase to a stable one. The sample was annealed for a week at room temperature and the DTA measurements were carried out again. The cooling DTA run from 300 K to 77 K showed no peak and the successive heating run from 89 K to 350 K only showed a peak at 332 K. The next cooling run showed two peaks at 290 K and 239 K. The phase relationship of the sample became clear by DTA. The typical DTA charts are shown in Fig. 4-3. The upper and lower curves indicate the quenched and annealed samples, respectively.

When the sample was loaded in a calorimeter sample cell, the color of the crystal was yellow which is the color characteristic of the high-temperature phase. That is to say, the sample was in an undercooled phase.

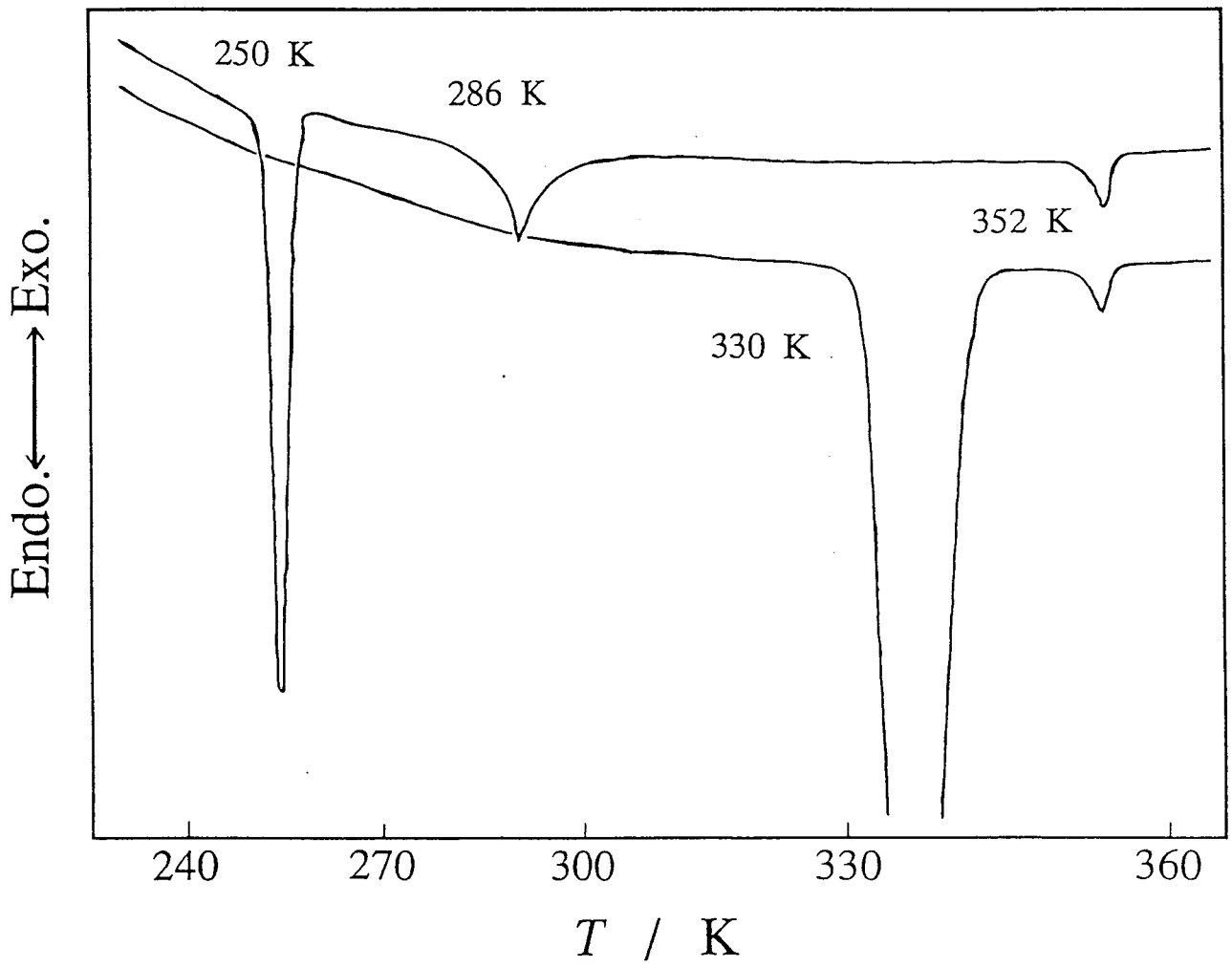

Fig. 4–3. Typical DTA runs of $(IPA)_2CuCl_4$. The upper line indicates the heating run of the quenched sample and lower line indicates that of annealed sample. The heating rates of both runs were about 3.5 K / min.

In order to get the green low-temperature phase, it was annealed at about 300 K for a week. To make sure that the sample was in the stable phase, heat capacity measurements in the temperature range from 230 K to 300 K were carried out. If there remains the yellow phase in the calorimeter cell, the anomalies at 250 K and 286 K would be found in the heat capacities. It took about a month to get completely the stable phase. During that period the sample was annealed at various temperatures and cooled down to liquid nitrogen temperature for several times and preliminary heat capacity measurements to check the phase relationship were carried out many times.

The heat capacity of the stable phases were measured from 11 K to 365 K. Heat capacities of both the stable and the metastable phases of $(IPA)_2CuCl_4$ are tabulated in Table 4–1 and shown in Fig. 4–4. As can be seen in Fig. 4–4, two transitions were found in the stable phase. The two transitions in the metastable states, which were detected by means of DTA, were not measured by the present adiabatic calorimetry.

Superheating was observed in the thermochromic phase transition. During the enthalpy measurement, the temperature of the sample decreased suddenly from 325.208 K to 321.958 K, although the Joule-energy was continuously supplied. The relationship between the supplied electric energy and the measured temperature is shown in Fig. 4–5. The lowest temperature in the superheating period was taken to be the transition temperature of the thermochromic phase transition, T_{trs} = 321.958 K. The initial and the final parts of the data were fitted with linear equations, independently. The results are as follows;

$$\Sigma\Delta E_i(T) = 17.118T - 5394.7 \quad \text{(initial part)}, \tag{4–1}$$

$$\Sigma\Delta E_f(T) = 17.264T - 5374.6 \quad \text{(final part)}. \tag{4–2}$$

Where, $\Sigma\Delta E_i(T)$ and $\Sigma\Delta E_f(T)$ indicate the sum of the electric power supplied

Table 4–1. Molar heat capacity of $(IPA)_2CuCl_4$ (relative molecular mass: 325.595).

$\frac{T}{K}$	$\frac{Cp}{JK^{-1}mol^{-1}}$	$\frac{T}{K}$	$\frac{Cp}{JK^{-1}mol^{-1}}$	$\frac{T}{K}$	$\frac{Cp}{JK^{-1}mol^{-1}}$
		Series 1			
229.258	319.50	245.386	333.63	261.156	347.61
231.069	320.99	247.156	335.43	262.886	349.33
232.874	322.59	248.921	336.81	264.612	351.05
234.675	324.31	250.682	338.39	266.334	352.92
236.472	325.80	252.438	340.23	268.052	354.59
238.264	327.36	254.189	341.93	269.766	355.85
240.051	329.03	255.937	343.32	271.476	357.27
241.834	330.59	257.681	344.83	273.182	359.10
243.612	332.04	259.420	346.47	274.885	360.70
		Series 2			
80.361	164.55	96.099	188.40	109.179	205.94
81.825	167.03	97.807	190.83	110.734	208.04
83.606	169.92	99.492	193.23	112.275	209.71
85.353	172.69	101.154	195.55	113.802	211.71
87.152	175.45	102.795	197.77	115.315	213.72
89.003	178.24	104.417	199.99	116.816	215.47
90.820	180.97	106.021	202.02	118.305	217.44
92.607	183.59	107.608	203.97	119.782	219.13
94.366	186.22				
		Series 3			
84.158	170.72	113.491	211.35	144.996	247.30
85.895	173.48	115.208	213.48	146.875	249.21
87.601	176.17	116.908	215.41	148.742	250.93
89.278	178.65	118.593	217.60	150.597	252.91
90.928	181.07	120.357	219.77	152.442	254.81
92.553	183.46	122.199	221.97	154.277	256.59
94.155	185.69	124.025	224.13	156.103	258.32
95.734	187.87	125.835	226.26	157.918	260.18
97.292	190.09	127.629	228.39	159.725	261.82
98.831	192.36	129.410	230.48	161.523	263.41
100.350	194.43	131.177	232.53	163.312	265.04
101.853	196.54	132.931	234.50	165.093	266.51
103.339	198.50	134.673	236.34	166.865	267.93
104.809	200.37	136.402	238.38	168.630	269.50
106.442	202.62	138.121	239.99	170.388	271.27
108.234	204.81	139.828	241.94	172.138	272.72
110.005	207.00	141.525	243.78	173.881	274.11
111.757	209.19	143.213	245.46	175.616	275.55

Table 4–1. (continued).

T / K	Cp / JK^{-1}mol^{-1}	T / K	Cp / JK^{-1}mol^{-1}	T / K	Cp / JK^{-1}mol^{-1}
177.345	277.19	179.154	278.81	181.041	280.39
		Series 4			
10.563	6.93	15.211	18.55	20.263	30.51
11.313	8.64	16.002	20.47	21.246	33.19
12.036	11.00	16.765	22.24	22.280	36.42
12.791	12.69	17.565	24.16	23.359	39.35
13.582	14.71	18.405	26.29	24.436	42.38
14.409	16.68	19.300	28.57	25.562	45.48
		Series 5			
23.805	40.42	65.160	137.93	112.366	210.02
24.980	43.79	66.720	140.83	113.706	211.49
26.112	46.95	68.238	144.59	115.035	213.21
27.254	50.06	69.718	146.31	116.354	214.80
28.440	53.38	71.163	148.92	117.800	216.68
29.669	56.70	72.576	151.48	119.371	218.69
30.937	60.27	73.960	153.78	120.929	220.69
32.242	63.83	75.317	156.12	122.475	222.59
33.593	67.47	76.649	158.31	124.010	224.34
34.989	71.20	77.957	160.50	125.533	226.19
36.332	74.69	79.345	162.82	127.046	228.00
37.589	77.89	80.882	165.34	128.549	229.79
38.776	80.88	82.466	167.75	130.042	231.54
39.902	83.67	84.096	170.50	131.525	233.14
41.080	86.48	85.774	173.19	132.999	234.77
42.399	89.73	87.423	175.77	134.465	236.45
43.786	93.09	89.044	178.28	135.922	237.88
45.181	96.45	90.639	180.64	137.371	239.42
46.549	99.51	92.211	182.97	138.812	241.09
47.927	102.61	93.762	185.13	140.245	242.73
49.319	105.69	95.291	187.27	141.671	243.89
50.653	108.59	96.801	189.27	143.199	245.55
51.970	111.36	98.293	191.45	144.827	247.11
53.308	114.25	99.766	193.56	146.447	248.83
54.632	117.08	101.223	195.56	148.058	250.68
55.912	119.73	102.663	197.59	149.661	252.17
57.152	122.24	104.088	199.38	151.256	253.85
58.357	124.59	105.500	201.14	152.843	255.30
59.530	126.96	106.897	203.04	154.423	256.81
60.673	129.25	108.282	204.85	155.995	258.44
61.988	131.89	109.655	206.56	157.560	259.84
63.554	134.93	111.016	208.32	159.119	261.27

Table 4–1. (continued).

T / K	Cp / JK^{-1}mol^{-1}	T / K	Cp / JK^{-1}mol^{-1}	T / K	Cp / JK^{-1}mol^{-1}
160.670	262.96	196.551	293.59	237.503	327.38
162.216	264.22	198.203	295.12	239.401	328.83
163.754	265.47	199.851	296.29	241.295	330.53
165.287	267.10	201.493	297.66	243.183	332.28
166.814	268.21	203.130	298.87	245.066	333.99
168.335	269.49	204.872	300.44	246.944	335.80
169.850	270.75	206.718	301.74	248.816	337.08
171.360	272.02	208.559	303.16	250.684	339.06
172.865	273.48	210.394	304.76	252.547	340.94
174.364	274.73	212.223	306.06	254.404	342.47
175.858	276.11	214.046	307.71	256.258	343.96
177.348	277.25	215.864	309.13	258.107	345.62
178.832	278.76	217.676	310.62	259.952	347.42
180.311	279.90	219.483	312.11	261.792	348.82
181.786	281.22	221.286	313.62	263.627	350.65
183.257	282.44	223.083	315.06	265.458	352.25
184.837	283.69	224.875	316.57	267.285	353.89
186.527	285.18	226.663	318.13	269.106	355.55
188.211	286.73	228.446	319.39	270.923	357.20
189.890	288.03	230.223	320.95	272.735	358.80
191.563	289.31	231.996	322.33	274.543	360.46
193.231	291.18	233.763	324.00	276.347	361.94
194.894	292.37	235.600	325.51	278.146	364.23
		S e r i e s 6			
241.161	329.79	270.799	356.89	297.459	381.18
243.049	331.67	272.612	358.52	299.197	383.05
244.933	333.20	274.421	360.15	300.937	384.40
246.811	335.04	276.224	361.92	302.679	385.99
248.685	336.53	278.024	363.46	304.419	387.62
250.554	338.35	279.819	365.15	306.157	389.17
252.418	339.99	281.610	366.78	307.892	390.81
254.277	341.67	283.396	368.40	309.624	392.67
256.131	343.45	285.178	369.98	310.990	393.93
257.981	345.18	286.954	371.65	311.990	394.83
259.826	346.83	288.726	373.08	312.990	395.60
261.667	348.40	290.490	374.64	313.988	396.29
263.503	350.29	292.242	376.64	314.985	397.27
265.334	351.83	293.982	378.17	315.981	398.06
267.161	353.68	295.719	379.11	316.975	398.83
268.982	355.05				

Table 4–1. (continued).

T/K	Cp/JK^{-1}mol^{-1}	T/K	Cp/JK^{-1}mol^{-1}	T/K	Cp/JK^{-1}mol^{-1}
		Series 7			
235.739	325.16	251.646	339.71	265.496	352.29
237.525	327.04	253.391	341.33	267.209	353.73
239.306	328.36	255.132	342.62	268.918	355.12
241.083	330.09	256.870	344.21	270.624	356.88
242.854	331.69	258.603	345.77	272.324	358.62
244.621	333.05	260.332	347.32	274.021	359.89
246.384	334.72	262.057	348.95	275.714	361.78
248.142	336.25	263.778	350.69	277.403	363.40
249.896	337.91				
		Series 8			
305.534	389.42	308.783	391.95	310.404	393.41
307.160	390.63				
		Series 9			
361.670	442.99	362.732	444.13		
		Series 10			
8.797	7.07	14.162	17.46	19.966	33.50
9.874	9.86	15.065	19.88	20.952	36.30
10.684	8.02	16.018	22.52	21.991	39.31
11.485	10.01	16.999	25.19	23.031	42.35
12.420	12.53	18.004	27.99	24.047	45.26
13.318	15.14	18.992	30.80		
		Series 11			
25.093	48.12	40.340	88.70	55.806	122.99
26.152	51.17	41.622	91.77	57.235	125.85
27.251	54.21	42.841	94.68	58.618	128.61
28.442	57.60	44.007	97.47	59.959	131.14
29.683	61.01	45.189	100.22	61.294	133.73
30.923	64.43	46.390	102.86	62.624	136.34
32.204	67.99	47.622	105.65	63.921	138.73
33.525	71.49	48.884	108.38	65.186	141.11
34.840	74.98	50.180	111.20	66.422	143.42
36.218	78.51	51.508	114.05	67.632	145.56
37.615	82.00	52.865	116.94	68.818	147.74
38.986	85.37	54.325	119.99	69.981	149.85

Table 4–1. (continued).

$\frac{T}{K}$	$\frac{Cp}{JK^{-1}mol^{-1}}$	$\frac{T}{K}$	$\frac{Cp}{JK^{-1}mol^{-1}}$	$\frac{T}{K}$	$\frac{Cp}{JK^{-1}mol^{-1}}$
71.123	151.84	115.203	217.48	172.839	285.11
72.245	153.71	116.840	219.76	174.552	286.81
73.457	155.89	118.462	221.87	176.258	288.69
74.757	158.11	120.071	223.92	177.956	290.63
76.033	160.20	121.745	226.06	179.648	292.62
77.289	162.37	123.485	228.35	181.333	294.39
78.523	164.30	125.209	230.44	183.011	296.28
79.739	166.41	126.920	232.53	184.682	298.10
80.938	168.21	128.618	234.74	186.347	300.11
82.119	170.10	130.303	236.91	188.006	302.05
83.421	172.26	131.975	238.86	189.658	303.92
84.839	174.43	133.636	240.86	191.305	305.87
86.237	176.66	135.286	242.73	192.945	307.58
87.615	178.67	137.002	244.85	194.579	309.32
88.973	180.84	138.783	246.88	196.327	311.56
90.314	182.90	140.553	249.03	198.189	313.64
91.636	185.11	142.376	251.19	200.043	315.86
92.941	187.16	144.252	253.27	201.890	318.21
94.231	189.17	146.115	255.48	203.730	320.31
95.507	191.01	147.966	257.64	205.562	322.61
96.769	192.70	149.806	259.65	207.387	324.91
98.018	194.57	151.635	261.73	209.204	327.09
99.255	196.23	153.454	263.73	211.015	329.40
100.480	197.98	155.262	265.78	212.818	331.75
101.693	199.69	157.060	267.87	214.614	334.20
102.896	201.40	158.848	269.87	216.403	336.56
104.088	203.24	160.627	271.80	218.185	338.92
105.394	204.68	162.397	273.70	219.960	341.40
106.810	206.59	164.158	275.53	221.730	343.89
108.214	208.41	165.910	277.43	223.493	346.24
109.604	210.28	167.654	279.27	225.251	348.96
110.983	212.06	169.391	281.08	227.003	352.22
112.350	213.89	171.118	283.71	228.754	355.30
113.705	215.58				
		Series 12			
315.964	398.16	322.450	524.99	324.987	402.37
317.612	399.70	322.680	486.77	325.340	402.41
319.257	401.03	322.955	452.64	325.693	402.11
320.899	402.29	323.264	426.79	326.045	403.05
322.538	403.59	323.594	414.12	326.397	403.38
322.018	587.60	323.935	408.30	326.927	403.56
322.126	573.35	324.283	401.72	327.633	404.00
322.268	551.03	324.635	402.45	328.791	405.16

Table 4-1. (continued).

T / K	Cp / $JK^{-1}mol^{-1}$	T / K	Cp / $JK^{-1}mol^{-1}$	T / K	Cp / $JK^{-1}mol^{-1}$
330.399	406.41	344.775	416.98	355.334	1191.85
332.006	407.79	346.360	419.20	355.761	1042.47
333.611	409.07	347.941	420.90	356.322	438.57
335.214	410.24	349.518	423.92	357.000	439.06
336.814	411.75	351.085	431.44	358.112	440.32
338.411	412.75	352.622	465.30	359.655	440.75
340.006	413.91	353.697	525.62	361.195	442.71
341.598	415.34	354.309	605.76	362.732	444.33
343.188	416.52	354.868	781.65	364.267	446.07
		Series 13			
197.794	313.20	236.297	360.54	283.734	406.75
199.673	315.47	238.257	363.09	285.449	430.74
201.544	317.57	240.336	365.64	287.103	446.69
203.408	320.00	242.431	367.95	288.773	456.66
205.264	322.27	244.550	370.14	290.534	435.37
207.112	324.54	246.696	371.30	292.472	380.15
208.953	326.95	248.880	373.25	294.463	378.22
210.787	329.38	251.096	471.99	296.395	383.62
212.614	331.81	252.818	724.22	298.292	390.20
214.434	334.38	254.771	397.18	300.061	389.46
216.247	336.76	257.347	361.99	301.717	387.80
218.054	339.35	259.951	356.67	303.370	387.72
219.853	342.08	262.510	354.83	305.019	389.12
221.647	344.86	265.166	353.05	306.665	391.08
223.439	348.43	267.879	352.43	308.307	391.80
225.237	351.68	270.580	352.11	309.944	393.44
227.056	351.64	273.178	355.55	311.578	394.95
228.894	351.94	275.607	361.75	313.206	396.67
230.743	353.26	277.840	370.27	314.831	398.28
232.596	355.29	279.919	375.03	316.675	399.50
234.449	358.33	281.882	380.74		
		Series 14			
336.088	411.61	345.137	419.41	353.422	511.95
337.905	413.17	346.934	421.70	354.036	571.57
339.719	414.58	348.724	425.76	354.604	696.18
341.529	416.02	350.503	433.90	355.099	950.98
343.335	417.55	352.248	464.09		
		Series 15			

Table 4–1. (continued).

T/K	Cp/JK^{-1}mol^{-1}	T/K	Cp/JK^{-1}mol^{-1}	T/K	Cp/JK^{-1}mol^{-1}
275.964	398.09	307.453	387.25	321.748	1370.05
278.266	395.61	309.423	391.43	322.302	1050.66
280.681	396.36	311.339	394.03	323.414	542.91
283.114	396.49	313.224	397.97	325.105	409.75
285.660	402.05	315.095	398.38	326.937	405.45
288.326	413.73	316.952	399.49	328.770	406.46
291.171	372.65	318.803	401.93	330.600	409.34
294.910	371.20	320.677	371.14	332.424	413.18
297.848	360.19	322.206	675.13	334.246	410.63
300.623	362.16	321.616	3534.18	336.068	411.56
303.136	368.17	321.547	2074.60	337.887	413.37
305.382	380.39				
		Series 16			
193.906	308.36	198.210	313.58	200.346	316.18
196.063	311.02				
		Series 17			
340.411	415.96	342.223	417.21	344.031	419.61
		Series 18			
309.100	392.44	322.118	400.09	334.954	410.86
310.970	393.78	323.963	401.87	336.775	412.39
312.836	394.73	325.805	404.40	338.593	414.08
314.699	395.82	327.640	406.62	340.407	415.62
316.559	396.69	329.475	406.44	342.216	417.38
318.415	397.69	331.306	409.47	344.022	419.43
320.268	398.58	333.131	411.22	345.822	422.23
		Series 19			
185.089	298.22	191.654	305.95	198.124	313.64
187.288	300.84	193.821	308.47	200.260	316.16
189.477	303.53	195.977	311.15		
		Series 20			
340.309	415.67	343.918	419.41	347.503	426.21
342.116	417.33	345.715	422.16		

Table 4–1. (continued).

T / K	Cp / JK^{-1}mol^{-1}	T / K	Cp / JK^{-1}mol^{-1}	T / K	Cp / JK^{-1}mol^{-1}
		Series 21			
319.988	650.45	320.653	425.17	321.865	400.45
320.142	697.39	320.801	428.09	322.216	401.48
320.206	785.76	320.950	432.98	322.568	400.46
320.042	414.74	321.104	414.40	322.921	401.55
320.201	417.16	321.261	422.22	323.274	401.42
320.354	425.88	321.513	399.94	323.628	401.14
320.505	424.81				
		Series 22			
324.725	401.92	342.925	420.22	354.737	779.61
326.563	403.60	344.723	422.65	355.212	948.11
328.398	405.74	346.517	424.47	355.769	464.87
330.228	407.90	348.305	428.46	356.443	440.44
332.049	415.06	350.079	437.67	357.650	443.24
333.865	411.38	351.823	460.87	359.386	440.64
335.683	411.99	352.998	500.39	361.121	442.84
337.500	413.82	353.619	542.52	362.851	445.09
339.313	415.32	354.203	630.53	364.578	447.17
341.121	417.41				

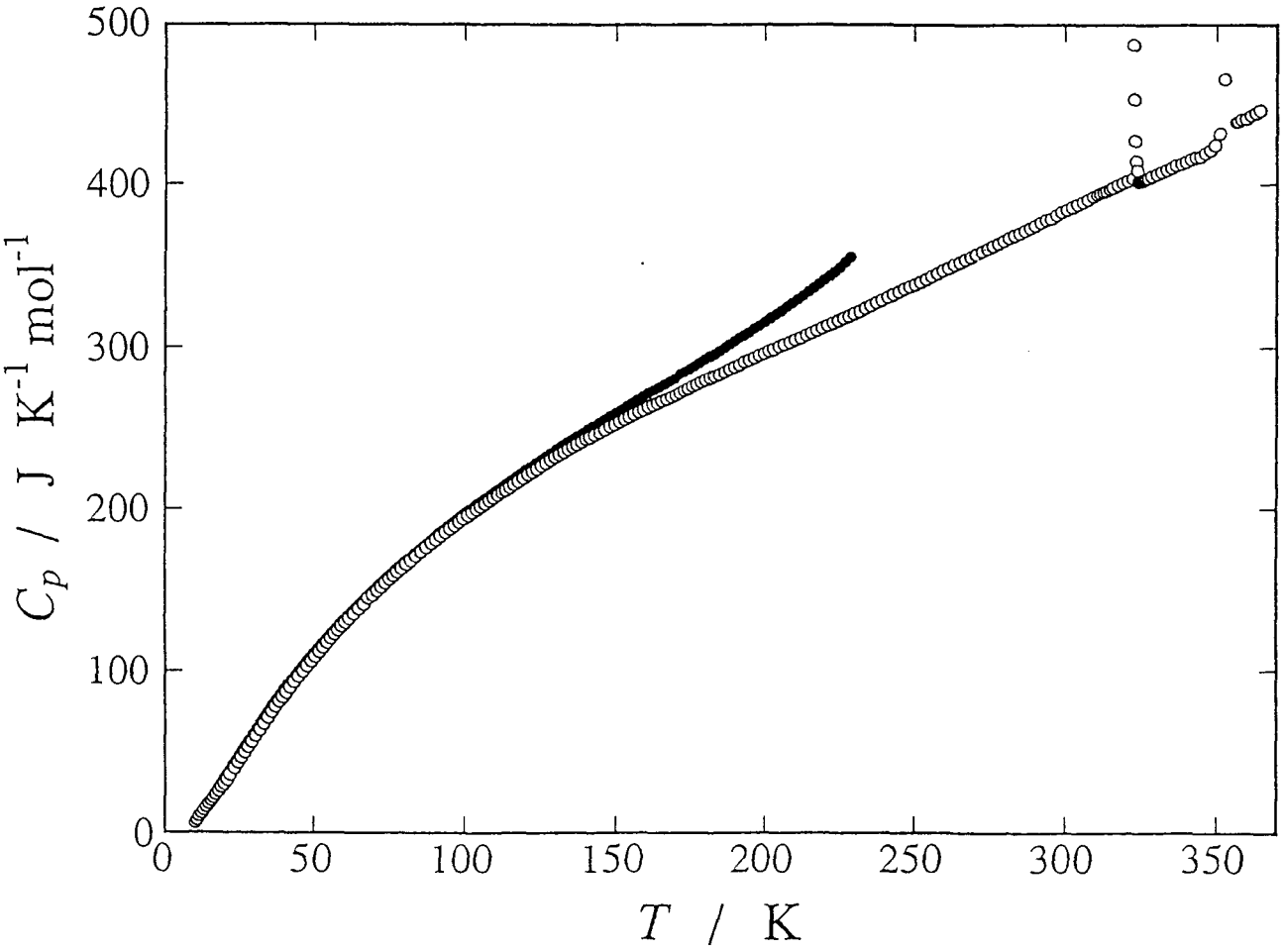

Fig. 4–4. Molar heat capacities of $(IPA)_2CuCl_4$. Open circles show the data of stable phase, while filled circles show the data of metastable phase.

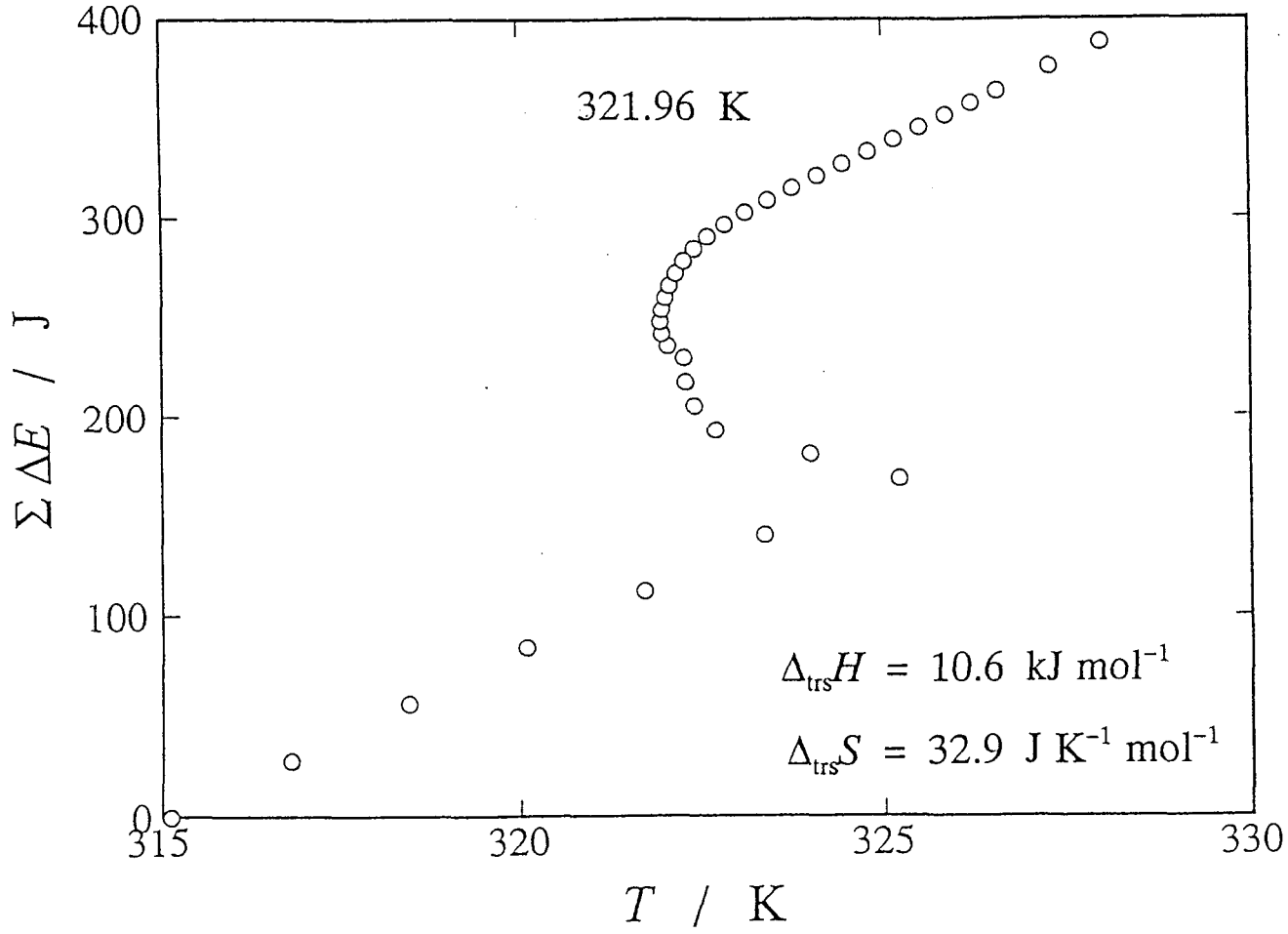

Fig. 4–5. Relationship between the supplied electric power and the temperature. $\Sigma\Delta E$ on the ordinate indicates the sum of the electric power supplied to the sample and sample container.

to the sample and the sample container. The transition enthalpy can be estimated from the difference between two values at T_{trs}, and the amount of sample in the calorimeter cell. Since $\Delta(\Sigma\Delta E)$ at T_{trs} is 167.12 J and a mole factor is 63.344 mol^{-1}, then $\Delta_{trs}H$ amounts to 10.59 kJ mol^{-1}. An enthalpy of transition divided by a transition temperature gives an entropy of transition: in this case, $\Delta_{trs}S$ = 32.88 J K^{-1} mol^{-1}. Based on DSC study, Bloomquist *et al.* [4] have reported $\Delta_{trs}H$ = 12.1 kJ mol^{-1} and $\Delta_{trs}S$ = 37.7 J K^{-1} mol^{-1}. These values are by 14.5 % larger than those of the present work.

Figure 4–6 shows the excess heat capacity of the transition occurring at 355.33 K. To calculate this curve, we determined the normal heat capacity curves. These curves were determined by the least squares fitting method for the heat capacity data in the vicinity of this transition peak. Two straight lines were determined by use of eight C_p data points from 335.2 K to 346.4 K and four points from 359.7 K to 364.3 K, independently. These two straight lines have been connected vertically at the transition temperature, 355.33 K. Subtraction of the normal heat capacities from the observed values gives the excess heat capacities, ΔC_p, due to the phase transition illustrated in Fig. 4–6. The enthalpy of transition, $\Delta_{trs}H$, and the entropy of transition, $\Delta_{trs}S$, were determined by integrations of ΔC_p with respect to T and ln T, respectively, to give $\Delta_{trs}H$ = 1.026 kJ mol^{-1} and $\Delta_{trs}S$ = 2.89 J K^{-1} mol^{-1}.

Heat capacity measurements for the quenched metastable phase were carried out from 9 K to 228.8 K. It was impossible to measure the heat capacity above that temperature. The temperature drift rate after an energy input had large positive values which made it meaningless to determine the heat capacity. That drift was due to an enthalpy relaxation from the metastable to the stable phases. It has been proved that there exist two phase transitions in the temperature range from 220 K to 310 K by DTA measurements carried out prior to heat capacity measurements. If there were no transition, it should have been possible to interpolate the heat capacities

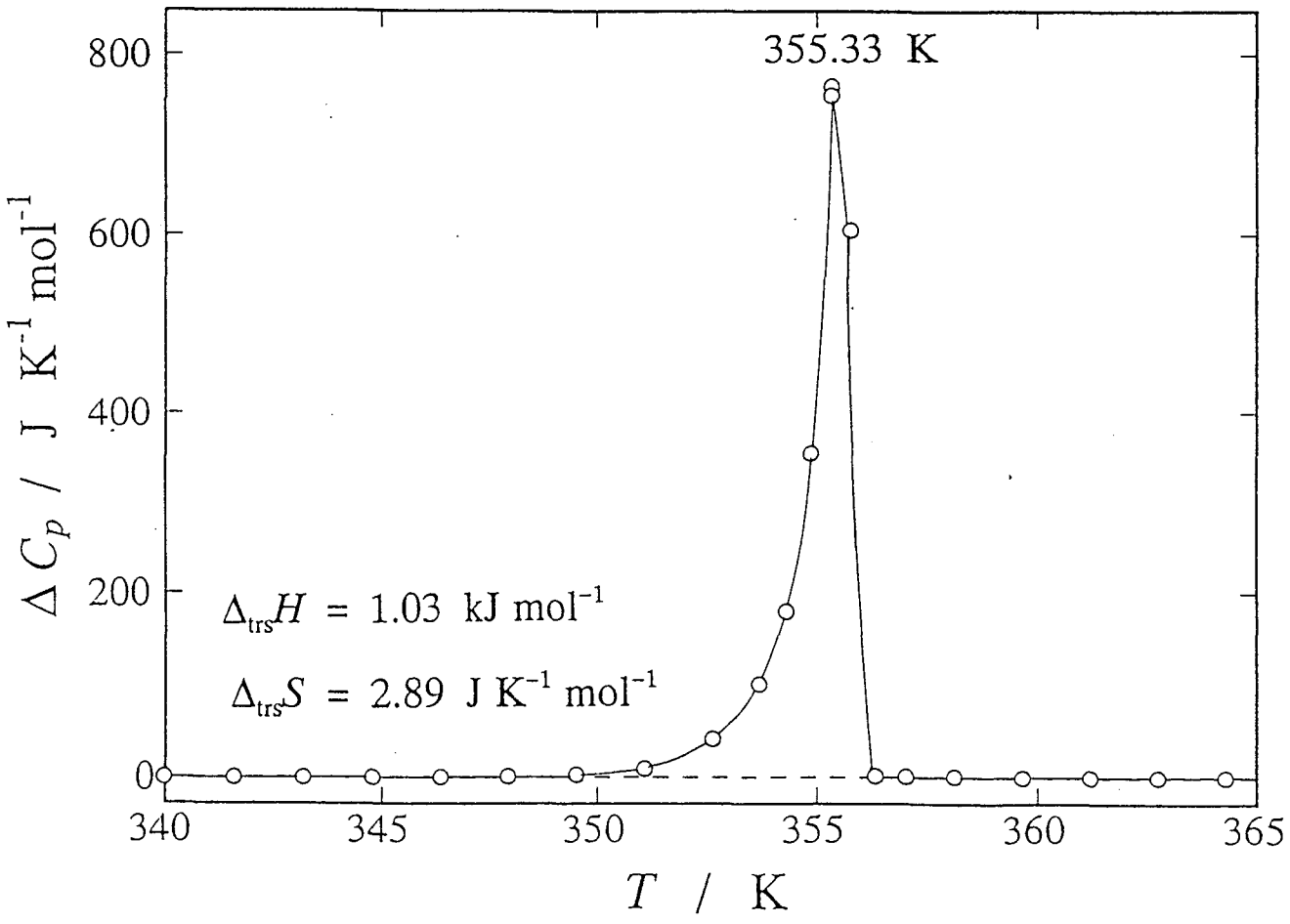

Fig. 4–6. Excess heat capacity, ΔC_p, of $(IPA)_2CuCl_4$.

by use of the effective frequency distribution method [11] as in Chapter 3. Once the interpolation were achieved, not only enthalpy but also entropy could be estimated. In order to get the enthalpy relationship between the stable phase and the metastable phase, the molar enthalpy from 201 K to 339.5 K was measured by a continuous heating. The sample was in the stable phase at 339.5 K. H°(339.5 K) - H°(201 K) is equal to 54.31 kJ mol^{-1}.

To compare the molar enthalpies of between the stable and the metastable phases at 0 K, the molar enthalpies at 339.5 K through two paths were evaluated from the heat capacity data: one passes through the stable phase and the other through the metastable phase. On extrapolating the heat capacities from 15 K down to 0 K, the data were fitted to polynomial functions. The actual functional form of each polynomial is as follows.

$$C_p(\mathrm{J\ K^{-1}\ mol^{-1}}) = \mathrm{A}(T/\mathrm{K})^3 + \mathrm{B}(T/\mathrm{K})^5 + \mathrm{C}(T/\mathrm{K})^7 + \mathrm{D}(T/\mathrm{K})^9 \qquad (4\text{–}3)$$

$$\mathrm{A} = 8.93673 \times 10^{-3}$$
$$\mathrm{B} = -2.10231 \times 10^{-5}$$
$$\mathrm{C} = 2.46651 \times 10^{-8}$$
$$\mathrm{D} = -1.08285 \times 10^{-11}$$

for the stable phase, and

$$\mathrm{A} = 9.29762 \times 10^{-3}$$
$$\mathrm{B} = -1.96653 \times 10^{-5}$$
$$\mathrm{C} = 2.07512 \times 10^{-8}$$
$$\mathrm{D} = -8.41532 \times 10^{-12}$$

for the metastable phase. The calculated values are given in Table 4–2. The

Table 4–2. Evaluation of the molar enthalpy of $(IPA)_2CuCl_4$.

stable phase		metastable phase	
T / K	H / kJ mol^{-1}	T / K	H / kJ mol^{-1}
0 - 14.022	0.0640	0 - 14.593	0.0787
14.022 - 339.50	95.196	14.593 - 201.00	36.398
		201.00 - 339.50	54.313
molar enthalpy at 339.50 K	95.260		90.790

enthalpies at 339.50 K determined through the stable and the metastable phases are 95.260 kJ mol^{-1} and 90.790 kJ mol^{-1}, respectively. The difference between these two values provides the enthalpy difference at 0 K. The quenched metastable phase is thus at 4.47 kJ mol^{-1} above the stable phase at 0 K.

$(IPA)_2CuCl_4$ changes its coordination geometry drastically through the thermochromic phase transition [3,4]. As described in §4–1, it contains two kinds of ribbons of $CuCl_4^{2-}$ anions in the green low–temperature phase. In the yellow high–temperature phase, it contains discrete isolated distorted tetrahedral $CuCl_4^{2-}$ anions. As in the case of $(IPA)CuCl_3$, this phase of $(IPA)_2CuCl_4$ was easily undercooled down to liquid helium temperature. Thermochromic complexes which change their coordination geometries through the phase transition tend to have metastable phases.

The electronic spectra were recorded over the range of 200 to 900 nm on a Shimadzu UV–2200. The results are shown in Fig. 4–7. The spectrum of the yellow high–temperature phase at room temperature was obtained as follows, first the green low–temperature phase was heated up with a heat gun and cooled down to room temperature, then set up in the spectrometer and the spectrum measured. As can be seen in Fig. 4–7, there are two features in the spectra, three overlapped bands in the range of 200 to 500 nm and another band at about 800 nm. The bands recorded around 400 nm are assigned to be the charge–transfer band and the other is the d–d band [7]. The absorption bands of the two phases are the same in the range of 200 to 500 nm (the charge–transfer bands), but the bands in the range of 600 to 900 nm (the d–d band) are significantly different. This change in the d–d absorption is the origin of the color change.

Standard thermodynamic functions derived from the present calorimetric data are given in Table 4–3. For C_p values below 14 K, the polynomial function was used for the extrapolation.

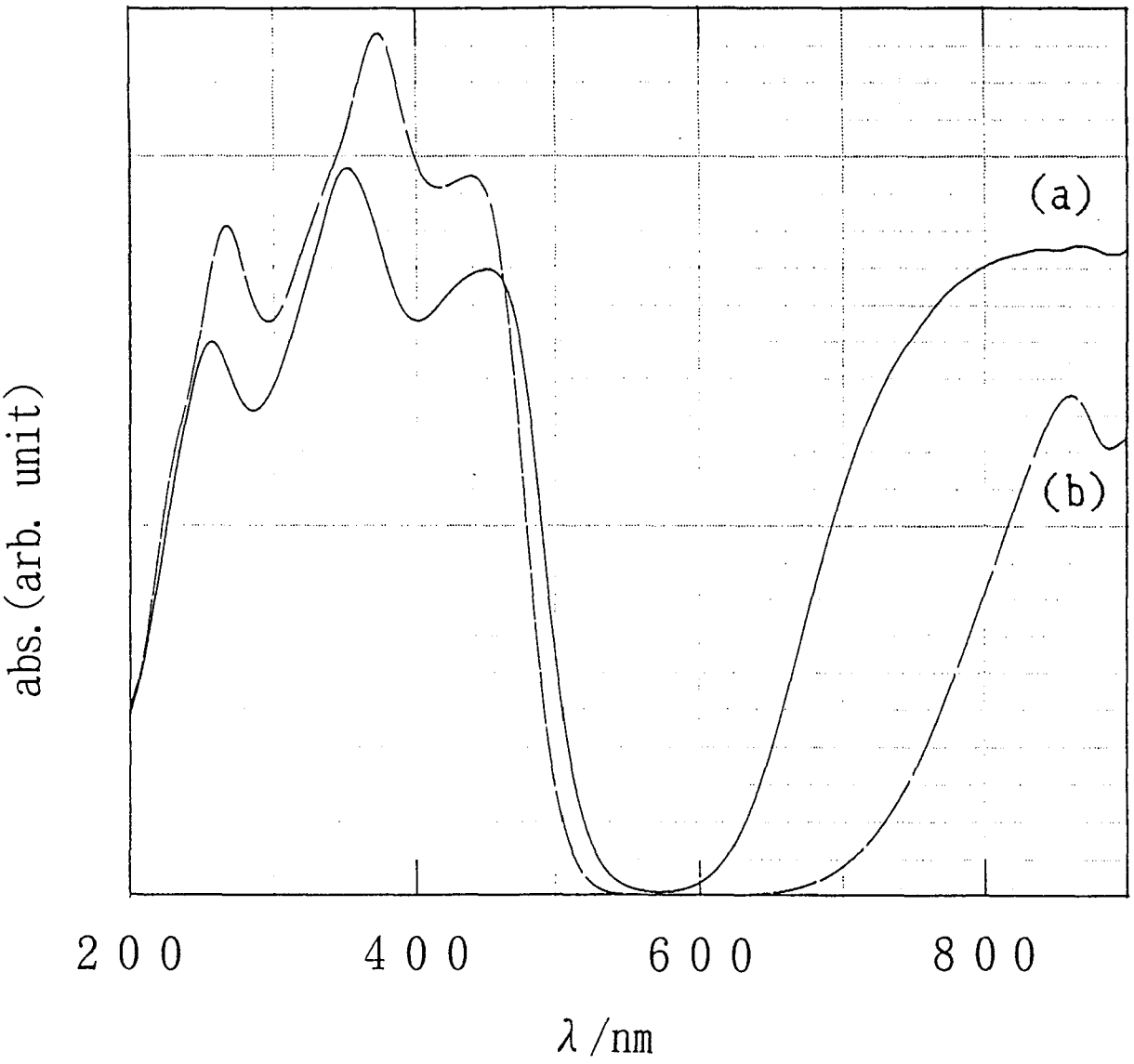

Fig. 4-7. Uv-vis spectra for $(IPA)_2CuCl_4$ at room temperature. (a) and (b) indicate the green and yellow phases, respectively.

Table 4–3. Standard thermodynamic functions for $(IPA)_2CuCl_4$ in the unit of J K^{-1} mol^{-1}; the values in parentheses are extrapolated.

T/K	$C_p^\bullet$	$S^\bullet$	$(H^\bullet-H_0^\bullet)/T$	$-(G^\bullet-H_0^\bullet)/T$
5	(1.05)	(0.360)	(0.269)	(0.091)
10	(7.08)	(2.592)	(1.914)	(0.679)
15	18.00	7.417	5.365	2.052
20	29.98	14.272	10.058	4.214
30	57.63	31.648	21.307	10.340
40	83.91	51.911	33.748	18.163
50	107.17	73.190	46.152	27.038
60	127.90	94.594	58.080	36.514
70	146.82	115.781	69.459	46.322
80	163.90	136.521	80.211	56.311
90	179.69	156.748	90.398	66.350
100	193.88	176.419	100.043	76.376
110	207.01	195.522	109.178	86.345
120	219.50	214.066	117.846	96.220
130	231.49	232.112	126.132	105.980
140	242.45	249.666	134.046	115.620
150	252.53	266.731	141.603	125.128
160	262.23	283.340	148.839	134.501
170	270.88	299.502	155.770	143.732
180	279.66	315.236	162.410	152.826
190	288.11	330.583	168.805	161.778
200	296.42	345.579	174.984	170.595
210	304.41	360.234	180.957	179.278
220	312.54	374.582	186.751	187.831
230	320.75	388.656	192.399	196.257
240	329.37	402.489	197.926	204.563
250	337.94	416.117	203.363	212.754
260	346.98	429.544	208.712	220.833
270	356.08	442.812	214.001	228.811
280	365.31	455.929	219.242	236.687
290	374.21	468.905	224.434	244.472
300	383.67	481.751	229.583	252.168
310	393.01	494.478	234.700	259.779
320	401.60	507.093	239.781	267.311
273.15	359.01	446.959	215.657	231.302
298.15	381.92	479.383	228.632	250.750

References to Chapter 4.

[1] H. Remy and G. Laves, *Ber Dtsch. Chem. A*, **66**, 401 (1933).

[2] R. D. Willett, J. R. Ferraro and M. Choca, *Inorg. Chem.*, **13**, 2919 (1974).

[3] D. N. Anderson and R. D. Willett, *Inorg. Chim. Acta*, **8**, 167 (1974).

[4] D. R. Bloomquist, R. D. Willett and H. W. Dodgen, *J. Am. Chem. Soc.*, **103**, 2610 (1981).

[5] D. R. Bloomquist and R. D. Willett, *Coord. Chem. Rev.*, **47**,125 (1982)

[6] P. Steadman and R. D. Willett, *Inorg. Chim. Acta*, **4**, 367 (1970).

[7] R. D. Willett, O. L. Liles, Jr. and C. Michelson, *Inorg. Chem.*, **6**, 1885 (1967).

[8] M. Yoshikawa, M. Sorai, H. Suga and S. Seki, *J. Phys. Chem. Solids*, **44**, 311 (1983).

[9] A. Nishimori, Y. Nagano and M. Sorai, *unpublished result.*

[10] R. D. Willett, J. A. Haugen, J. Lebsack and J. Morrey, *Inorg. Chem.*, **13**, 2510, (1974).

[11] M. Sorai and S. Seki, *J. Phys. Soc. Jpn.*, **32**, 382 (1972).